STUDY OF HIGH STRENGTH REINFORCED CONCRETE EXTERIOR BEAM-COLUMN JOINTS UNDER CYCLIC LOADING

BY

ANAS MOHAMMAD IBRAHIM ALKHATIB

A Thesis Presented to the
DEANSHIP OF GRADUATE STUDIES

KING FAHD UNIVERSITY OF PETROLEUM & MINERALS

DHAHRAN, SAUDI ARABIA

In Partial Fulfillment of the
Requirements for the Degree of

MASTER OF SCIENCE

In

CIVIL ENGINEERING

MAY 2015

KING FAHD UNIVERSITY OF PETROLEUM & MINERALS

DHAHRAN- 31261, SAUDI ARABIA

DEANSHIP OF GRADUATE STUDIES

This thesis, written by **Anas Mohammad Ibrahim Alkhatib** under the direction his thesis advisor and approved by his thesis committee, has been presented and accepted by the Dean of Graduate Studies, in partial fulfillment of the requirements for the degree of **MASTER OF SCIENCE IN CIVIL ENGINEERING.**

Dr. Mohammed H. Baluch
(Advisor)

Dr. Omar A. Al-Swailem
Department Chairman (A)

Dr. Mohammed AL-Osta
(Co-Advisor)

Dr. Salam A. Zummo
Dean of Graduate Studies

Dr. Muhammad K. Rahman
(Member)

7/6/15
Date

Dr. Ahmed Ibrahim
(Member)

Dr. Al Farabi M. Sharif
(Member)

DICTATED TO

MY BELOVED PARENTS,

AND

MY BROTHERS & SISTERS

ACKNOWLEDGMENTS

In the first place, I shall thank Allah (Glory be to Him) for blessing me with hale, faith and illuminating ideas to accomplish this study.

Thanks are due to all those who helped directly or indirectly in the preparation of this thesis, from family and friends to professors and- why not- computers. I have to admit that the merits of this work are theirs and the inadequacies are mine. I also grant my hearty thanks to The King Fahd University of Petroleum & Minerals for the chance it bestowed on me to accomplish my dream through its well-equipped labs and well-trained staff, and for helping me pursue my graduate studies and financially supporting my research.

I deeply appreciate the encouragement, immense knowledge and great efforts provided by Dr. Mohammed H. Baluch, the major advisor, who greatly helped me in the conceptual aspects and whose guidance all through the experimental and modeling work was inspiring. Moreover, I acknowledge my gratitude to Dr. Mohammed AL-Osta, the co-advisor, for his extensive guidance, insightful comments, and personal involvement in the experimental work of this study. My sincerest gratitude also goes to Dr. Muhammad K. Rahman whose knowledge and expertise in the modeling work and preparing for casting were very enlightening. Thanks to the other committee members Dr. Al Farabi M. Sharif and Dr. Ahmed Ibrahim for their instructive comments, great advice and support. Thanks to Dr. Hakeem for providing me the mix design of ultra-high performance

concrete. Acknowledgement is due to the Deanship of Scientific Research for funding this research.

I would like to pay thanks to the laboratory technicians Eng. Omer, Eng. Syed Imran Ali and Eng. Najam for their tremendous help and endless efforts during all the stages of my experiments. My deep appreciation shall go to Dr. Nedal T. Ratrout, the Chairman of the Department, and to other faculty members for their support and outstanding expertise.

I would like to show my great appreciation to my colleagues at the University for their friendship and support during my graduate studies. Special words of thanks are due to my family for their encouragement and unfailing support during the years of my study.

TABLE OF CONTENTS

LIST OF TABLES

LIST OF FIGURES

LIST OF ABBREVIATIONS

BCJ	:	Beam-Column Joint
SFC	:	Steel Fibre Concrete
UHPC	:	Ultra-High Performance Concrete
SSG	:	Steel Strain Gauge
SFRC	:	Steel Fibre Reinforced Concrete
RCBCJ	:	Reinforced Concrete Beam Column Joint

ABSTRACT

Full Name : Anas Mohammad Ibrahim Alkhatib

Thesis Title : [Study of High Strength Reinforced Concrete Exterior Beam-Column Joints Under Cyclic Loading]

Major Field : [Civil Engineering]

Date of Degree : [May, 2015]

Beam-column joints are one of the most common elements of existing buildings that collapse under shear forces which are mainly caused by earthquakes. During a seismic event, damage may occur in beam-column joints (BCJ). Under an earthquake, a complex combination of shear and flexural stresses acts simultaneously within the joint. The beam-column joint (BCJ) in moment resisting frame structures which designed according to early codes have insufficient shear reinforcement and inadequate development length. The damage in this area may result in collapse of the structure. The ductility of the beam column joint is enhanced by adding transverse reinforcement which results in the joint becoming highly congested. Recently, steel fibre reinforced concrete (SFRC) and ultra-high performance concrete (UHPC) have been used in various applications.

The main focus of this research, entitled “Study of High Strength Reinforced Concrete Exterior Beam-Column Joints Under Cyclic Loading” was to investigate the behavior of BCJs under monotonic and cyclic loadings for three different scenarios: (1) normal reinforced concrete beam-column joints (2) beam-column joints strengthened with steel fibre reinforced concrete (SFRC) (3) beam-column joints strengthened with ultra-high performance concrete (UHPC). In addition to variation in joint concrete, two different

diameters of longitudinal steel, 12 mm and 18 mm and two stirrups or ties were used within the joint for some specimens.

The results showed that, steel fibre enhanced the tensile strength of concrete and hence the shear capacity of the joint. The high strength concrete used in the BCJ specimens reinforced with 18 mm bars whether it is UHPC or SFRC converted the mode of failure from joint shear failure to beam flexural failure, which enhanced the ultimate load carrying capacity by more than 60%. While the high strength concrete did not improve the load carrying capacity of specimens reinforced with 12 mm bars, because all the specimens reinforced with 12 mm bars failed due to the beam flexural failure. The stirrups in the normal concrete joint region played a role in improving the shear carrying capacity and the hysteresis behavior of the joint, the load carrying capacity was improved by 23 %, while the effect of the stirrups in the high strength concrete joint region could not be observed. Regarding the cyclic results, the energy dissipated and the stiffness were enhanced after strengthening the BCJ specimens with either UHPC or SFRC.

Numerical modeling of BCJs with and without strengthening was conducted by using the finite element analysis software (ABAQUS 6.13) to predict the behavior and failure modes of the BCJ specimens under monotonic load. ABAQUS numerical results with damage plasticity model were noted to yield reasonably accurate results of BCJ specimens under monotonic loading. The Concrete Damage Plasticity (CPD) Model was noted to predict not only beam flexural failure mode of the BCJ, but also the softening mode of failure resulting from shear failure of the joint.

ملخص الرسالة

الاسم الكامل: أنس محمد إبراهيم الخطيب

عنوان الرسالة: دراسة الخرسانة عالية الاداء في نقاط التقاء الاعمدة والجسور تحت تاثير الاحمال الدورية.

التخصص: الهندسة المدنية

تاريخ الدرجة: 5/ 2015

إن الخرسانة هي واحدة من مواد البناء الأكثر شيوعاً حيث إن لها قوة ضغط عالية ولكن لسوء الحظ فهي ضعيفة تحت الشد. و بالتالي و لتقوية مقاومة هذه المادة لتقاوم قوى الشد، فإنه يجب تحضير مزيج من مواد أخرى. ان القضبان الفولاذية هي المادة الأكثر استخداما لتسليح الخرسانة العادية ولتمكينها من مقاومة ضغوطات الشد و التي تنجم بشكل اساس عن الاثقال الثابتة و الزلزالية و الانفجارية. تسبب قوى الشد صدوع في الخرسانة و الذي يؤدي إلى انهيار أو دمار البناء. فخلال الحدث الزلزالي، يحدث دمار في نقاط التقاء الاعمدة و الجسور (BCJ). من الممكن ان ينجم عن الدمار في هذه المنطقة انهيار البناء. من الممكن تعزيز الليونة في منطقة التقاء الاعمدة و الجسور عن طريق زيادة التعزيزات المستعرضة و التي تجعل منطقة الالتقاء ممتلئة بشكل عالٍ. تم استخدام الخرسانة المعززة بالياف الفولاذ (SFRC) و الخرسانة عالية الاداء (UHPC) حديثاً في تطبيقات مختلفة.

ان التركيز الاساسي لهذا البحث المعنون " دراسة الخرسانة عالية الاداء في نقاط التقاء الاعمدة والجسور تحت تاثير الاحمال الدورية " هو دراسة سلوك الBCJ تحت الاثقال الرتيبة و الدورية في ثلاثة تصورات مختلفة: (1) الخرسانة عادية التعزيز في منطقة التقاء الاعمدة و الجسور (2) الخرسانة المعززة بألياف الفولاذ في منطقة التقاء الاعمدة و الجسور (SFRC) (3) الخرسانة عالية الاداء في منطقة التقاء الاعمدة و الجسور (UHPC) . بالاضافة الى استخدام نوعين من حديد التسليح في تسليح عينات BCJ احدهما 12 ملم والاخر 18 ملم.

اظهرت النتائج ان استخدام UHPCو SFRC في تقوية عينات BCJ المسلحة بقضبان حديد بقطر 18 لم حول طبيعة الانهيار من انهيار في منطقة التقاء الجسر مع العمود الى انهيار في الجسر. ان استخدام UHPCو SFRC طور قوة تحمل العينات لاكثر من 60%. بينما استعمال الباطون عالي الاداء في العينات المسلحة بقضبان 12 ملم لم

يطور من قوة التحمل لان العينات انهارت بسبب انهيار الجسرز ان استعمال الكانات في الباطون العادي حسن قوة تحمل العينة حيث زادت بحوالي 23% ولكن تاثير الكانات في UHPCوSFRC لم يكن ملحوظا. ان الطاقة الكامنه زادت بعد تقوية العينات ب UHPCو SFRC.

كما و تم القيام بالنمذجة الرقمية لنقاط الالتقاء بعد تقويتها و بدونها عن طريق استخدام برنامج تحليل العناصر المحدودة (ABAQUS) لعمل نموذج عناصر محدودة. ساعد هذا في تفسير السلوك المضبوط ل BCJ تحت تاثير الاحمال الستاتيكية. ان نتائج ABAQUS الرقمية كانت دقيقة ولوحظ ان CDP قادر على التنبؤ ليس فقط بالانهيار الناتج عن الجسر ولكن ايضا بالانهيار الناتج عن نقطة التقاء الجسر بالعمود.

CHAPTER 1

INTRODUCTION

1.1 General

Reinforced concrete is one of the most common composite materials, which is used in a wide range of structures such as buildings, dams, bridges etc. The familiarity of this material comes from it is strength, durability, fire resistance, ease of manufacturing and low environmental impact. Many reinforced concrete structures lose their durability due to aggressive environment and due to cyclic loadings which are caused generally by earthquakes.

Beam-column joints are one of the most common elements of existing buildings that collapse under shear forces which mainly caused by earthquakes. The damage in the joints has been observed in recent destructive earthquakes in many countries around the world. The beam-column joint (BCJ) in moment resisting frame structures which designed according to early codes have insufficient shear reinforcement and inadequate development length. That is the main cause of joint failure. Therefore, other materials should be used in order to increase the ductility of the BCJs, such as Carbon Fibre Reinforced Polymer (CFRP), Glass Fibre Reinforced Polymer (GFRP), steel fibres, Shape Memory Alloys (SMA) and ultra-high performance concrete (UHPC).

Steel fibers is one of the materials that is used to enhance the ability of the structures to resist tensile forces such as seismic loads, blast and shock loads, splitting erosion and abrasion, and high temperature by making the concrete tougher and more ductile. It is very ductile material with high tensile strength and different shapes and styles. The steel fibre reinforced concrete (SFRC) is normal concrete with a specific amount of steel fibres. The properties of the SFRC mainly depend on the concrete mix proportions, steel fibre content, fibre shape and bond characteristics. The workability of the concrete will be affected by adding steel fibre to the mixture. Therefore, important requirements should be considered when the concrete mixture includes steel fibres like the amount of mortar, maximum aggregate size, and role of additives like superplasticizers.

1.2 Need of Research

Many researches were conducted to study the behavior of BCJ under cyclic load experimentally and numerically e.g. Hanson and Connor (1967), Megget and Park (1971), Meinheit and Jirsa (1981), Durrani and Wight (1982).Several international codes of application have been undertaking revisions to include the research outcomes into practice. New design and detailing aspects has been incorporated into codes to prevent joint failure (Anderson et al. 1996, Mugurama et al 1995, Saatcioglu et al. 2001). However, other ductile materials like steel fibres in new construction and techniques for their use need to be enhanced. Depending on the literature review, few experimental studies have been conducted on BCJs with high strength concrete weather it is SFRC or UHPC.

1.2.1 Seismicity of the Kingdom

Many studies were carried out to estimate the seismic activities and seismic hazards along the western cost of Saudi Arabia. Depending on the peak ground acceleration PGA, a zonation map was created for the Kingdom for 50 years life time with 10% probability of being increased (Figure 1-1). The Kingdom was divided into four zones depending on the uniform building code (UBC 1991), Table 1-1 shows PGA values, no risk level is considered for zone of SZN=0, while low risk level for zone of SZN=1, whereas moderate risk level is considered for zone of SZN=2A and 2B, and high seismic risk level is considered for zones of SZN = 3 and 4. Most of the Kingdom areas are considered to be of no and low risk level depending on the seismic zonation map, while areas along the western cost is included in the zone of moderate risk level.

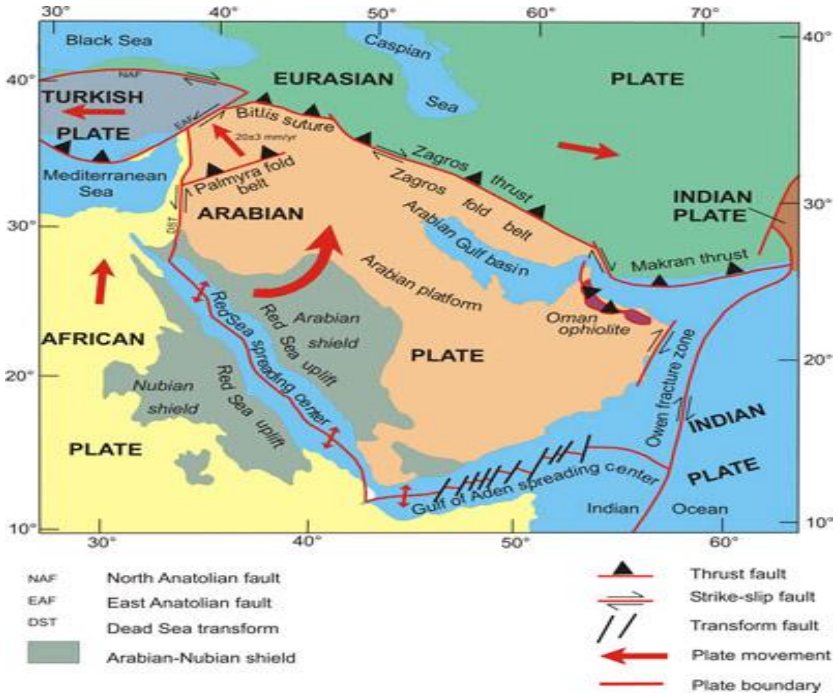

Figure 1-1: Kingdom seismic zonation map

Table 1-1: PGA values and corresponding seismic zones number according to UBC

SZN	PGA in g's
0	< 0.05
1	0.05 to 0.10
2A	0.10 to 0.15
2B	0.15 - and above

Some areas in the Kingdom fall in fault zones. The seismic hazards to human life and buildings are increased by increasing the population. Recently, Arabian Peninsula was exposed to frequent earthquakes, because it is sited close to the active seismic boarders on the north eastern as well as the western borders. (stated by Geologist in an interview in Asharq Al Awsat). They also stated that the Arab plate move 2 cm annually towards Iranian and Turkish plate, which causes expansion in Red Sea area and collision between the eastern region in the Arab plate with the neighbor plates.

Haql earthquake with magnitude 7.3 on the Richter scale shook Gulf of Aqaba causing severe damage in both sides of the gulf. In September 2005, an earthquake with magnitude 3.7 on the Richter scale frightened the residents in Otaibah near the Holy Mosque. In 2006, an earthquake with magnitude of 4.1 on the Richter scale shook the city of Haradh in Eastern of Saudi Arabia. SGS (Saudi ground services) is responsible for monitoring all earthquakes within the kingdom. The old stations which were included in the previous seismograph networks are now part of SGS national network. SGS can detect routinely any earthquake with magnitude more than 2 within Saudi Arabia. Since the western part has high seismicity, most of the stations located in that area.

1.3 Objectives of this Research

The main objective of this research is to investigate the feasibility of using SFRC and UHPC for strengthening RC beam-column joints (BCJs) for new RC construction.

The following tasks will be carried out in order to meet the above stipulated objective:

- Examine the mechanical properties of SFRC and UHPC.
- To inspect the behavior of steel fibre reinforced concrete beam column joint specimens (SFRC-BCJ) under monotonic and cyclic loading experimentally.
- To study the behavior of ultra-high performance concrete beam-column joint specimens (UHPC-BCJ) under monotonic and cyclic loading experimentally.
- Simulate BCJ's in ABAQUS environment to predict the behavior and failure modes of the joints. The parameters of the numerical model will be calibrated by comparing the numerical results to the experimental data.

CHAPTER 2

LITERATURE REVIEW

2.1 Mechanical Properties of High Strength Concrete

Concrete is a brittle material therefor; other materials should be used to improve concrete tensile strength. Steel fibre is one of the most materials used to enhance the ductility and most of the concrete mechanical properties. Hakeem MSc thesis.[1] studied the physical and mechanical properties of the Ductal concrete as well as its behavior related to durability. The mix proportion of the Ductal concrete is as shown in Table 2-1. The results showed that the compressive strength of the Ductal material was 163 MPa with elastic modulus of 57 GPa. The compressive strength was increased by using heat-cool cycles. The flexural strength of fibre reinforced Ductal was about 31 MPa. Ductal concrete water absorption and permeability were low according to the durability tests. The coefficient of chloride diffusion was smaller than that of normal concrete.

Table 2-1: Ductal mix proportion [1]

Ductal Mix Component	Weight (kg/m^3)	Percent by weight
Premix	2202	87.2
Water	136	5.4
Superplasticizer	30	1.2
Steel Fibers	157	6.2

Song et al.[2] studied the mechanical properties of high strength concrete (HSC) with several percentages of steel fibres which were 0.5%, 1%, 1.5%, and 2%. Each of the compressive and splitting tensile strength was conducted on 15 cylindrical concrete specimens and the flexural strength was investigated on fifteen beams according to ASTM C1018 specification. The results showed that the mechanical properties of the HSC were improved by mixing it with the steel fibre (Figure 2-1). The tensile strength and the modulus of rupture increased by increasing the percentage of the steel fibres and the maximum value of the compressive strength was at 1.5% fibre content (Figure 2-2).

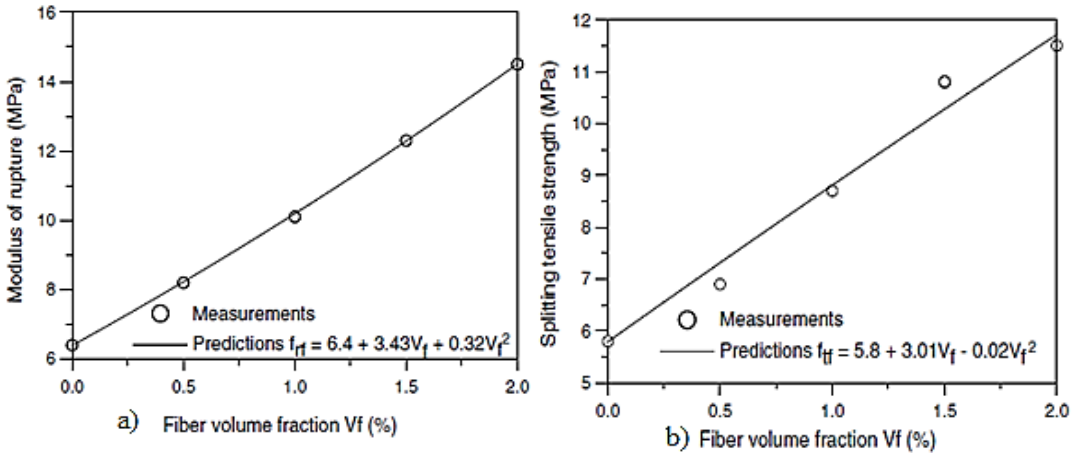

Figure 2-1: The variation of modulus of rupture and splitting tensile strength with the fibre volume fraction [2]

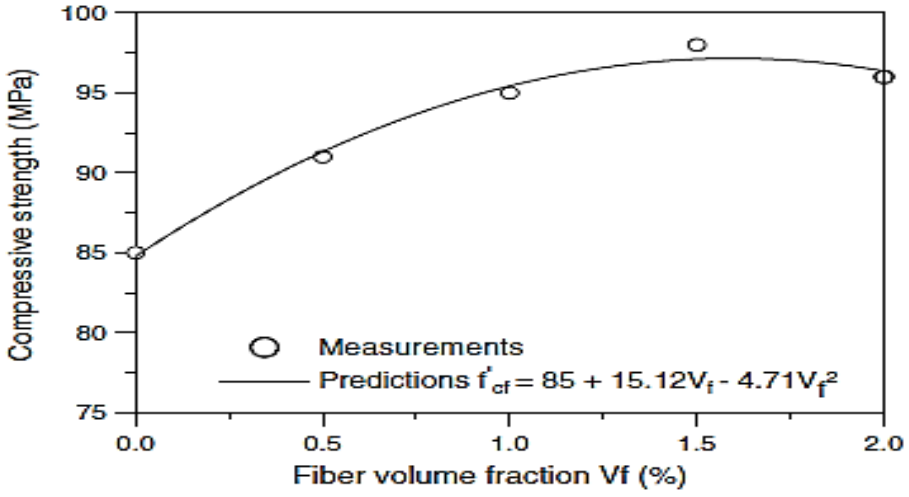

Figure 2-2: The variation of compressive strength with fibre volume fraction [2]

Shende et al.[3] investigated the mechanical properties of SFRC. The parameters of the study were the percentages of the steel fibre which were 0%, 1%, 2%, and 3%, and the aspect ratios which were 50, 60, and 67. The results presented that the flexural strength, compressive strength, and split tensile strength were higher for specimens containing 3% steel fibre with aspect ratio equal to 50 (Figure 2-3 to 2-5).

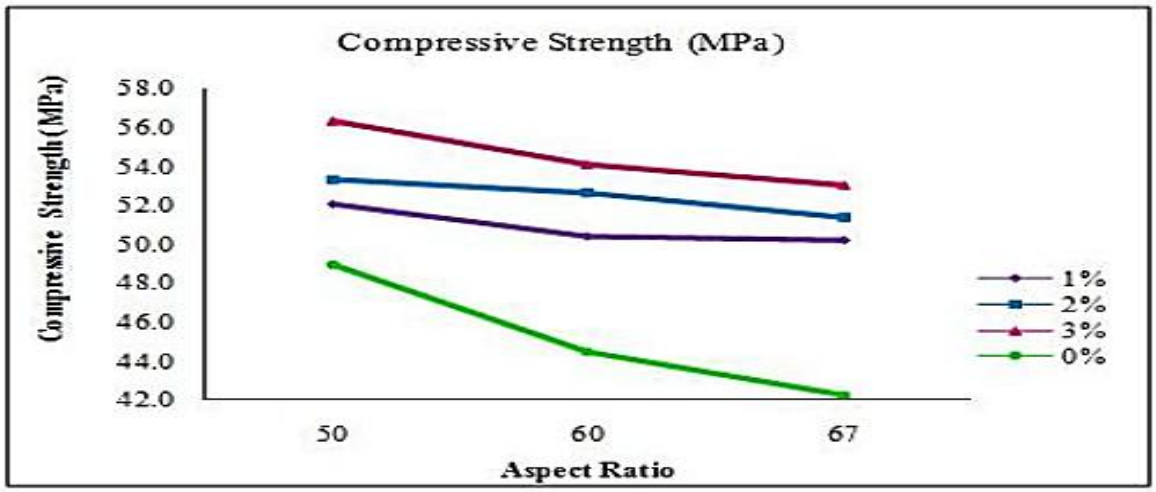

Figure 2-3: Percentages change in 28 days M-40 grade concrete compressive strength [3]

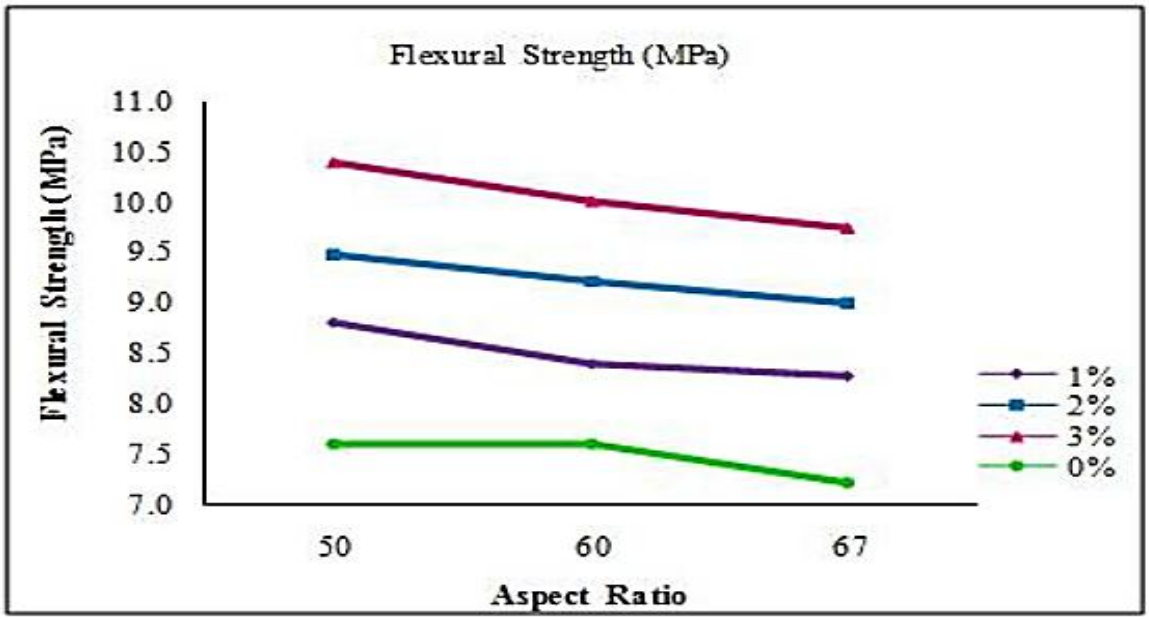

Figure 2-4: Percentages change in 28 days M-40 grade concrete flextural strength [3]

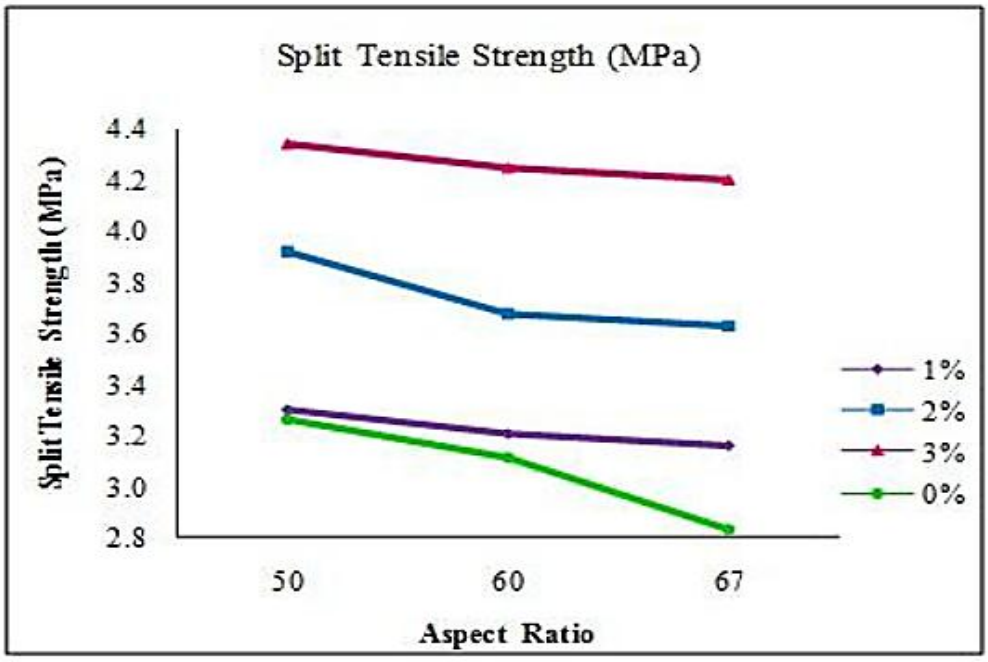

Figure 2-5: Percentage change in 28 days M-40 grade concrete split tensile strength [3]

Gao et al [4] investigated the mechanical properties of the steel fibre high strength light weight concrete. Five percentages of the steel fibres were used, which were 0%, 0.6%, 1%, 1.5%, and 2% with three different aspect ratios of 46, 58, and 70. The results showed that the compressive strength was improved by increasing the volume and the aspect ratios of the steel fibres. The density of the fresh concrete was improved by increasing the volume of the steel fibre while the aspect ratio of the fibres did not affect the fresh concrete density. The splitting tensile and flexural strength increased by increasing the volume of the steel fibres (Figure 2-6).

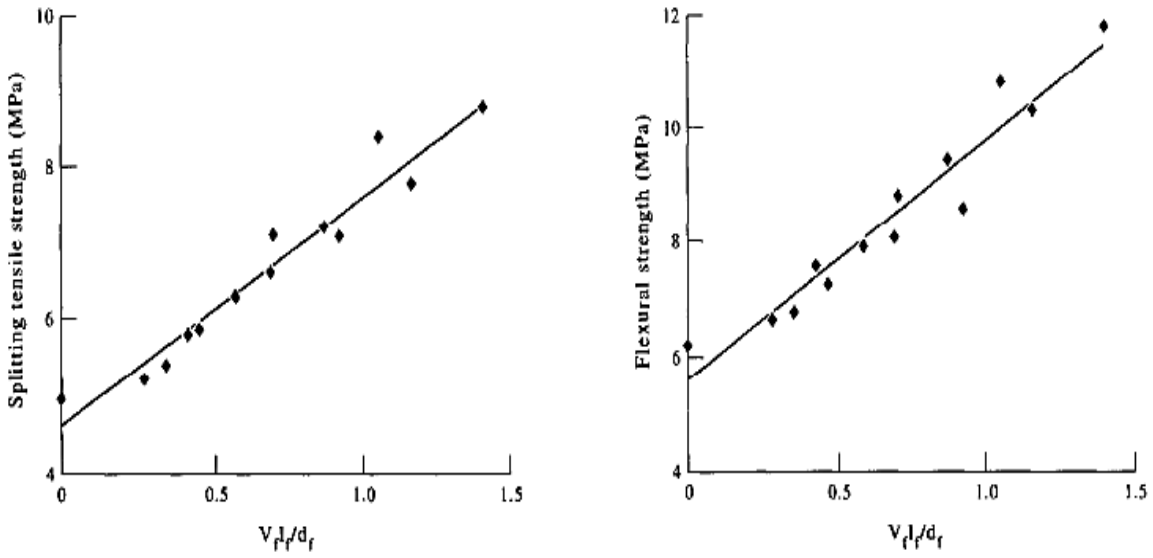

Figure 2-6: (a) Effect of $V_f l_f/d_f$ on splitting tensile strength (b) Effect of $V_f l_f/d_f$ on flexural strength [4]

Barros et al.[5] investigated the flexural behavior of steel fibre reinforced self-compacting concrete. The experiment was conducted on twelve slabs which were categorized into three groups depending on the value of steel reinforcement ($\rho_{SL)}$. Each group consists of four slabs, two of them without steel fibre and the other two with 45 Kg/m³ of hooked end steel fibre. The results showed that the load carrying capacity enhanced by adding 45Kg/m³ steel fibre and the highest value of the load carrying capacity was achieved at the lowest value of ρ_{SL} (Figure 2-7).

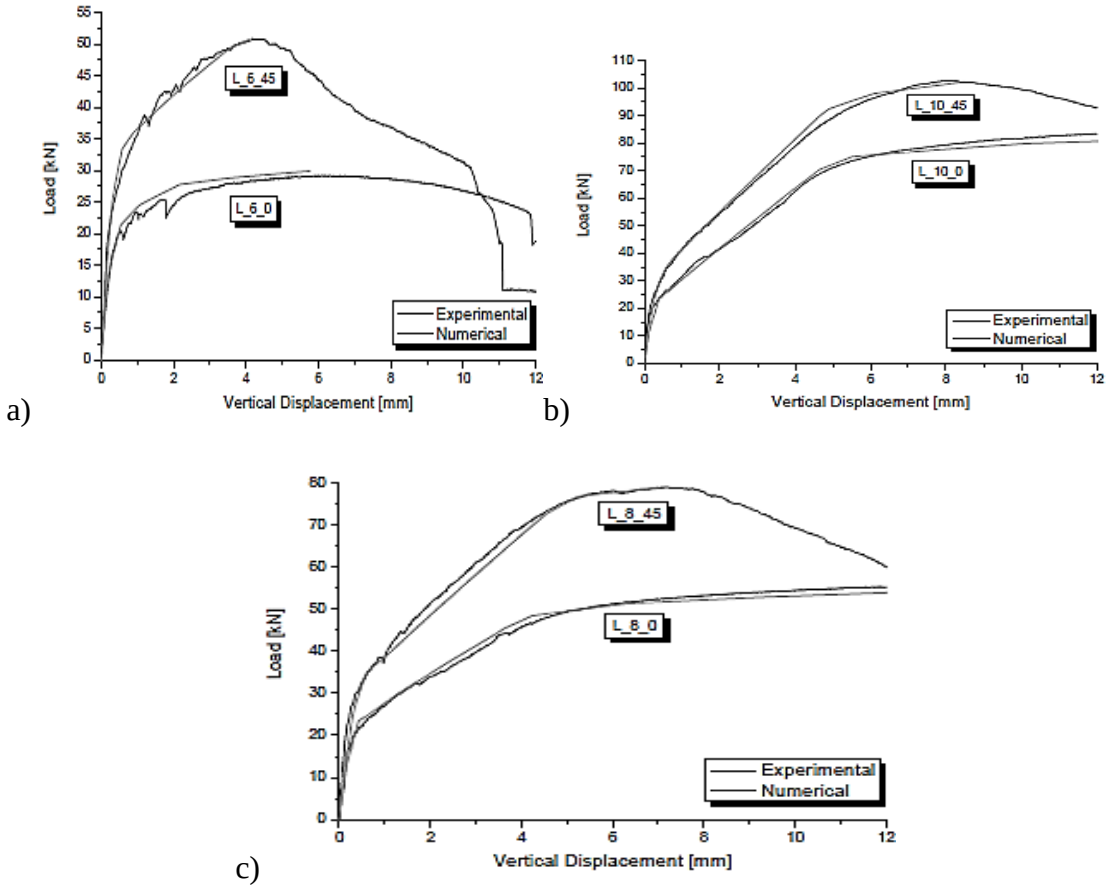

Figure 2-7: Load central deflection curves of series (a) L_ 6 (b) L_8(c) L_10. [5]

Prem et al. [6] explored the mechanical properties of UHPC. The variables of the study were the volume and the aspect ratio of the steel fibre. The results showed that the tensile strength of the concrete improved by adding the steel fibre with high aspect ratio. The relationship between the flexural strength and the reinforcement index was linear, and the compressive strength was slightly affected by the reinforcement index.

El-Dieb et al [7] studied the possibility of producing ultra-high self-compacting (UHSC) concrete by using local material with steel fibre and they investigated the mechanical properties of UHSC. The results showed that UHSC can be produced locally and the ductility was improved by adding the steel fibre. The total charge passing through the

concrete was increased by increasing the volume of the steel fibre. The bulk chloride diffusion coefficient did not affected by the volume of the steel fibre. The compressive and tensile strength were increased by increasing the quantity of the steel fibre.

Park et al [8] examined the effect of blending fibres on the tensile behavior of ultra-high performance hybrid fibre reinforced concrete (UHP-HFRC). Two types of fibres were used which were micro fibre with different volumes and macro fibres with different length or geometry. The results showed that the post cracking, strain capacity and the multiple micro-cracking behaviors were higher when macro fibre with twisted geometry was used. All tensile stress vs. strain curves of UHP-HFRC were directly depending on the type of the macro fibre.

Ramli et al [9] studied the mechanical strength of ultra-high self- compacting concrete with several percentages of steel fibre. The results showed that the flexural strength, toughness indexes, compressive strength, and static modulus of elasticity were enhanced by increasing the dosage of the steel fibre up to 1.75% as a volume fraction from the concrete volume.

Mazloom et al [10] studied the effect of different percentages of silica fume on the mechanical properties of high strength concrete. The main objective of the research was to study the effect of binder systems including different percentages of silica fume on short and long term mechanical properties of high strength concrete. Cement was replaced by different percentages of silica fume which were 0%, 6%, 10%, and 15%. The outcomes of the study showed that the workability of the concrete decreased as the percentage of silica fume increased. The percentage of the silica fume did not affect the

total shrinkage of the concrete while concrete autogenously shrinkage increased as the amount of silica fume increased whereas the basic creep decreased as the amount of silica fume increased.

Yew et al [11] studied the mechanical properties of hybrid nylon-steel fibre reinforced concrete as well as the polypropylene-steel fibre reinforced concrete. The total volume fraction of the fibre was 0.5%, whereas the volume fraction of steel fibre was 0.4% and the volume fraction of micro fibre (nylon or polypropylene fibre) was 0.1%. The results showed that the splitting tensile strength, the compressive strength, and the modulus of rupture of nylon-steel fibre reinforced concrete were more than that for polypropylene-steel fibre reinforced concrete. That was due to the better distribution of the nylon fibre in the concrete.

Sivakumar et al [12] investigated experimentally the mechanical properties of high strength concrete reinforced by hybrid fibres with max volume fraction of 0.5%. The variables of the study were the volume fraction of the hybrid fibre and the hybrid fibre combinations, which were steel-polypropylene fibres, steel-polyester fibres, steel-glass fibres, and steel fibre only. The results showed that the steel fibre played a significant rule towards the energy absorbing mechanisms, while the non-metallic fibre delayed the formation of micro-cracks. That was the reason for improving the strength and the flexural properties for the hybrid fibre concrete. Comparing between the steel fibre concrete and the concrete reinforced by different combinations of fibre, the mechanical properties improved more when the concrete reinforced by steel-polypropylene fibre, while the other different combinations caused decreasing in the flexural toughness.

Rubi et al [13] investigated the mechanical properties of hybrid fibre reinforced concrete (HFRC). M40 grade concrete was reinforced by steel-polypropylene fibres with volume fraction of 0.5%. The results showed that the compressive strength and the splitting tensile strength of HFRC with volume fraction of 75% steel fibre and 25% of polypropylene fibre were the highest. The improvement in the compressive strength was due to the high elastic modulus of steel fibre and low elastic modulus of polypropylene fibre.

Hsie et al [14] studied the mechanical properties of polypropylene hybrid fibre reinforced concrete. Two types of polypropylene fibres were used, which were coarse monofilament and staple fibres. The results showed that the compressive strength, the splitting tensile strength, and the flexural properties for polypropylene hybrid fibre reinforced concrete were better than the mechanical properties of single fibre reinforced concrete. The staple fibre restrained the cracks due to its fineness, while the monofilament took the stresses after the concrete cracked due to its high elastic modulus and stiffness.

Singh et al [15] studied experimentally the strength and the flexural toughness of hybrid fibre reinforced concrete (HyFRC) with different combinations of steel-polypropylene fibres. The different dosages of steel-polypropylene fibres were 100-0%, 75-25%, 50-50%, 75-25%, and 100-0% by volume. The results showed that the compressive strength, the flexural strength and the flexural toughness were highest when the concrete contained 75% steel fibre and 25% polypropylene fibre.

Nili et al [16] investigated the impact resistance and strength performance of concrete mixtures with water to cement ratios of 0.36 and 0.46. The mixtures also contained silica

fume and four different volume fraction of polypropylene fibre, which were 0%, 0.2%, 0.3% and 0.5%. The silica fume was used as a replacement material. The results showed that, the addition of polypropylene fibre improved the mechanical strength, while the silica fume played a significant rule in distributing the fibre uniformly.

2.2 Behavior of Reinforced Concrete Beam-Column Joint Under Cyclic Loadings

Ahmed [17] studied the behavior of exterior beam column joint under cyclic and static loads. The joints had insufficient reinforcement detailing. Three types of specimens were tested. The variable of the study was the reinforcement detailing. The results showed that the ultimate capacity of the joint with high beam reinforcement reached when the load exceeded the shear capacity of the joint, while the joints with low beam reinforcement failed when the load exceeded the flexural strength of the beam.

Braga et al [18] studied the behavior of reinforced concrete beam column joints under inelastic seismic load. Low strength concrete and smooth bars were used to form three interior joints and one exterior joint. The behavior of the joints was studied by increasing the horizontal cyclic drift up to failure. The results of the experiment showed that the cracks occurred in the joint due to the splitting of the bar while the failure in the exterior joint was caused by shear (Figure 2-8).

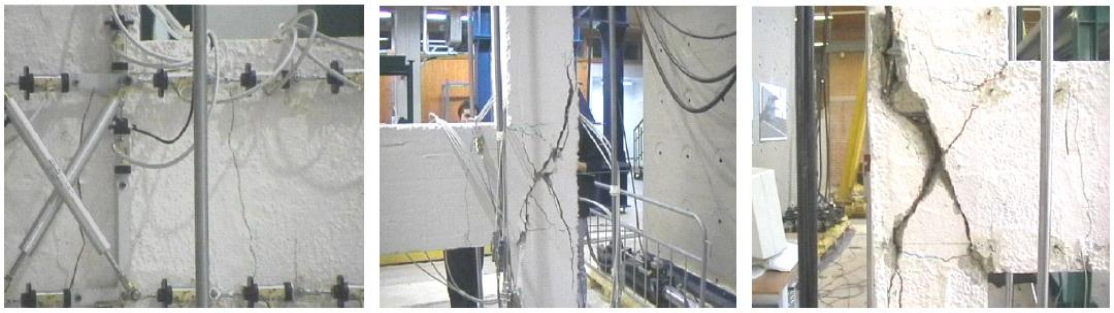

Figure 2-8: Cracks pattern at failure of T-joint specimen [18]

Pampanin et al [19] investigated the behavior of the beam column-joints which were designed under gravity load with six 2/3 scaled reinforcement concrete. The study was conducted on six joints, two exterior knee joints, two exterior tee joints, and two interior cruciform joints. The joint region has lack of reinforcement detailing, and smooth bars also used with insufficient anchorage hook (Figure 2-9). The results of the experiment showed that the bars with hooked end slipped and the concrete at the face of the exterior specimen crushed as illustrated in Figure 2-10.

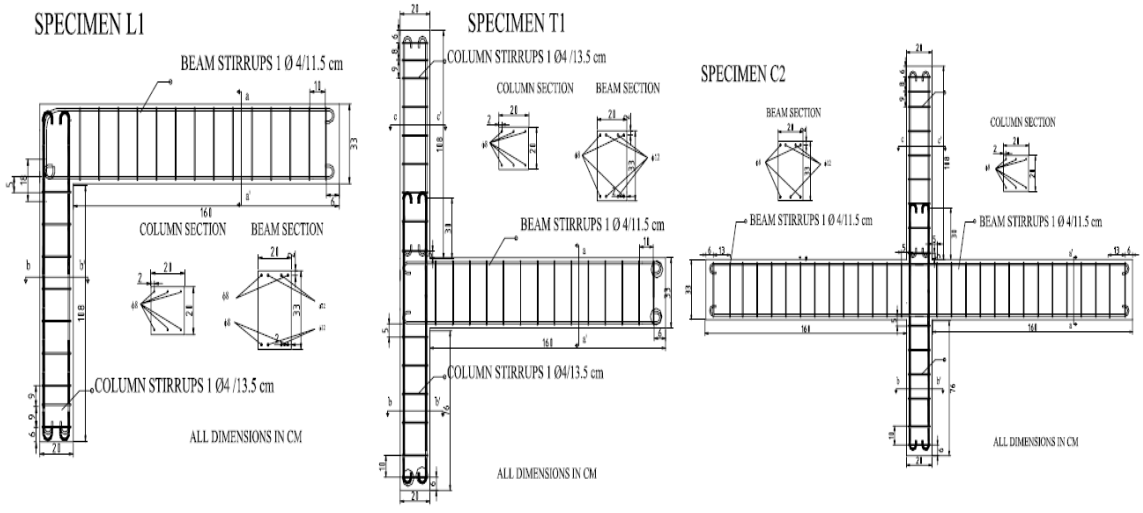

Figure 2-9: Joint sizes and reinforcement details for (a) Knee joint (b) Tee joint and (c) Interior [19]

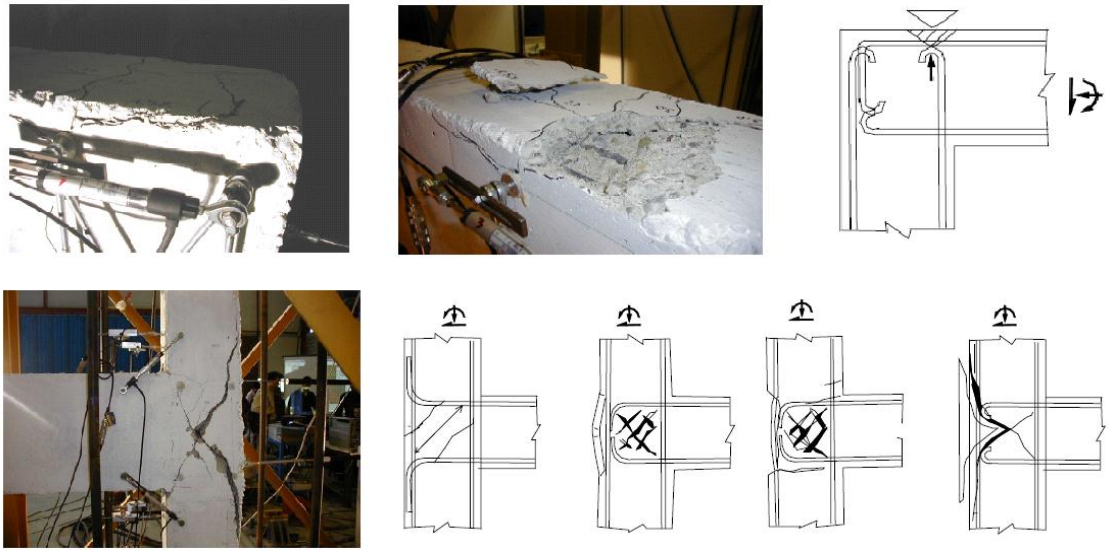

Figure 2-10: Failure mechanisms of Knee and Tee joint [19]

Halahla [20] investigated the behavior of the beam column joint under cyclic loading. He studied the behavior of non-retrofitted normal concrete beam-column joints and other specimens retrofitted with CFRP numerically and experimentally. The results showed that the capacity of the joints improved after retrofitting.

Pantelides et al.[21] studied the behavior of exterior beam column joint with and without retrofitting using FRP laminates under quasi-static cyclic loading. The experiment was conducted on two specimens, one of them was constructed without any type of strengthening, and the other one was retrofitted by FRP (Figure 2-11). The results showed that the ductility, axial load, bearing capacity and lateral load capacity were improved (Figure 2-12).

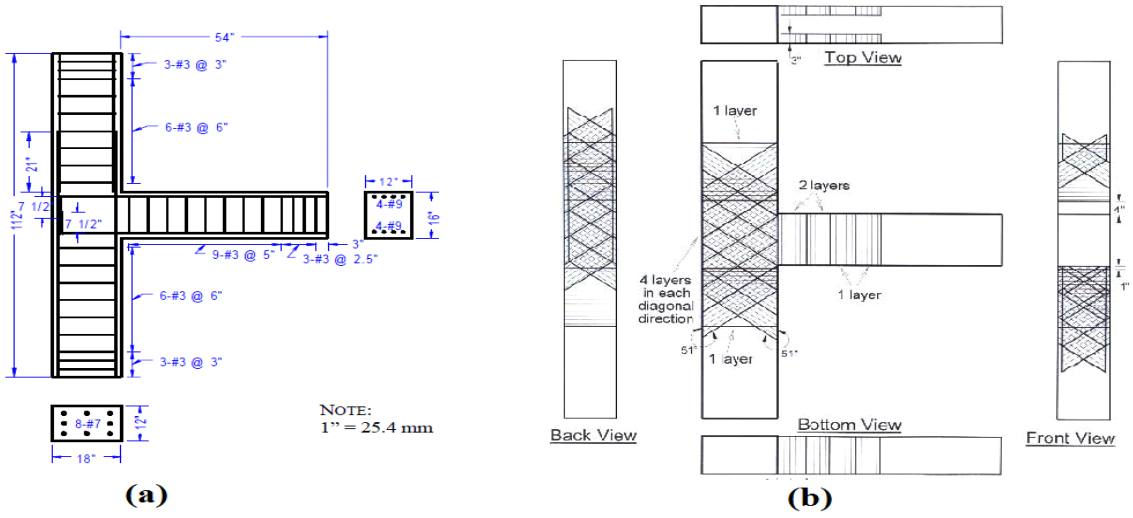

Figure 2-11: (a) Geometry of BCJ specimen and reinforcement detailing (b) Exterior BCJ retrofitted with FRP [21]

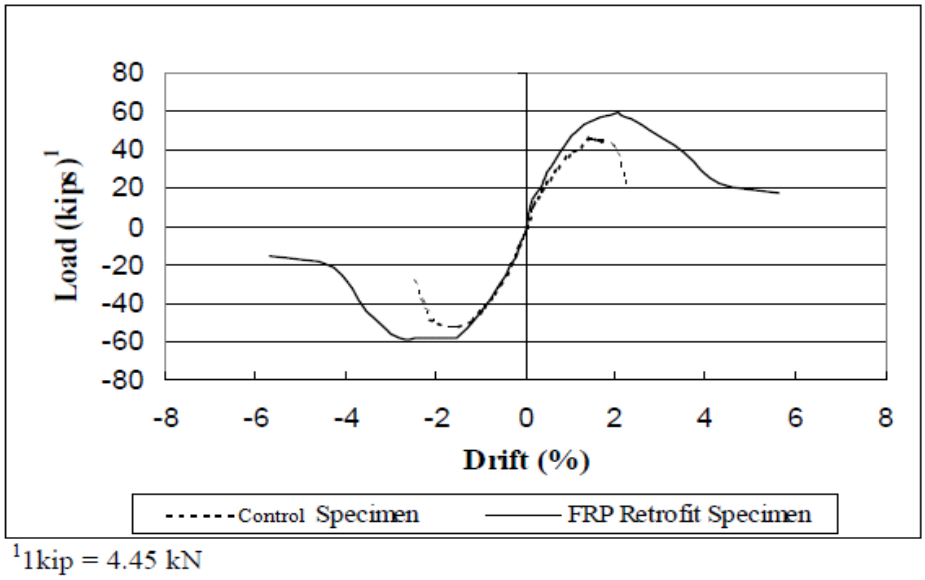

Figure 2-12: Control and FRP retrofit specimen backbone curve [21]

Gencoglua et al. [22] studied the effect of seismic load on four exterior beam column joints. One specimen was considered as a control, the other two specimens were retrofitted using CFRP fabrics on the tension zones of the specimens. The second one was designed according to ACI-318.02 as shown in Figure 2-13. The results showed that

the load carrying capacity and the energy absorbing was higher in the specimen retrofitted by CFRP (Figure 2-14).

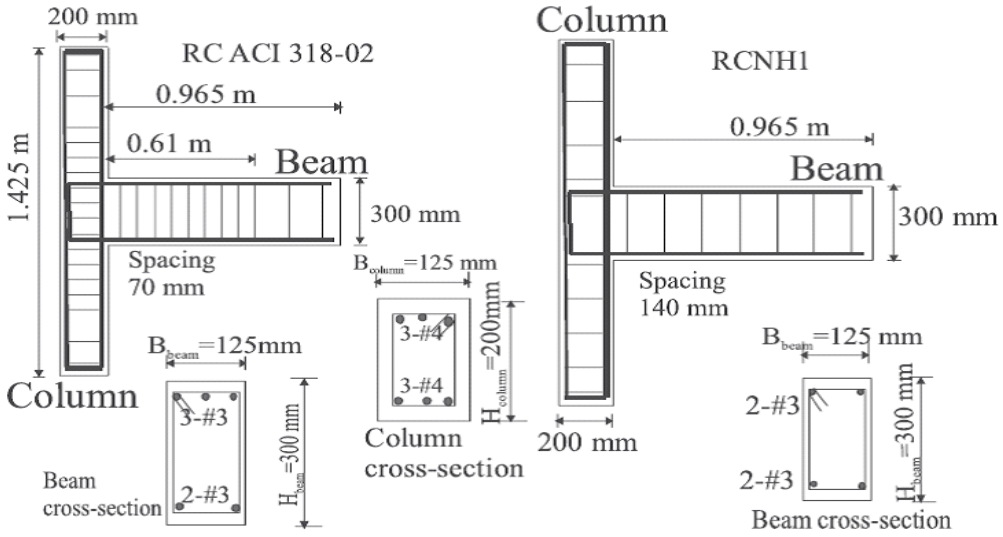

Figure 2-13: Geometry and reinforcement detailing for exterior BCJ Specimens [22]

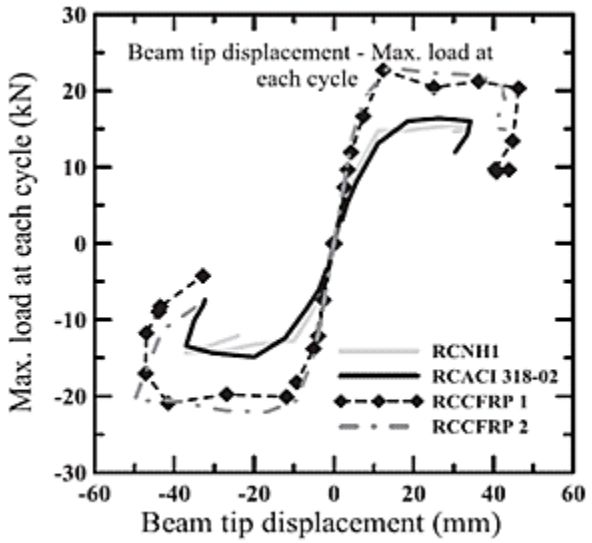

Figure 2-14: Load versus displacement graph for BCJ specimens [22]

Sasmal et al. [23] studied the behavior of reinforced concrete beam column joint specimens, which were retrofitted by FRP under seismic load. The Specimens were designed according to the Indian code considering seismic specifications, but

reinforcement details according to ductility were not considered. The specimens were retrofitted using FRP after being repaired with epoxy mortar and low viscous polymer as shown in Figure2-15. The results showed that the retrofitted specimens can return back to its original stiffness and it showed more ductility than the original specimen.

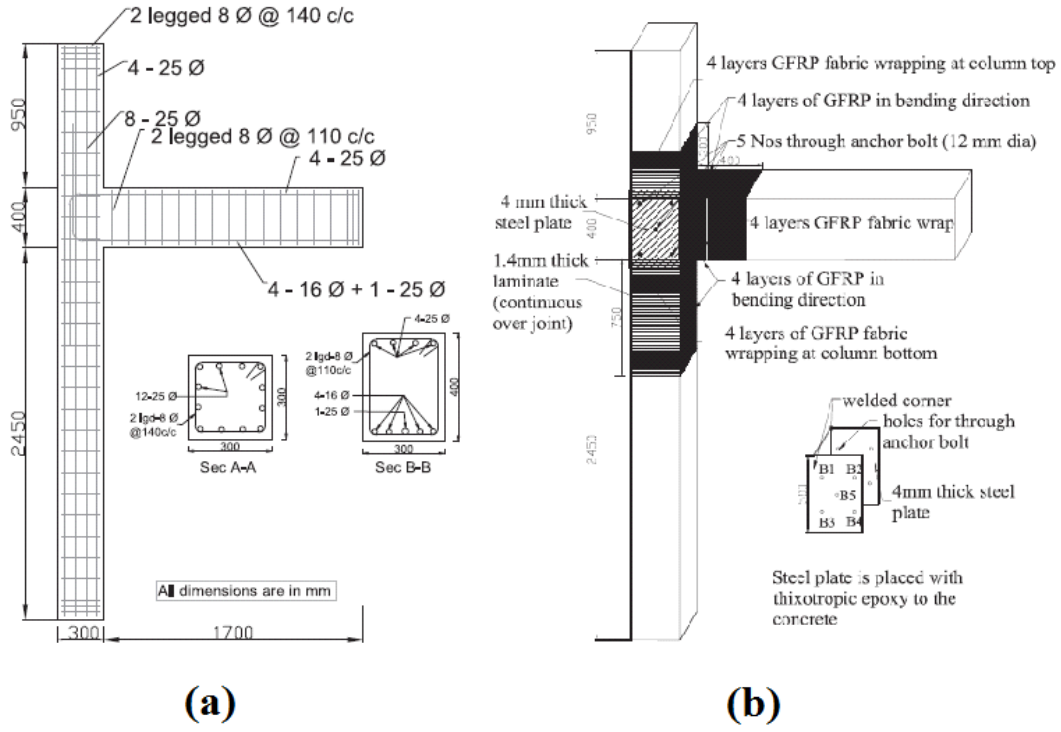

Figure2-15: (a) NonDuctile' specimen reinforcement detailing and (b) Retrofitting pattern for damaged 'NonDuctile' specimen [23]

Alsayed et al. [24] studied the behavior of beam-column joint retrofitted with CFRP under cyclic loads. The study was conducted on specimens of beam-column joint, four of them were control specimens while the other were retrofitted with CFRP by using two different scenarios of retrofitting. In the first scenario the CFRP was applied on the joint region, beam, and part of the column, while in the second scenario the CFRP was applied on the joint area only. The control specimens were tested under cyclic load then it

retrofitted again by CFRP. The results showed that shear resistance, deformation capacity, and stiffness were improved by using CFRP.

Karayannis et al. [25] investigated the behavior of exterior beam column joint retrofitted with thin reinforced concrete jacket. Ten specimens were constructed and exposed to increasing cyclic loading. The loaded specimens were retrofitted using reinforced concrete jackets then the retrofitted specimens were tested under the same type of loading. The variables of the study were the lateral reinforcement in the joint area and the reinforcement of the jackets. The results showed that the load carrying capacity and the energy distortion of the retrofitted specimens were improved (Figure 2-16).

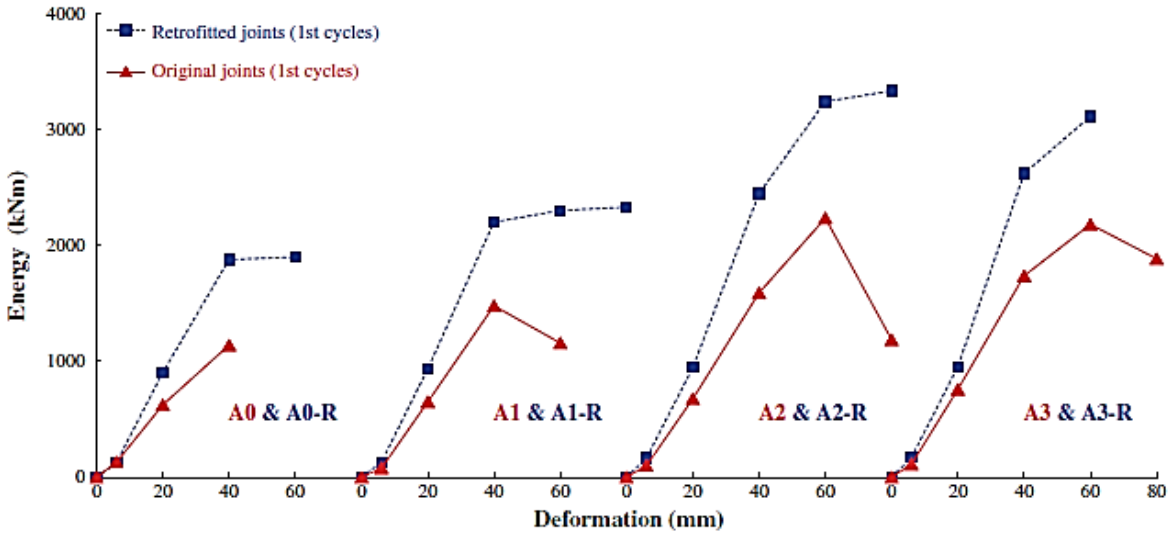

Figure 2-16: Energy dissipated of the tested specimens of BCJ strengthened with SFRC . [25]

2.3 Beam – Column Joint Strengthened with SFRC

Oinam et al. [26] investigated the behavior of reinforced concrete (RC) exterior beam column joints under cyclic loads. The experiment was conducted on three specimens of

exterior beam column joint which were made from steel fibre reinforced concrete (SFRC), polypropylene fibre reinforced concrete (PFRC), and plain reinforced concrete (PRC). All the specimens had the same cross section and reinforcement detailing. The results showed that the stiffness, energy dissipation, and ductility were improved by using steel fibres in the mixtures (Figure 2-17 and 2-18).

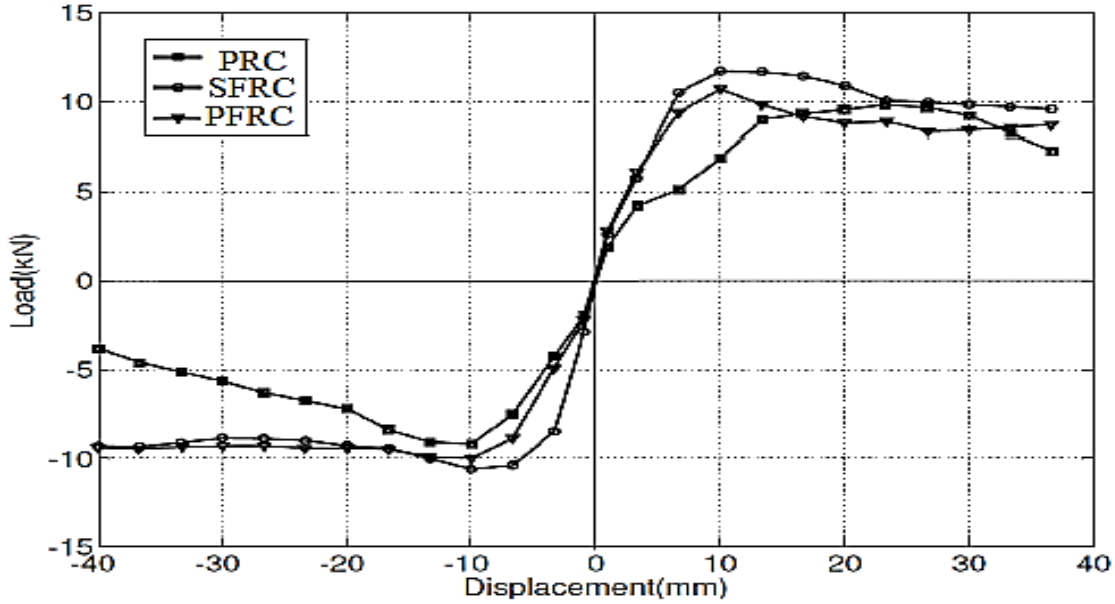

Figure 2-17: Envelopes of hysteresis loops for PRC, SFRC and PFRC specimens [26]

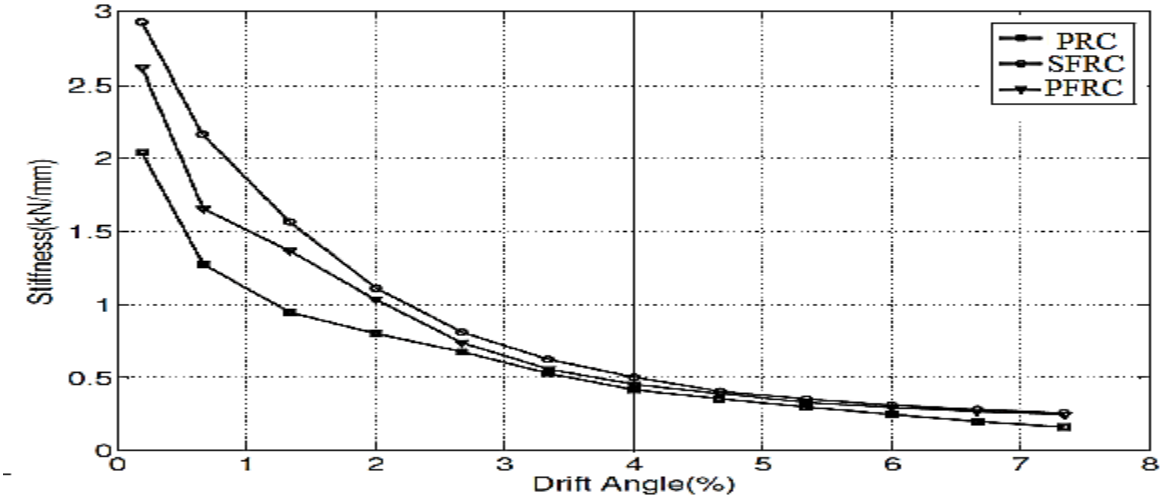

Figure 2-18: Stiffness vs. drift angle curve for PRC, SFRC and PFRC specimens [26]

Perumal et al. [27] investigated the behaviour of exterior reinforced concrete beam column joint under seismic load. The experiment was conducted on five specimens of exterior beam column joints which were made from M60 concrete and also from different combinations between steel and poly polypropylene fibres as listed in Table 2-2. The results showed that when using fibre combination (1.5% steel fibre and 0.2% polypropylene fibre) the beam column joint strength, deformation capacity, energy dissipation capacity and damage tolerance was significantly improved.

Table 2-2: Details of the test specimens [27]

Specimen Idetification	III O2	III S2	III F12	III F 22	III F32
Detailing of Lateral Reinforcement	Without Seismic Detailing	With Seismic Detailing	Without Seismic Detailing	Without Seismic Detailing	Without Seismic Detailing
% of Steel fibre	--	--	1.5	1.5	1.5
% of Polypropylene Fibre	--	--	0	0.2	0.4

Sarsam et al. [28] studied the behavior of thirteen high strength concrete beam column joints with and without steel fibres. The results showed that the joints with fibres have good integrity at failure load (Figure2-19), the ductility of the joints was improved, and the cracks became smaller during the test comparing with joints without fibres.

Figure2-19: Specimens after failure [28]

Ganesan et al. [29] studied the behavior of ten beam column joints which were made from M60 grade concrete with steel fibres under cyclic load. The amounts of fibres were changed from 0.25% to 1%. The results approved that using steel fibres in the joint improve the strength, ductility (large displacement with small cracks (Figure 2-20), integrity, and stiffness.

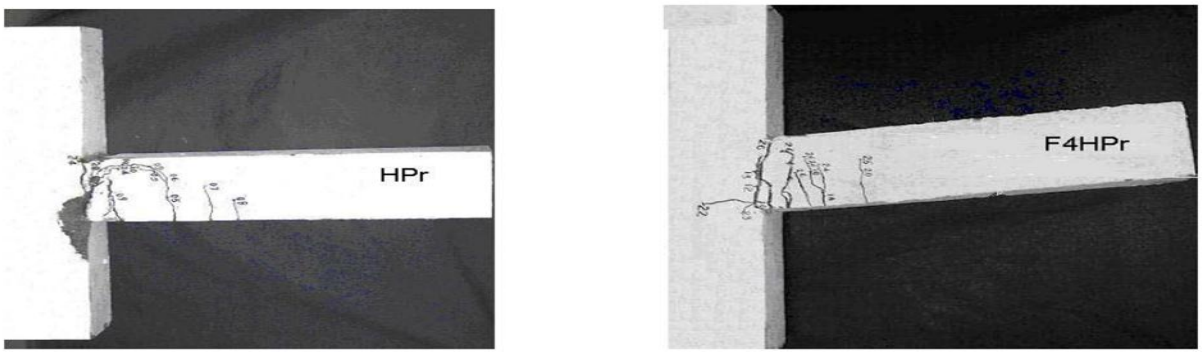

Figure 2-20: (a) HPC (high performance concrete specimen after failure; (b) SFRHPC (steel fibre reinforced high performance concrete) specimen after failure [29]

Wang et al.[30] investigated the behavior of beam column joint strengthened with steel fibres under cyclic loads. The results of the tests showed that using steel fibres in the joint improved the abrasion resistance, the ductility without adding transverse reinforcement

(Figure 2-21), and the durability by resisting freeze and thaw reactions and weight loss during abrasion test.

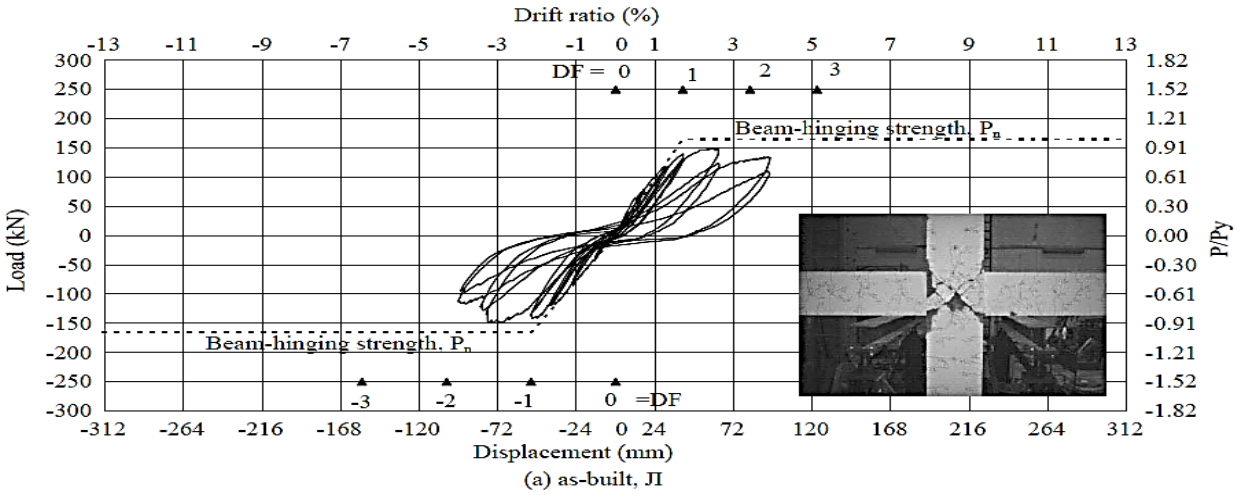

Figure 2-21: Hysteresis loop of BCJs [30]

Gencoglu et al. [31] investigated the behavior of reinforced concrete exterior beam column joint. The experiment was conducted on four specimens, the first specimen was cast using plain concrete which was reinforced according to Turkish Earthquake Code, the second one was with transverse reinforcement inside the joint region, the third one was made from steel fibre reinforced concrete and only one stirrup was placed in the joint region, and the fourth one was cast using plain concrete with steel fibre but without any transverse reinforcement inside the joint (Figure 2-22). The results showed that steel fibre can be used to improve the ductility and minimize the number of transverse reinforcement.

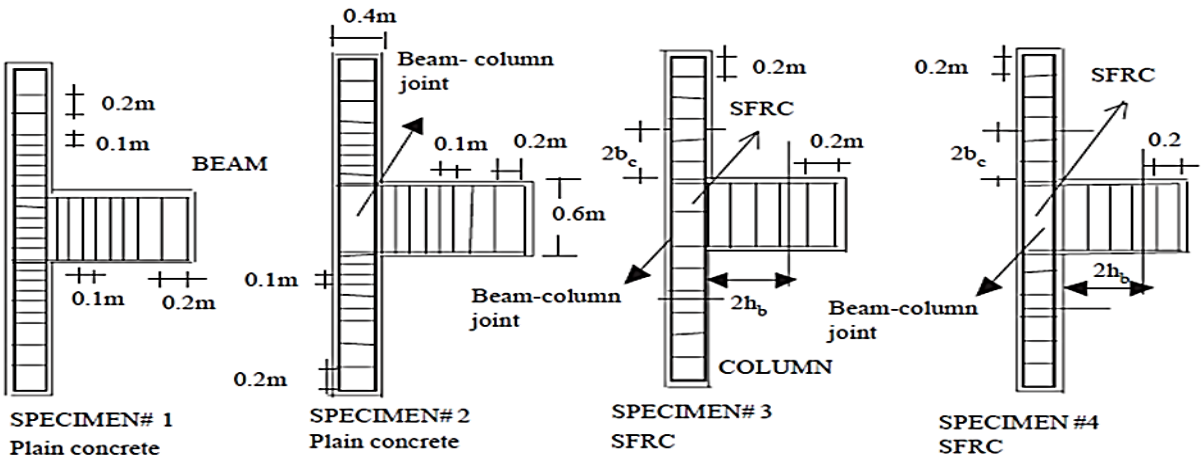

Figure 2-22: Dimensions and reinforcement of the test specimens [31]

Rohm et al. [32] studied the behavior of the reinforced concrete beam-column joint under cyclic loading. The study was conducted on specimens designed according to the Indian code and other specimens strengthened with steel fibre reinforced concrete in the joint area. The results showed that the presence of steel fibre in the joint shifted the cracks from the joint to the beam.

Keerthana et al. [33] investigated the behavior of hybrid fibre reinforced concrete beam-column joints under cyclic loading. Crimped hook end steel fibre with different aspect ratios and volume fractions was applied in the joint. The results showed that, the strength, stiffness, and energy dissipation for the beam column joint specimens which were strengthened with hybrid steel fibre reinforced concrete were improved.

2.4 Reinforced Concrete Beam-Column Joint Strengthened with UHPC

Ha et al. [34] studied the performance of high strength reinforced concrete beam column joint under cyclic loads. The experiment was conducted on five specimens of high ductile fibre reinforced exterior beam column joint with and without transverse reinforcement Table 2-3. The load carrying capacity and the energy dissipation capacity of the specimens with high strength mortar in the joint region were higher than the other specimens (Figure2-23).

Table 2-3: Design parameters of test specimen [34]

Specimen	Main objectives and design parameters
BCJC	*Evaluation of structural performance ACI Building Code 318M-08 and ACI-ASCE 352 Recommendation
BCJNS	*Evaluation of structural performance ACI Building Code 318M-08 and ACI-ASCE 352 Recommendation *No shear reinforcement within joint region
BCJNS*$P_{1.0}$	*No shear reinforcement within joint region *PVA 1.0% content of joint region
BCJNS*$P_{1.5}$	*No shear reinforcement within joint region *PVA 1.5% content of joint region
BCJNS*P_2	*No shear reinforcement within joint region *PVA 2.0% content of joint region
Note) B : Beam, C : Column, J : Joint, S* : Shear reinforcement, P : PVA	

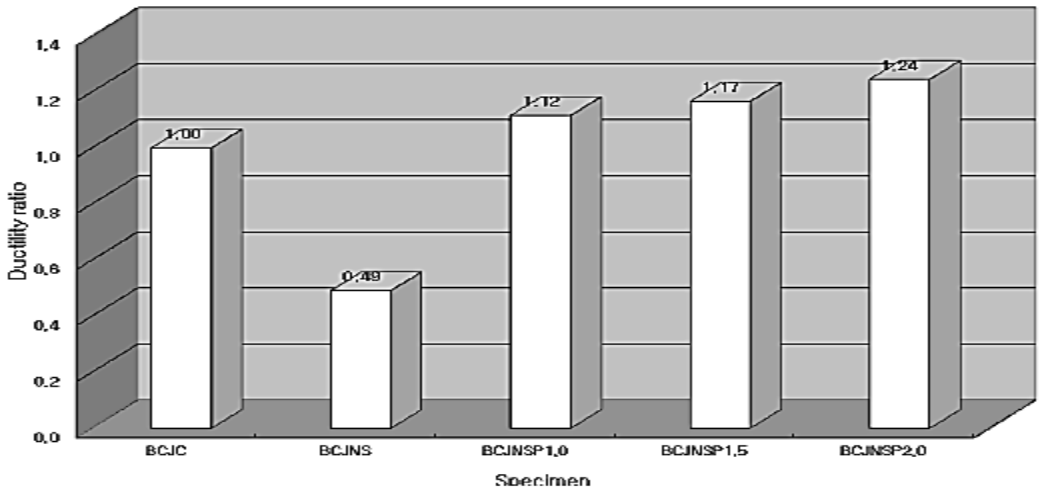

Figure2-23: Cumulative energy dissipation capacity for several specimens [34]

2.5 Previous FEM Simulation of Beam-Column Joint

Ahmed et al. [17] modeled low strength reinforced concrete exterior beam column joints. The joints were tested experimentally in Istanbul Technical University Ilki et al. [35]. DYANA software was used to model the joints. Drucker-Prager model was used in the analytical investigation. The joint cracks obtained in the experimental test were closely similar to that obtained analytically. The experimental results of the cyclic load test were closely matched with DYANA results. Ahmed further extended this work to modeling of normal strength beam-column connections, focusing on shear deficient joints.

Mostofinejad et al. [36] created a model of reinforced concrete BCJ retrofitted with FRP over lays using ANSYS software. They studied the effect of slipping and extending the anchorage steel. The numerical results were closely matched with experimental results. Ravi et al. [37] modeled three models of reinforced concrete BCJs. One joint has seismic detailing, and the other two specimens were without seismic detailing, one of them was

retrofitted with CFRP. Sagbas et al. [38] predicted the failure mode of exterior and interior BCJs under cyclic loading. They created models using FEM Vec Tor2.

Mitra et al. [39] modeled two interior beam-column joints using DYANA software. They studied the load deflection response and compression stress distribution. Kaya et al. [40] investigated the behavior of precast BCJ experimentally and analytically by creating nonlinear 3D model using ANSYS software. The results showed that the initial stiffness of the ANSYS model was lower than that in the experimental model.

CHAPTER 3

THEORETICAL PRELIMINARIES

3.1 Shear Strength Requirements of Exterior BCJ

BCJ in the moment resisting frame structure is the intersection between beam and column. It is used to transfer bending moments and shear forces from the beam and axial load and shear forces from the column as shown in Figure 3-1, where N is the axial load applied on the column, V is the beam shear force, τ_v is the resulting shear stress, and σ_N is the axial stress.

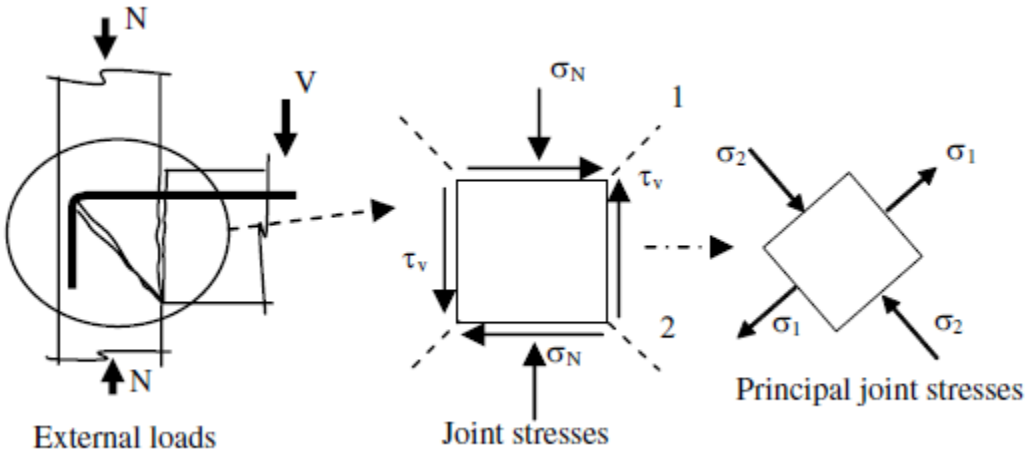

Figure 3-1: BCJ external loads, stresses in the joint intersection, and principal joint intersection stresses [35]

The principal joint stresses can be evaluated as:

$$\sigma_{1,2} = \frac{\sigma_x + \sigma_y}{2} \pm \sqrt{\left(\frac{\sigma_x - \sigma_y}{2}\right)^2 + \tau^2_{xy}} \qquad [3.1]$$

where:

σ_N = column axial stress.

σ_y = stress in the beam longitudinal direction.

τ_{xy} = shear stress.

So equation [3.1] can be written as

$$\sigma_{1,2} = \frac{\sigma_N}{2} \pm \sqrt{\left(\frac{\sigma_N}{2}\right)^2 + \tau_v^2} \qquad [3.2]$$

where:

σ_N = axial stress on the column which is equal to $\frac{N}{Ag}$ (negative when N compression)

τ_v = horizontal shear stress.

A_g = The gross sectional area of the column.

So τ_v can be written as:

$$\tau_v = \sigma_1 \sqrt{1 - \frac{\sigma_N}{\sigma_1}} \qquad [3.3]$$

From the splitting tensile test, concrete tensile strength can be measured and expressed as a function of $\sqrt{f'c}$ [(ACI)-ASCE Committee 326 1962], so, the tensile strength of the concrete can be expressed as $f_{ct} = c\sqrt{f'c}$ where c is a constant [0.5 value of c is recommended by ACI (2008a) when $f'c$ is measured by MPa]. Since there is no transverse reinforcement in the joint, the joint shear capacity depends only on the concrete shear capacity, so equation [3.3] can be written as:

$$\tau_{vc} = 0.5\sqrt{f'_c}\sqrt{\left(1 - \frac{N}{0.5\sqrt{f'_c}A_g}\right)} \qquad [3.4]$$

If the tensile principal stresses exceeded the tensile strength in the concrete the cracks will be developed in the joint Figure 3-2.

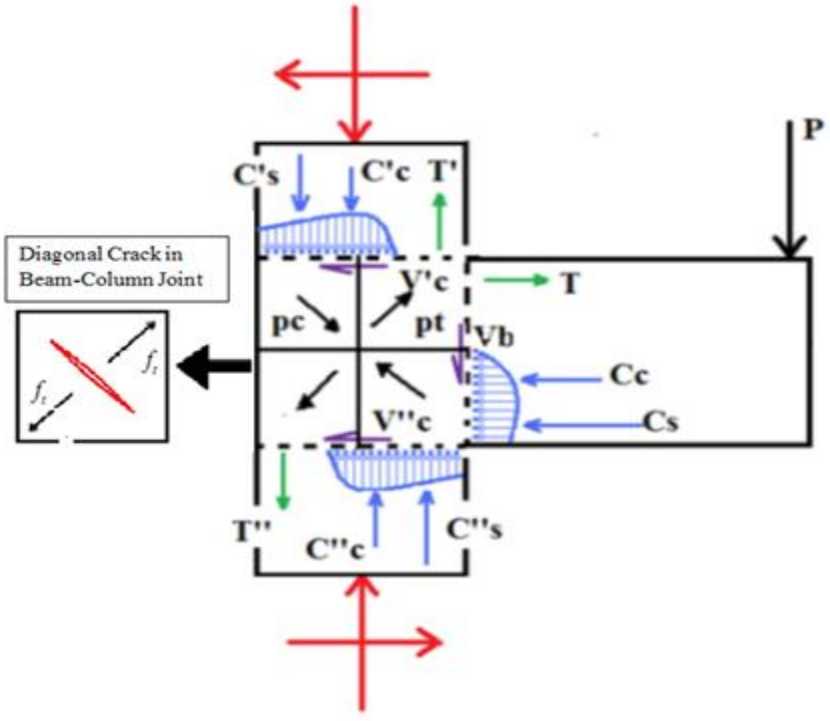

Figure 3-2: Shear crack in BCJ

3.2 Theoretical Shear Strength of SFRC-BCJ

The theoretical shear strength of SFRC-S-BCJ includes three components: shear strength of plain concrete, shear strength resisted with transverse reinforcement, and shear strength of steel fibre. Joint shear strength can be expressed as:

$$V_j = V_{con} + V_{fib} + V_s \quad [3.5]$$

where:

$$V_c \text{ (shear strength resisted by concrete)} = 0.1\ (1 + \frac{N}{bc+hc+fc})\ b_j\ h_j\ hc \quad [3.6]$$

$$V_s \text{ (shear strength resisted by stirrups)} = \frac{(Ash)\ (fyt)\ d}{S} \quad [3.7]$$

$$V_{fib} \text{ (shear strength resisted by steel fibre)} = 2\ \frac{Lf}{df}\ V_f \quad [41] \quad [3.8]$$

N = axial compressive load of column.

A_{sh} = area of transverse reinforcement within distance S.

bc = column width.

hc = column depth.

bj = joint effective width.

fc = axial compressive strength of concrete

d = beam steel bars diameter.

df = steel fibre diameter.

L_f = length of steel fibre

hj = effective depth of joint in the direction of shear.

V_f = volume fraction of fibres.

3.3 Failure Mode for Exterior BCJ

Pampanin et al [19] mentioned in his study that the poor reinforcement detailing can result in weak-column / strong-beam system. That develops soft story mechanism, causing global failure of the structure. The following shortcomings are stated by Pampanin et al [19]:

- Lack of shear reinforcement in the joint area.
- Inadequate column longitudinal reinforcement when taking into account seismic lateral forces.
- Insufficient anchorage detailing for longitudinal and transverse reinforcement.
- Lower quality of materials. e.g. joints were built from low strength concrete with smooth bars reinforcement.

During an earthquake, such joints suffer a large interaction of shear cracking and then formation of the shear hinges. To improve the ductility of the joint, different material with high tensile strength should be combined with the concrete in the joint area. This goal can be achieved by using high strength concrete, carbon fibre reinforced polymer (CFRP), shape memory alloy, and many other materials. That combination will improve

the capacity and the ductility of the joint, and also changing the system to strong column / weak beam.

CHAPTER 4

EXPERIMENTAL INVESTIGATIONS

4.1 Introduction

Several experimental tests were conducted in this research, which were:

1- Mechanical properties tests of NC (uniaxial compression and tension tests).

2- Mechanical properties tests of UHPC (uniaxial compression and tension tests).

3- Mechanical properties tests of SFC (uniaxial compression and tension tests).

4- Steel tensile test.

5- Full-scale BCJ test under monotonic and cyclic loading.

4.2 Mechanical Properties of Normal Concrete (NC)

The normal concrete which was used in casting the specimen of beam-column joint has required strength of 30 MPa with 110 mm slump and 25 mm maximum aggregate size. Many cylinders were cast at KFUPM lab and in Saudi ready mix company in Dammam. The cylinders were tested under compression and tensile loading.

4.2.1 Concrete Compressive Strength (NC)

Three normal concrete cylinders were tested under compression load (Figure 4-1). Two cross concrete strain gauges were fixed on the surface of the concrete cylinder to measure the concrete strain. The cylinders were loaded with a suitable load rate. The data logger was used to monitor and record the strain with different load values. The stress-strain curve was plotted (Figure 4-2). The compressive strength was 34 MPa and the elastic modulus was 29000 MPa. From the slump test the concrete slump was 110 mm (Figure 4-3). Loading and unloading test was conducted on cylinders under compression load to get the compression damage parameters which are used in the modeling part using ABAQUS code.

Figure 4-1: Cylinder test for normal concrete compressive strength

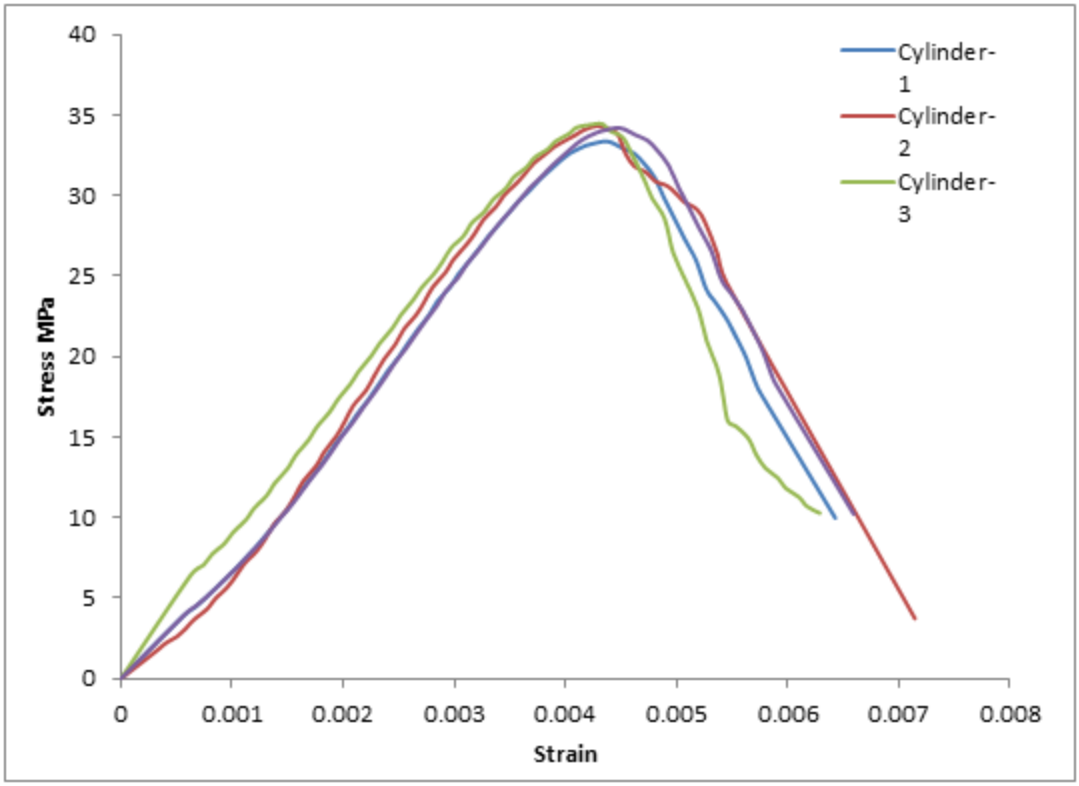

Figure 4-2: Normal concreter stress-strain response under compression

Figure 4-3: Slump test for fresh concrete

4.2.2 Concrete Tensile Test

Split tensile test was conducted on three concrete cylinders to find indirectly the tensile strength of normal concrete. ASTM-D3967 and C496 cover testing apparatus, specimen preparation, and testing procedure for finding the splitting tensile strength (Figure 4-4). From the results of the split tensile test the average split tensile strength was calculated using equation [4.1]. The average tensile strength of the normal concrete was 2.2 MPa.

$$f_t = \frac{2P}{\pi l d} \qquad [4.1]$$

Where:

P: applied load (39.4 kN)

L: length of cylinder (150 mm)

D: diameter of specimen (75 mm)

f_t: split tensile strength.

Figure 4-4: Concrete specimen under split test.

4.3 Mechanical Properties of Steel Fibre Concrete (SFC)

SFC was used in casting the intersection area of beam-column joint specimens. Table 4-1 shows SFC mix design. The SFC cylinders and Dog Bone specimens were cast in Saudi ready mix company in Dammam. The Compressive test and splitting tensile test were conducted on the cylinders with dimensions of 75mm diameters and 150 mm depth, while the dog bone specimen was used in the direct tension test.

Table 4-1: SFC concrete mix proportions

Cement (Kg)	500
Water (Liter)	165
Coarse Aggregate (Kg)	925
Fine aggregate (Kg)	775
Super plasticizer (Liter)	3
Smooth steel fibre (% by weight of the total mix)	1.5
Hooked end steel fibre (% by weight of the total mix)	1.5

4.3.1 SFC Compressive Strength

The compressive strength was conducted on SFC cylinders with 75 mm diameter and 150 mm depth according to ASTM C39. The compressive strength test was conducted on three cylinders (Figure 4-5). The strain gauges were attached on the surface of the cylinders to measure the concrete strain. The load and the strain readings were recorded by using data logger. The average compressive strength was 53 MPa (Figure 4-6).

Figure 4-5: Cylinder test for steel fibre concrete compressive strength

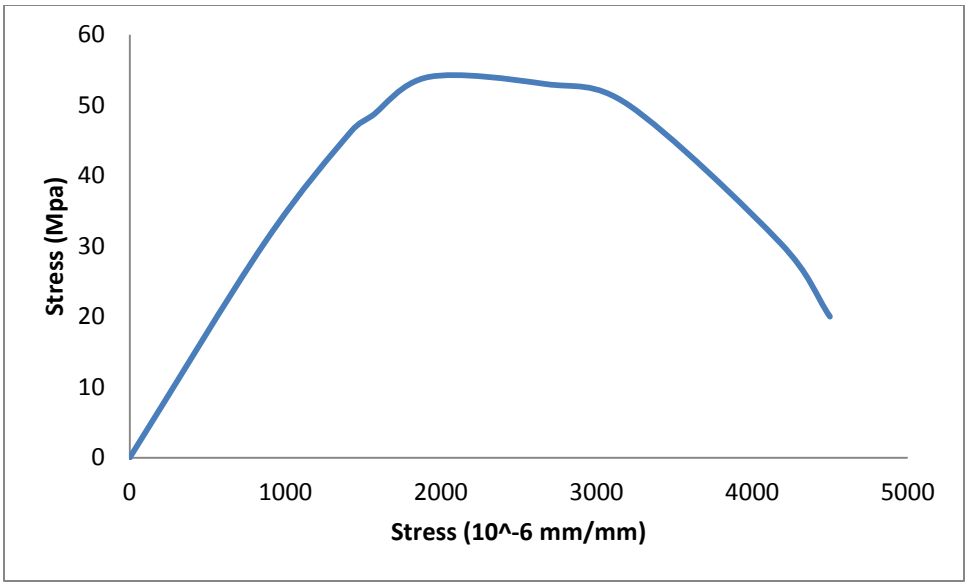

Figure 4-6: Steel fibre concrete stress-strain response under compression

4.3.2 Splitting Tensile Strength of SFC

Splitting tensile strength was used to determine the tensile strength of SFC indirectly according to ASTM C496. Three SFC cylinders were tested by compressive testing machine (Figure 4-7). The average splitting tensile strength was 3.85 MPa. Due to the presence of steel fibre the cylinder did not split into two parts.

Figure 4-7: Steel fibre concrete specimen under split test.

4.3.3 SFC Direct Tensile Test

SFC dog bone specimen with dimensions of 37 mm ×40 mm ×490 mm was tested under direct tension using an Instorn testing machine with capacity of 250 KN (Figure 4-8). The data logger was used to record load and strain readings during the test. The direct tension test was 1.85 MPa (Figure 4-9). CFRP was used in wrapping the top and bottom parts of the specimen to prevent any failure near the grips.

Figure 4-8: Dog bone specimen under direct tension test

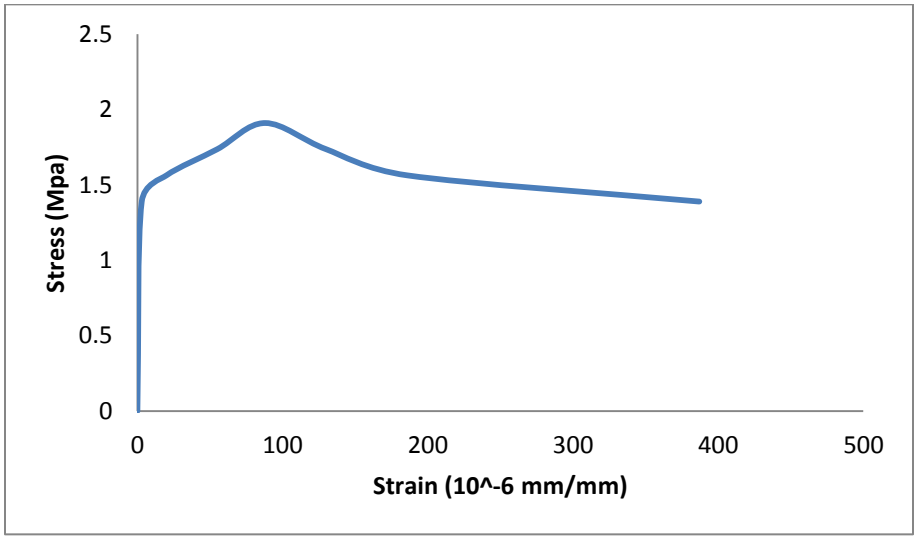

Figure 4-9: Concreter stress-strain response under tension

4.4 Mechanical Properties of UHPC

UHPC was used in casting the intersection area of two beam-column joint specimens. Table 4-2 shows UHPC mix design. The UHPC cylinders and Dog Bone specimens were cast in KFUPM lab. The Compressive test and splitting tensile test were conducted on the cylinders with dimensions of 75mm diameters and 150 mm depth, while the dog bone specimen was used in the direct tension test.

Table 4-2: UHPC concrete mix proportions

Cement (Kg)	900
Water (Liter)	190
Fine Materials (Kg)	1143.94
Super plasticizer (Kg)	44.8
Smooth steel fibre (% by weight of the total mix)	3%
Hooked end steel fibre (% by weight of the total mix)	3%

4.4.1 UHPC Compressive Strength

The compressive strength was performed on UHPC cylinders according to ASTM C39. Three cylinders were tested under compression load (Figure 4-10). Strain of the concrete was monitored through the strain gauges which were connected with a data logger. The

load and the strain readings were got from the data logger. The average compressive stress was 108 MPa (Figure 4-11).

Figure 4-10: Cylinder test for UHPC compressive strength

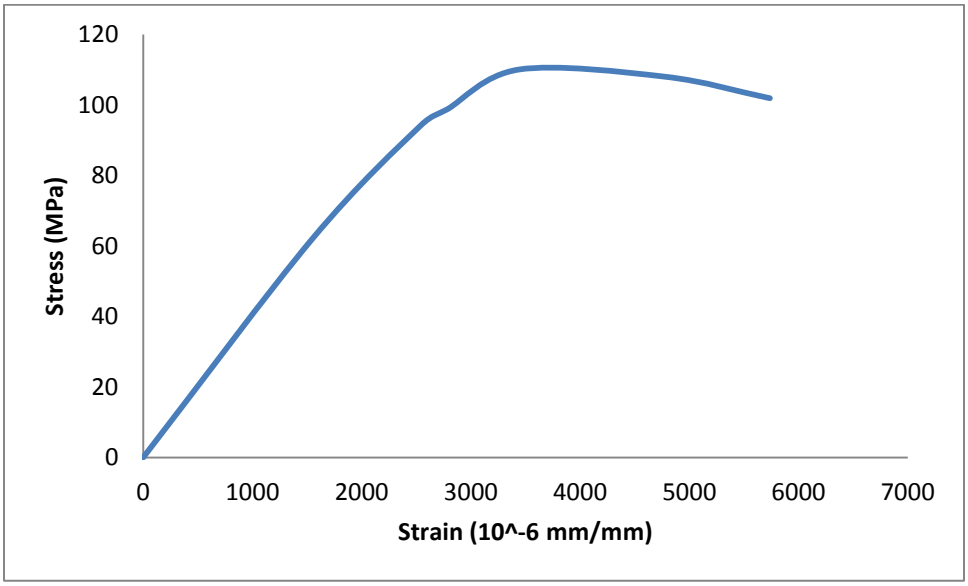

Figure 4-11: UHPC stress-strain response under compression

4.4.2 UHPC Splitting Tensile Strength

Splitting tensile strength was used to determine the tensile strength of UHPC indirectly according to ASTM C496. Three UHPC cylinders were tested by compressive testing machine (Figure 4-12). The average splitting tensile strength was 7.36 MPa. Due to the presence of steel fibre the cylinder did not split into two parts.

Figure 4-12: UHPC specimen under split test.

4.4.3 UHPC Direct Tension Test

UHPC dog bone specimen with dimensions of 37mm × 40 mm× 490 mm was tested under direct tension using an Instorn testing machine with capacity of 250 KN (Figure 4-13). The load and strain readings were recorded using data logger. CFRP was used in wrapping the top and bottom specimen to prevent any failure near the grips.

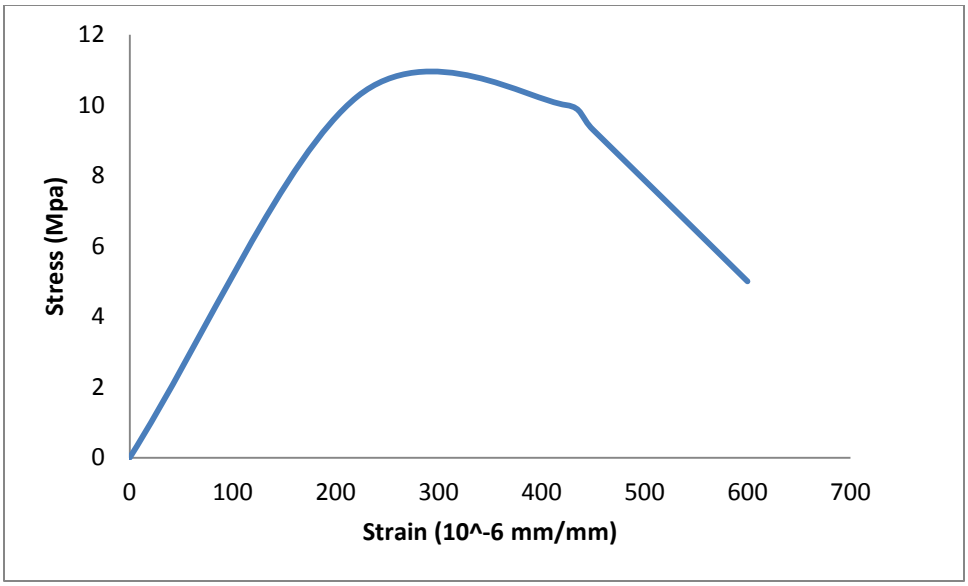

Figure 4-13: UHPC stress-strain response under tension

4.5 Steel Tensile Strength

The diameter of longitudinal steel bars which were used in reinforcing the specimens of BCJ were 12 mm and 18 mm while the diameter of transverse reinforcement of all specimens was 8 mm. The actual tensile strengths of the steel bars were determined by conducting a tensile test. Table 4-3 shows the properties of steel reinforcement and Figure 4-14 shows the steel stress-strain curve. The stress-plastic strain was used in the modeling (Figure 4-15).

Table 4-3: Yielding strength of steel reinforcement

Reinforcements	Diameter (mm)	Fy (MPa)
Φ8	8	480
Φ12	12	610

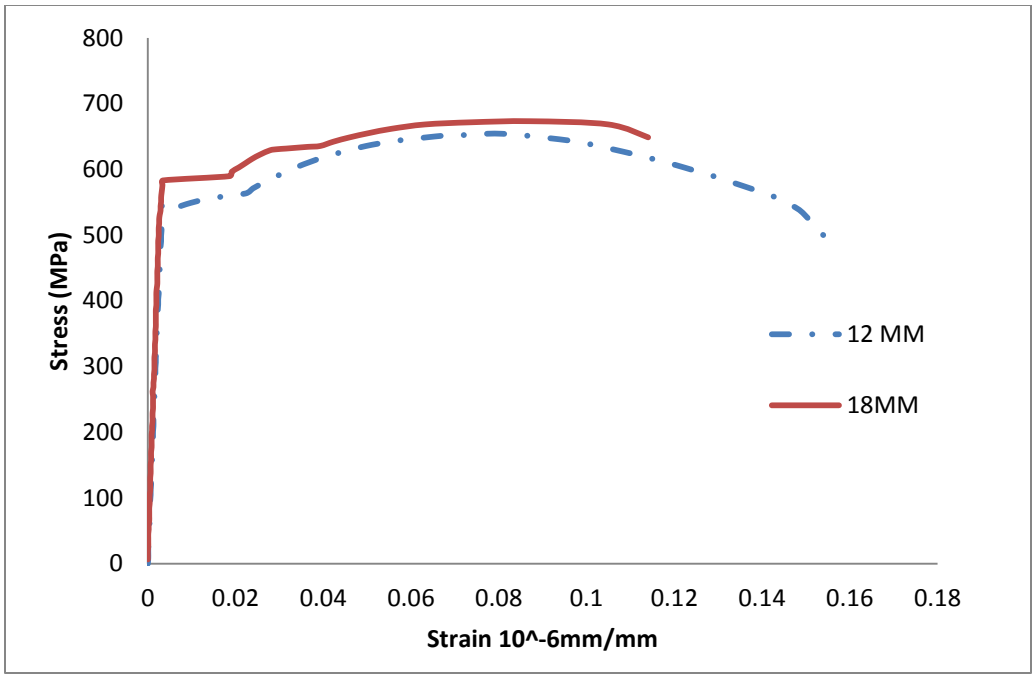

Figure 4-14: Stress-Strain response for 18 mm and 12 mm steel bars

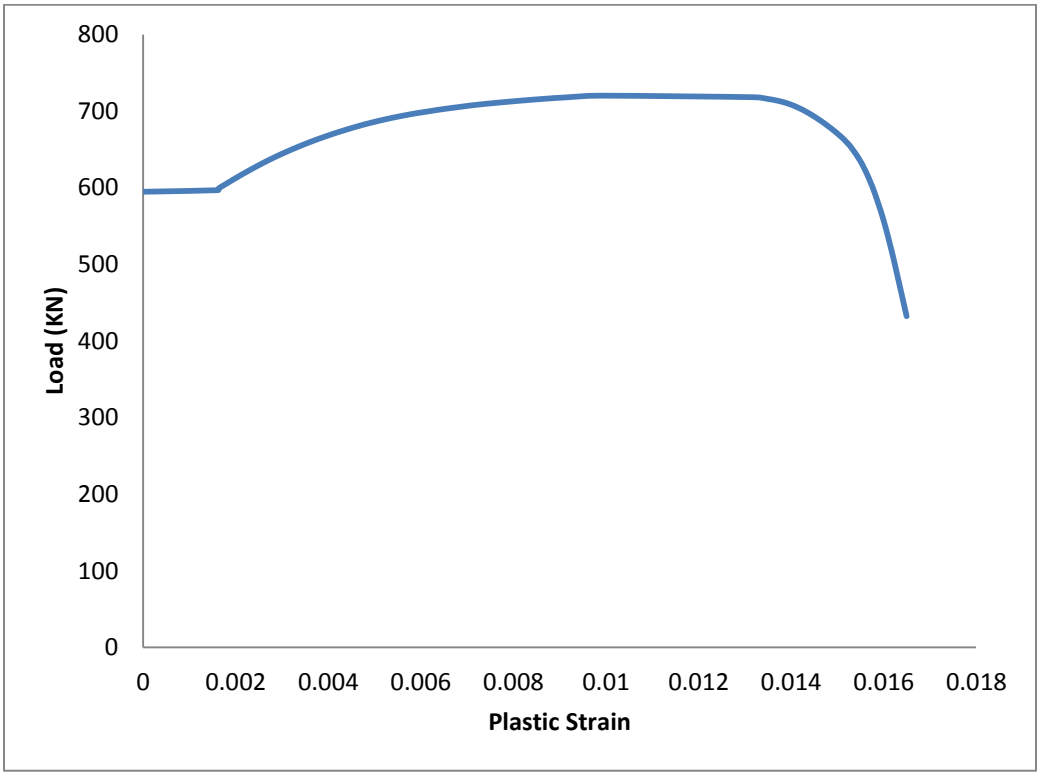

Figure 4-15: Stress-Plastic strain for steel

4.6 Steel Fibre

Steel fibre was used to enhance the concrete tensile strength. Two types of steel fibre were used in preparing SFC and UHPC (Figure 4-16), brass coated micro steel fibre with length of 13 mm and diameter of 0.2 mm and with aspect ratio of 65, and brass coated hooked ends steel fibre with length of 25 mm and diameter of 0.35 mm and with aspect ratio of 71.43. The tensile strength of the two types was 2500 MPa.

Figure 4-16: Brass coated steel fibre

4.7 Test Setup and Preparation

In order to investigate the behavior of exterior RCBCJ strengthened with high strength concrete, experimental test was conducted on sixteen BCJ specimens. The key parameters of the study were the reinforcement detailing and the type of high strength

concrete. Table 4-4 and 4-5 Show the difference and details of all specimens for the monotonic and cyclic tests.

Table 4-4: Specimens details for monotonic test

S.No.	No. of Specimens	Specimens	Details	Test Method
1	1	NC-BCJ-12MM	Control sample reinforced with normal steel Φ12 and no stirrups in the joint region	Monotonic
2	1	NC-BCJ-18MM	Control sample reinforced with normal steel Φ18 and no stirrups in the joint region	Monotonic
3	1	NC-BCJ-S-18MM	Control sample reinforced with normal steel Φ18 and stirrups in the joint region	Monotonic
4	1	SFRC-BCJ-12MM	Sample reinforced with normal steel Ø12, SFRC joint and no stirrups in the joint region	Monotonic
5	1	SFRC-BCJ-S-12MM	Sample reinforced with normal steel Ø12, SFRC joint and stirrups in the joint region	Monotonic
6	1	SFRC-BCJ-18MM	Sample reinforced with normal steel Ø18, SFRC joint and no stirrups in the joint region	Monotonic
7	1	SFRC-BCJ-S-18MM	Sample reinforced with normal steel Ø18, SFRC joint and stirrups in the joint region	Monotonic
8	1	UHPC-BCJ-18MM	Sample reinforced with normal steel Ø18, UHPC joint and no stirrups in the joint region	Monotonic

Table 4-5: Specimens details for cyclic test

S.No.	No. of Specimens	Specimens	Details	Test Method
1	1	NC-BCJ-12MM	Control sample reinforced with normal steel Φ12 and no stirrups in the joint region	Cyclic
2	1	NC-BCJ-18MM	Control sample reinforced with normal steel Φ18 and no stirrups in the joint region	Cyclic
3	1	NC-BCJ-S-18MM	Control sample reinforced with normal steel Φ18 and stirrups in the joint region	Cyclic
4	1	SFRC-BCJ-12MM	Sample reinforced with normal steel Ø12, SFRC joint and no stirrups in the joint region	Cyclic
5	1	SFRC-BCJ-S-12MM	Sample reinforced with normal steel Ø12, SFRC joint and stirrups in the joint region	Cyclic
6	1	SFRC-BCJ-18MM	Sample reinforced with normal steel Ø18, SFRC joint and no stirrups in the joint region	Cyclic
7	1	SFRC-BCJ-S-18MM	Sample reinforced with normal steel Ø18, SFRC joint and stirrups in the joint region	Cyclic
8	1	UHPC-BCJ-18MM	Sample reinforced with normal steel Ø18, UHPC joint and no stirrups in the joint region	Cyclic

4.8 Specimen Detailing

The cross section for beams and column was 250 mm× 300 mm, the column height was 1400 mm and the beam length was 900 mm [17]. The geometry of the BCJ specimens was chosen to fit with the existing testing frame (Figure 4-17).

Figure 4-17: BCJ testing frame at KFUPM lab

BCJ-12MM specimen reinforced with 12 mm steel bars. The beam reinforcement was three 12 mm steel bars for both top and bottom, with 8 mm closed stirrups at spacing of 75 mm. The longitudinal reinforcement of the column was 12 mm bars with 8 mm closed stirrups at spacing of 75 mm (Figure 4-18). BCJ-S-12MM specimen was reinforced with same reinforcement of BCJ-12MM specimens but with additional transverse reinforcement in the intersection area (Figure 4-19). BCJ-18MM specimen reinforced with 18mm bars as a flexural reinforcement in both beam and column with 8 mm close

stirrups at spacing of 75 mm (Figure 4-20). BCJ-S-18MM specimen was reinforced with same BCJ-18MM specimen reinforcement but with additional transverse reinforcement in the intersection area (Figure 4-21).

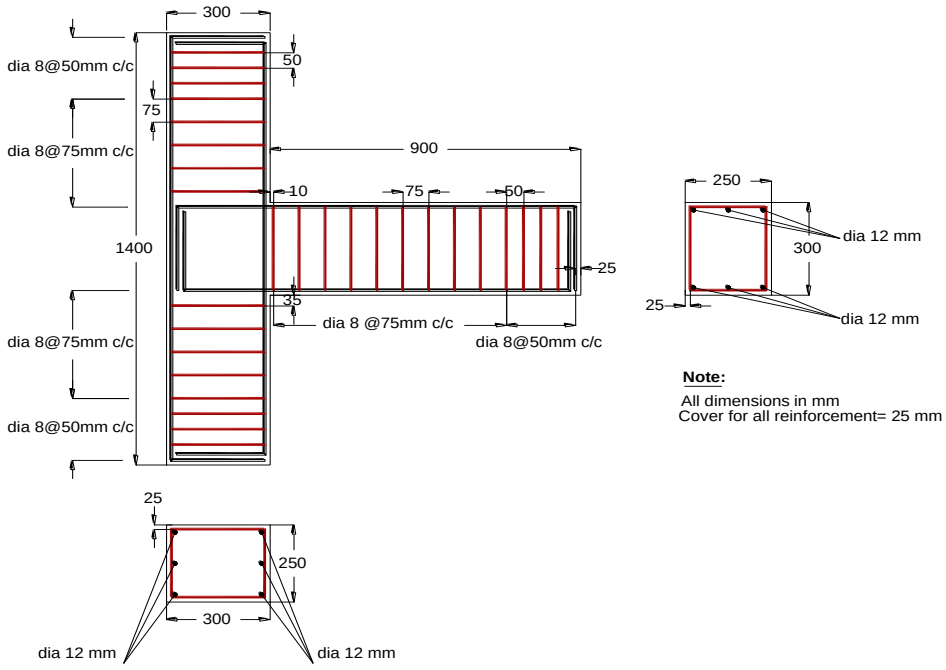

Figure 4-18: BCJ-12 MM specimen reinforcement details and dimensions [17]

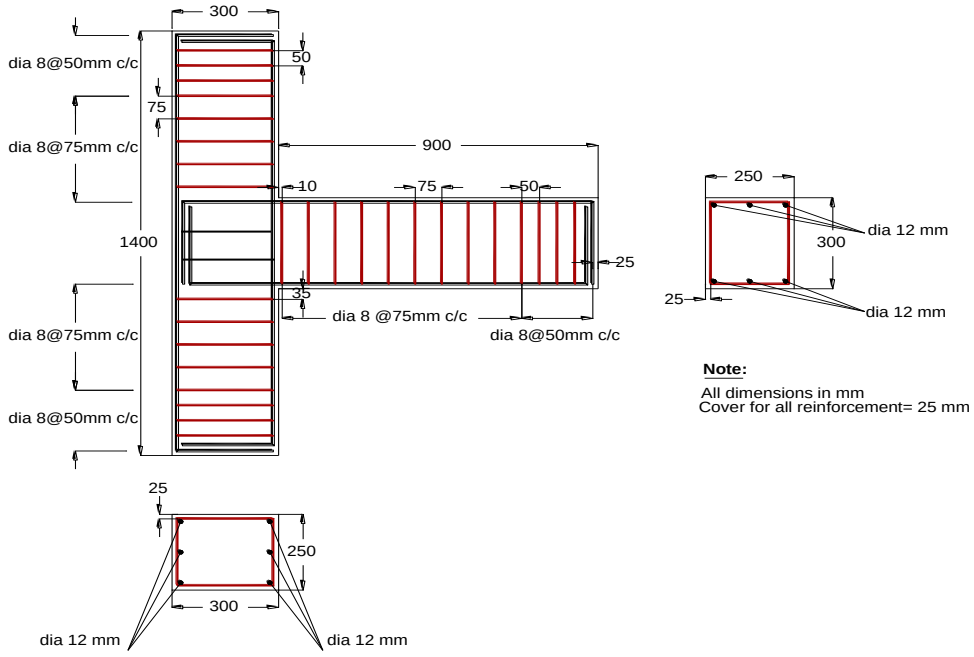

Figure 4-19: BCJ-S-12MM specimen reinforcement details and dimensions

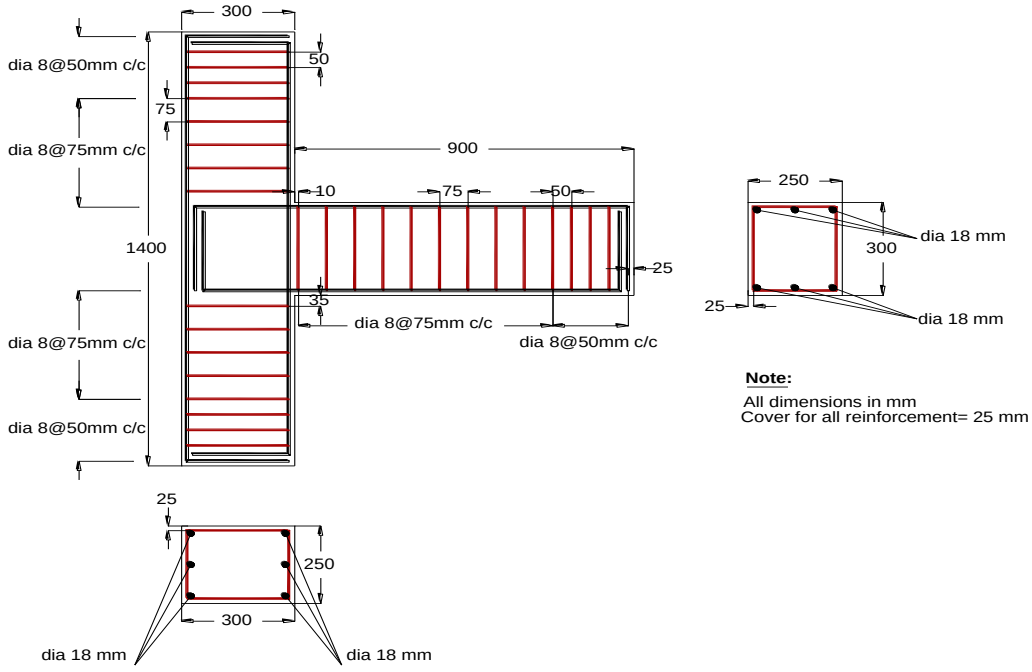

Figure 4-20: BCJ-18 MM specimen reinforcement details and dimensions [17]

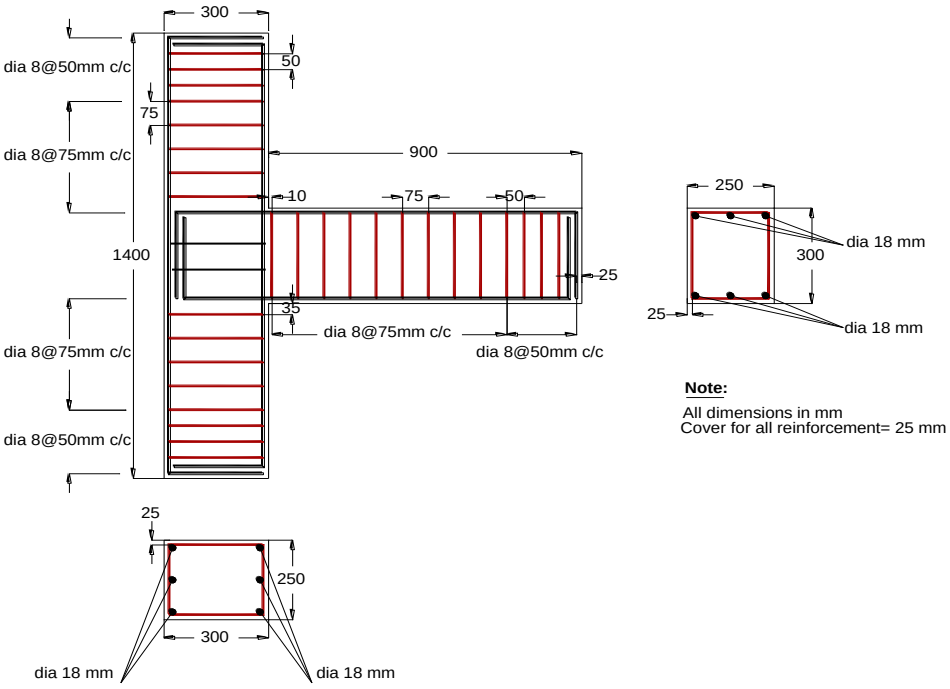

Figure 4-21: BCJ-S-18 MM specimen reinforcement details and dimensions

SFRC-BCJ specimen was cast using steel fibre concrete (SFC) in the intersection area while the rest of the specimen was cast using normal concrete. UHPC-BCJ specimen was cast using UHPC in the intersection area and the rest of specimen was cast using normal concrete (Figure 4-22).

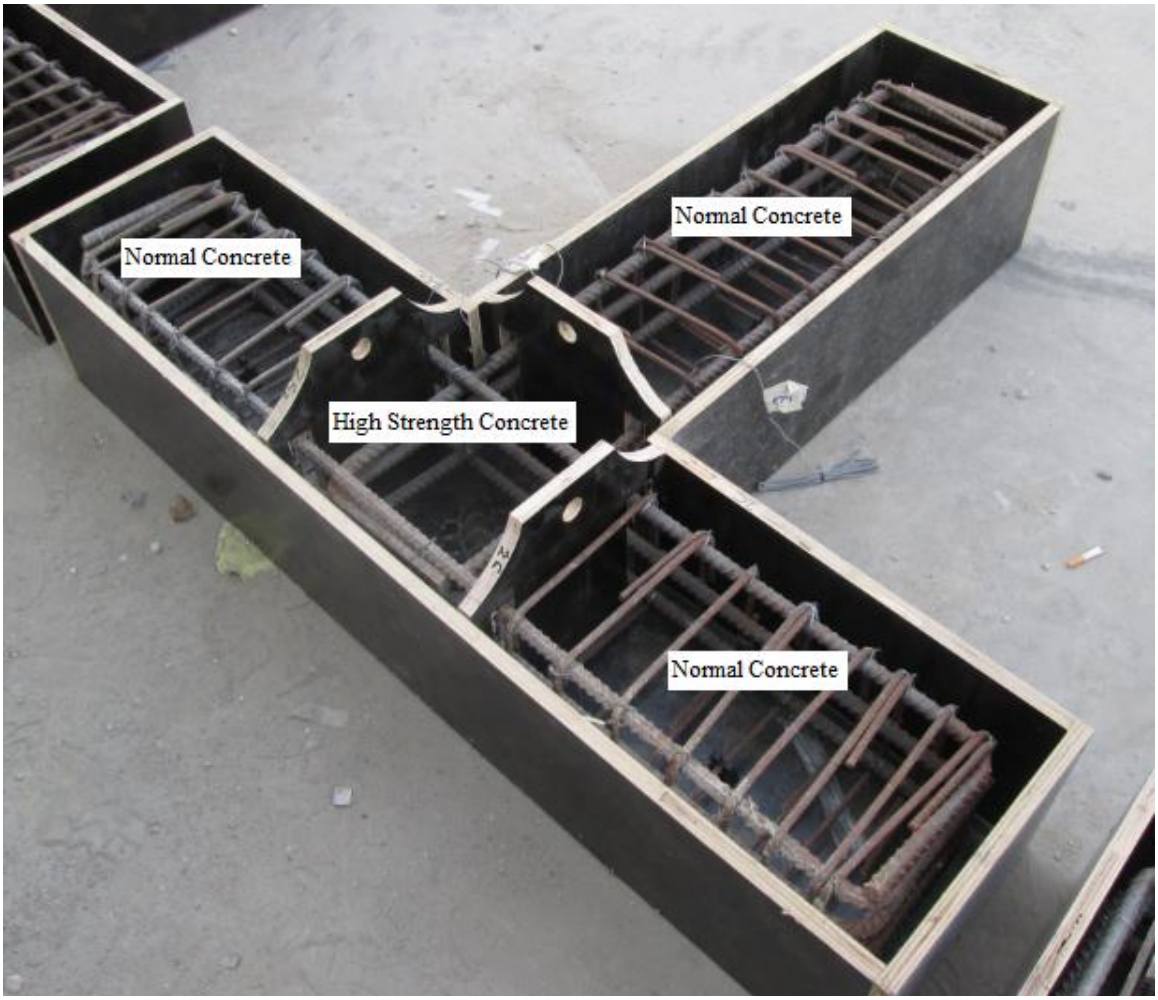

Figure 4-22: High strength concrete joint

4.9 Strain Gauges

Five steel strain gauges were fixed on the steel cage of each BCJ specimen. The locations of the steel gauges were grinded by grinder machine and other tools to make it smooth. By using special type of glue material, the gauges were attached on the reinforcement surfaces (Figure 4-23). Water proof plaster was used to protect the strain gauges during the casting process. The strain gauge resistance was 120 Ω and it was checked with voltmeter. Figure 4-24 represents the location of the steel gauges. Strain gauge numbers

1&2 (SSG# 1&2) were attached on the top reinforcement of the beam, strain gauge number 3 (SSG# 3) was attached on the bottom reinforcement of the beam, Strain gauge number 4 (SSG# 4) was attached on the column reinforcement, and strain gauge number 5 (SSG# 5) was attached on the stirrups just on the beam column interface.

Figure 4-23: Installation of strain gauges and check the voltage reading

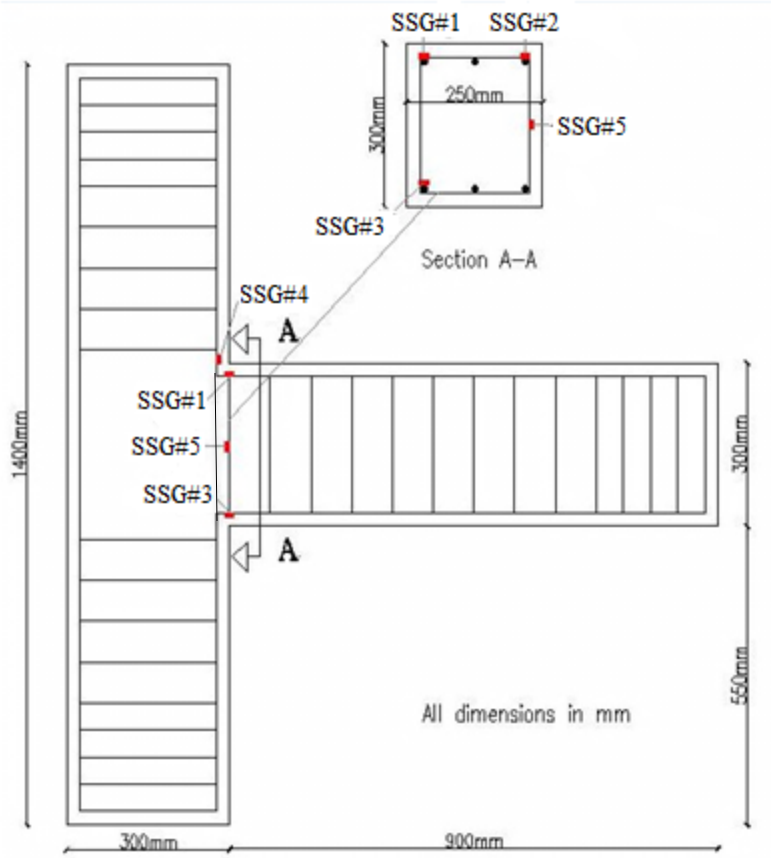

Figure 4-24: Strain gauges locations

4.10 Casting of Beam-Column Joints

Fair face ply wood was used to form the beam-column joint molds. After installing the steel gauges on the reinforcement and isolating them with water proof glue, the steel gages were installed in the molds. The reinforcement cover was adjusted with plastic spacers. The joint area was separated by partitions in order to cast the joint intersection using concrete with steel fibre and the rest of the specimen was cast using normal concrete. The specimens were cast in the concrete research lab of Saudi Ready Mix Company. The joint intersections area were cast first with steel fibre concrete, then the

remaining parts were cast using normal concrete. The partitions were removed before the concrete set. The vibrator was used to consolidate the concrete properly, and to make the two types of concrete behave as one unit. The surface of the concrete was leveled by trowels and steel hooks were installed in the concrete (Figure 4-25). The specimens were cured with wet jute and plastic sheets for 28 days (Figure 4-26).

Figure 4-25: Casting of beam-column joint specimens in Saudi Ready Mix research lab

Figure 4-26: Specimens curing with wet jute

4.11 Testing Set up for the Specimens

Self-reacting steel loading was used in testing the specimens of beam-column joint, with additional supporters to grip the column and to apply the load on the tip of the beam. The load was applied using two hydraulic jacks (Figure 4-27). One hydraulic jack with ultimate capacity of 30 tons was used for applying constant axial load on the top of the column while the other hydraulic jack with capacity of 10 tons was used in applying cyclic loading on the tip of the beam.

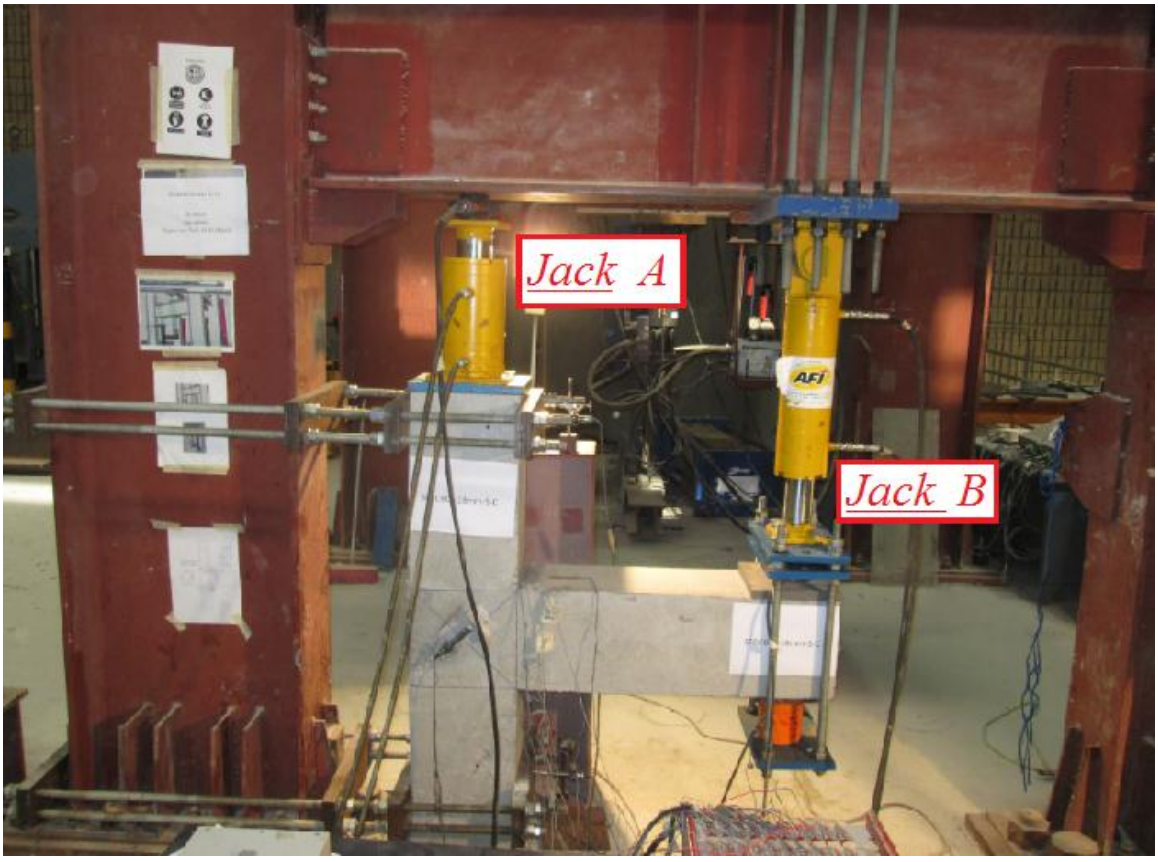

Figure 4-27: Hydraulic jacks

4.6 Instruments for Monotonic Test

Three load cells were used to monitor the load during the test (Figure 4-28). Two Load cells with capacity of 100 ton were fixed at top and bottom of the beam while the other one with capacity of 20 ton was fixed at the top of the column. Four LVDTs where used in the test. Two LVDT's were installed at the top and bottom of the column to monitor any rotations, and two LVDT's were attached at the intersection area to measure the diagonal crack openings. The beam deflection was monitored by string type LVDT. The strain in the concrete was measured by attaching concrete strain gauges on the surface of the concrete (Figure 4-29).

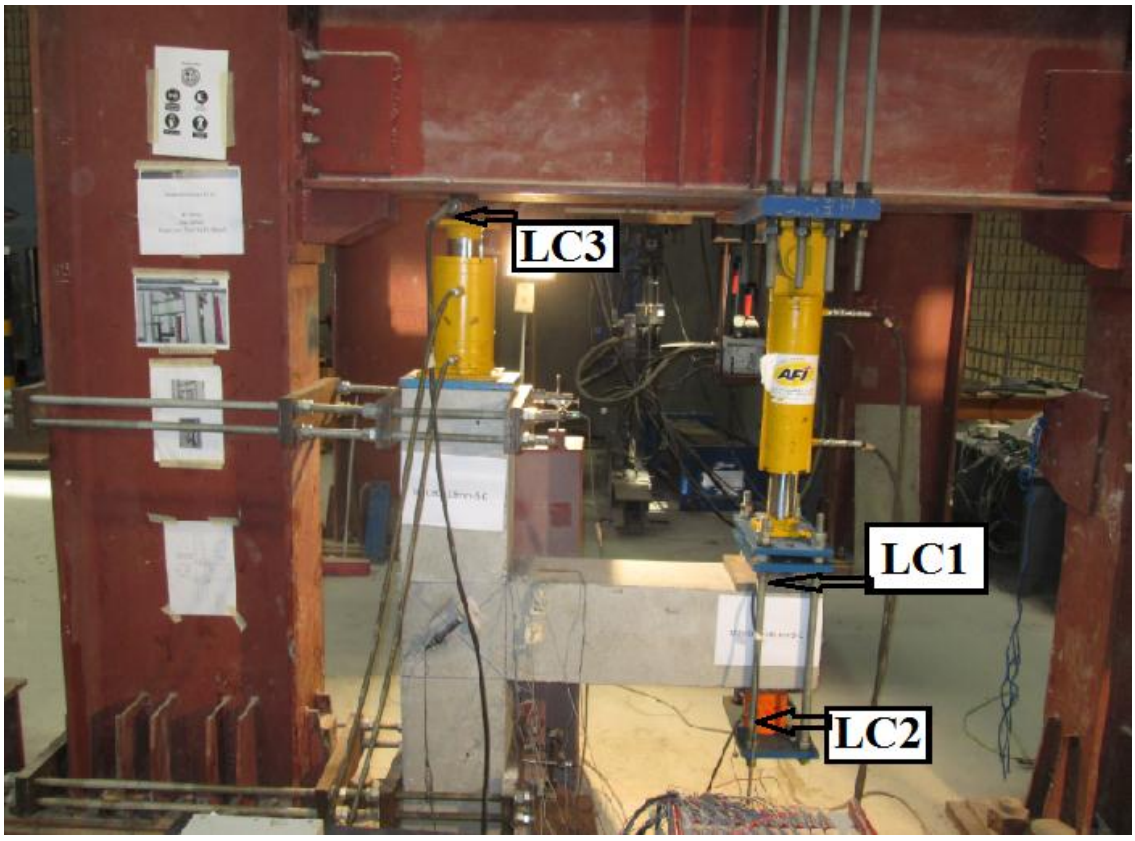

Figure 4-28: Load cells

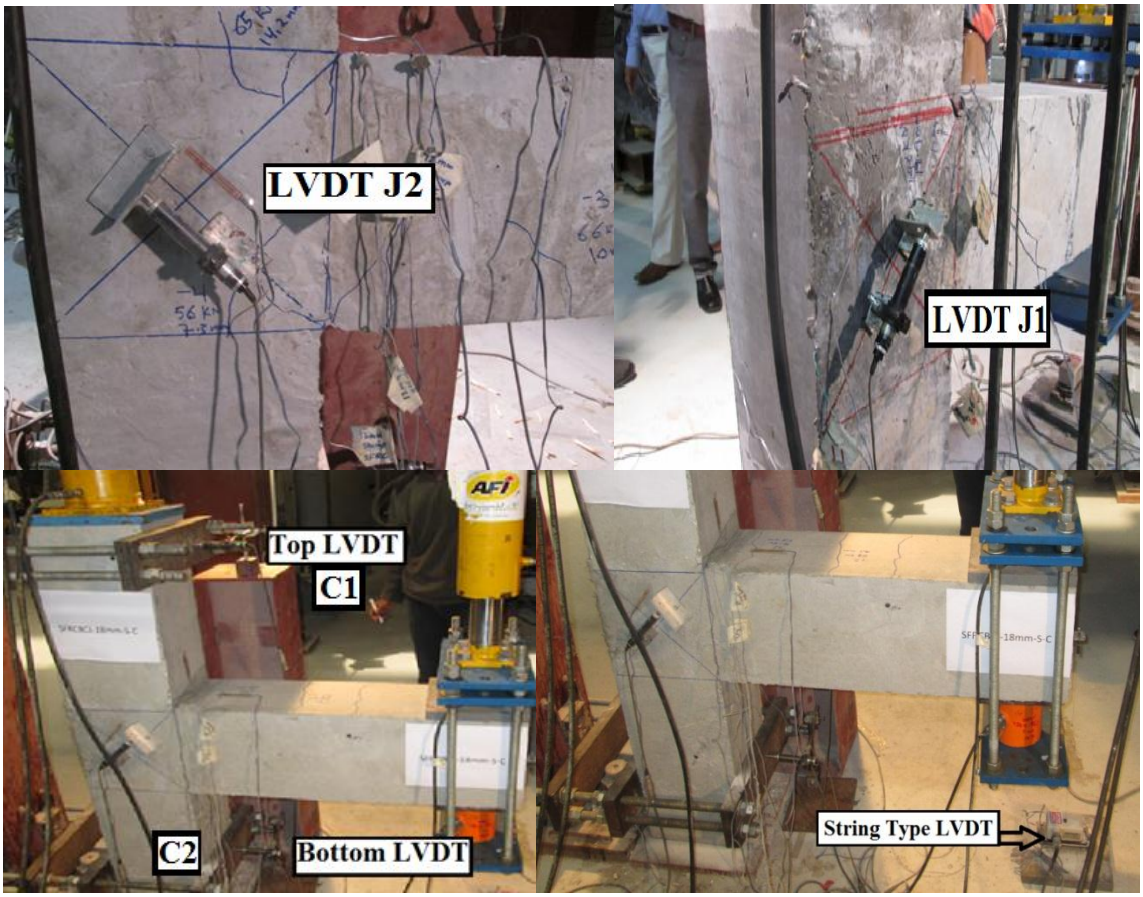

Figure 4-29: LVDT's and strain gauges used in testing specimens of BCJ

4.7 Test Program for the Specimens

Two types of loading were used in testing the specimens of BCJ. A constant axial load with value of 150 KN was applied first on the top of column then an increasing displacement was applied at the tip of the beam on both push and pull sides up to the failure of the specimen. Table 4-6 and Figure 4-30 show the displacement that was applied in every cycle. The specimens were monitored during the test with data logger, marking the cracks, and taking photos. The reading of the load cells, LVDTs, and strain gauges were extracted from the data logger.

Table 4-6: Cyclic load pattern during the test

Cyclic Loading			
No.	**Drift Ratio**	**Push**	**Pull**
	%	**mm**	**mm**
1	0.288%	2.6	-2.6
2	0.6%	5.4	-5.4
3	1.11%	10	-10
4	1.66%	15	-15
5	2.22%	20	-20
6	2.77%	25	-25
7	3.33%	30	-30
8	4.44%	40	-40
9	5.55%	50	-50
10	7.22%	65	-65

Drift Ratio = (Beam Tip Displacement/ Beam Length) × 100

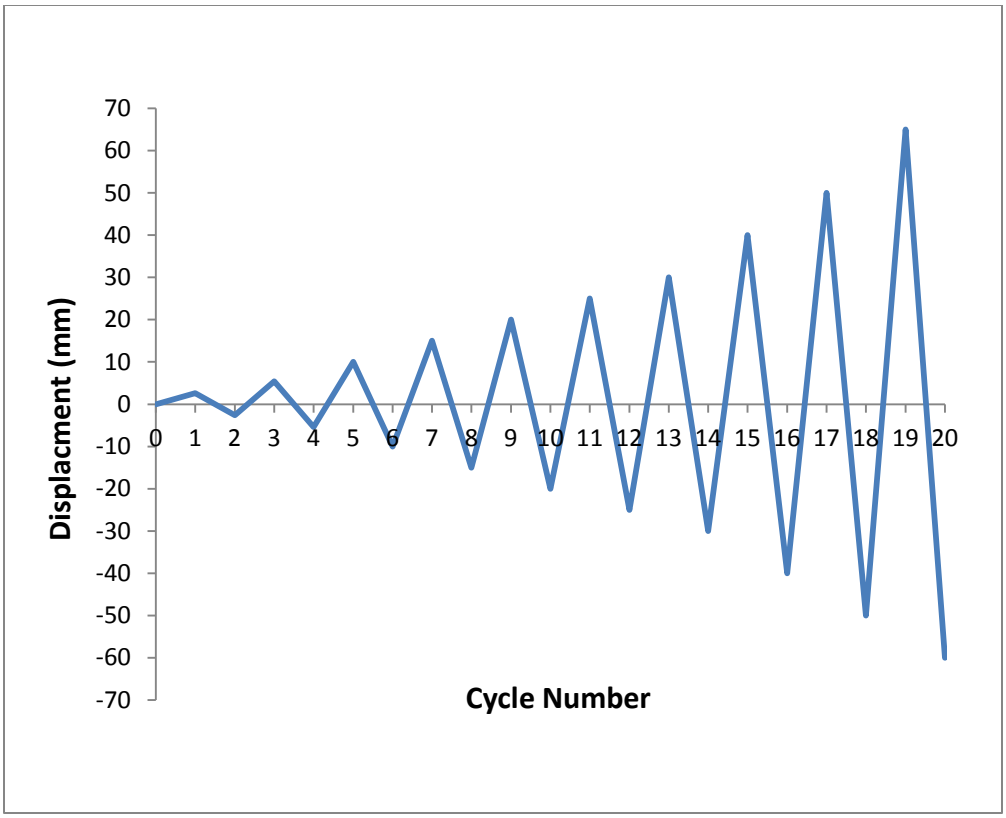

Figure 4-30 : Cyclic load pattern applied during the test

CHAPTER 5

EXPERIMENTAL TEST RESULTS

5.1 Monotonic Test Result for BCJ–12MM

BCJ-12MM specimen reinforced with 12 mm longitudinal steel bars and with 8 mm transverse reinforcement at spacing of 75 mm in both beam and column.

5.1.1 Monotonic Test Result for NC-BCJ–12MM

NC-BCJ–12MM specimen was cast using normal concrete. The load vs. displacement curve shows that the maximum load was 74 KN at displacement of 26.8 mm (Figure 5-1). At load of 24 KN and displacement of 2.2 mm the first flexural crack was formed adjacent to the beam-column interface, while the first diagonal crack in the joint intersection region was formed at load of 53 KN and displacement of 8.53 mm. during the test the diagonal cracks extended and the flexural cracks width increased. Due to the diagonal cracks in the joint region, the concrete cover spalled of from one side of the joint. The joint failed due to the beam flexural damage (Figure 5-2).

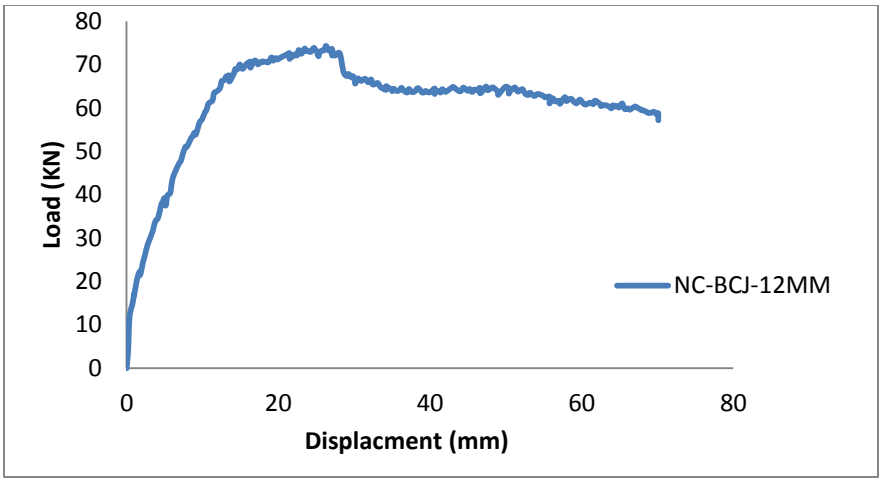

Figure 5-1: Load deflection response of NC-BCJ-12MM specimen

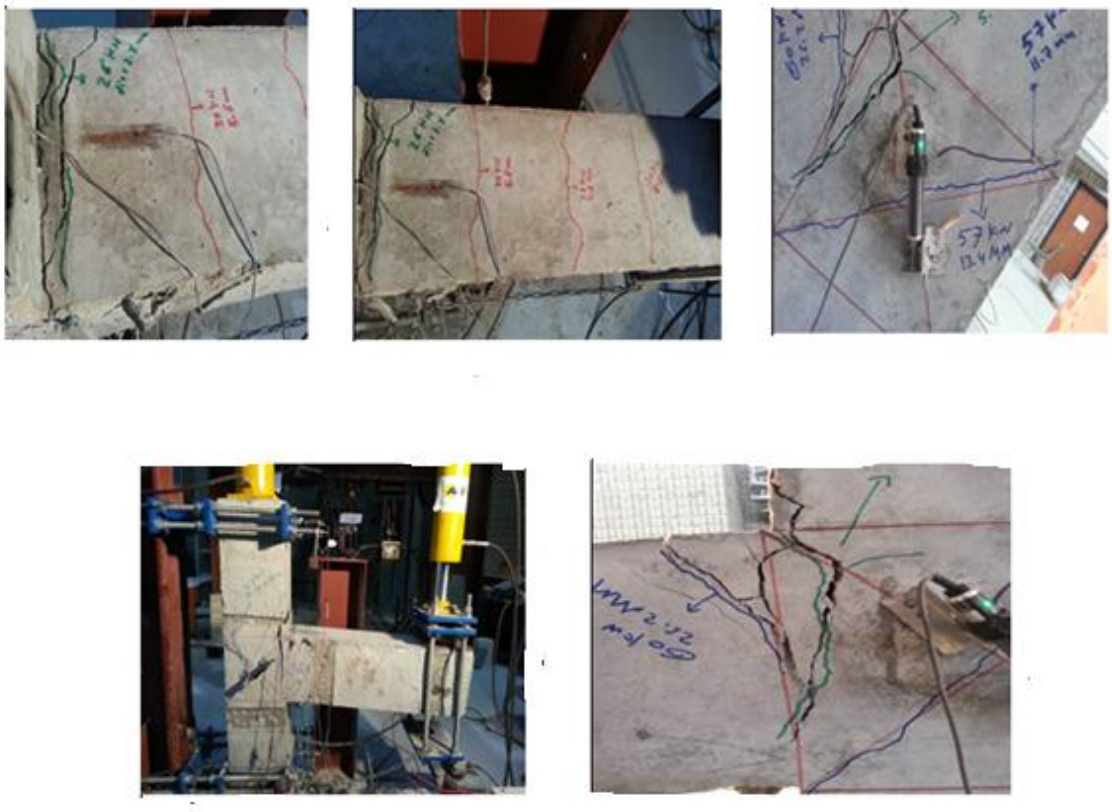

Figure 5-2 : Crack pattern specimen NC-BCJ-12MM

Different steel strain gauges were fixed in different locations on the steel reinforcement. Figure 5-3 shows the variation of steel strain of top and bottom beam reinforcement with

the load applied at the tip of the beam. The gauge installed on the top reinforcement showed that the strain had exceeded the yield strain on the reinforcement.

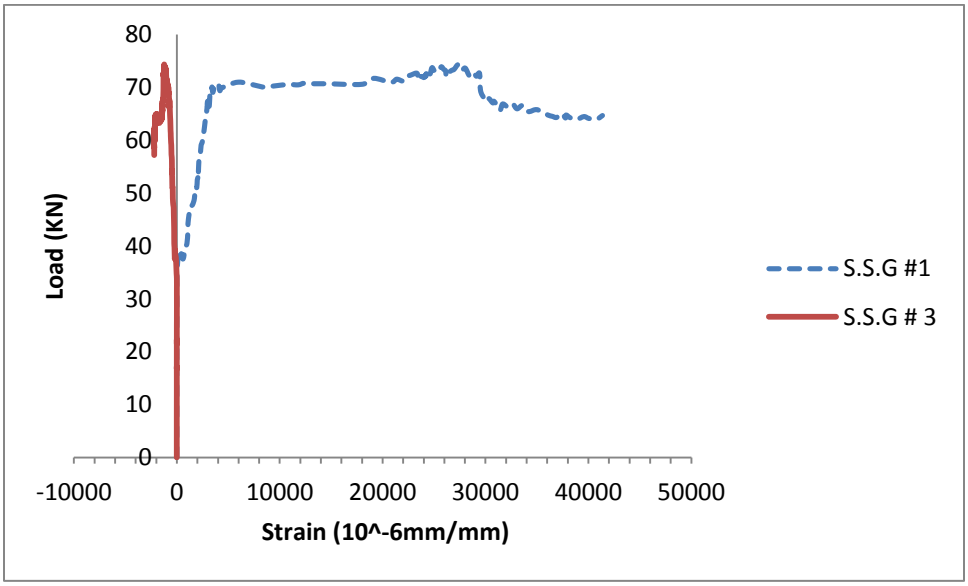

Figure 5-3: Load-strain curve for SSG# 1 and SSG# 2

5.1.2 Monotonic Test Result for SFRC-BCJ–12MM

SFRC-BCJ–12MM specimen was cast using steel fibre concrete in the intersection region while the rest of the specimen was cast using normal concrete. The load vs. displacement curve shows that the ultimate load was 79 KN at displacement of 50 mm (Figure 5-4). The first flexural crack appeared in the beam at load of 22 KN and at displacement of 1.63 mm. During the test no diagonal cracks formed in the joint while the flexural cracks became wider. The specimen failure was preferred beam flexural failure at the beam-column interface (Figure 5-5).

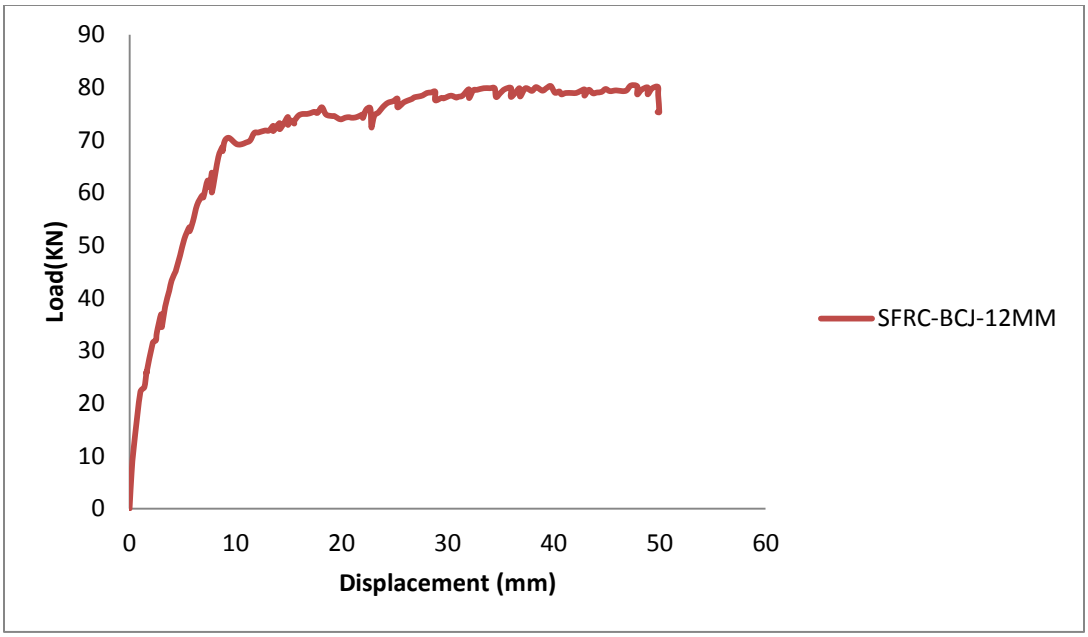

Figure 5-4: Load deflection response of SFRC-BCJ-12MM specimen

Figure 5-5: Crack pattern specimen SFRC-BCJ-12MM

Steel strain gauges were fixed on the steel reinforcement to monitor the strain (Figure 5-6). The strain of the top reinforcement had exceeded the yield strain of the reinforcement.

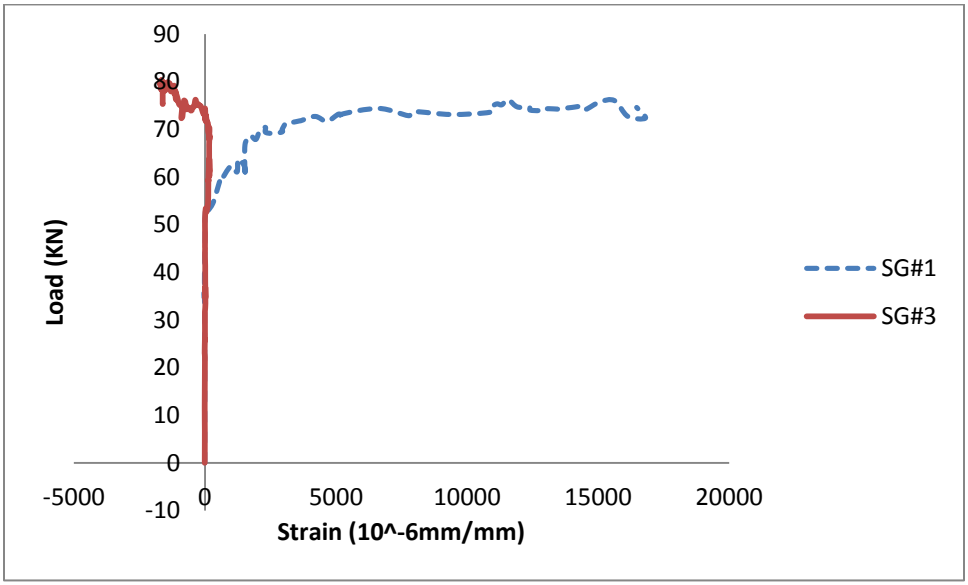

Figure 5-6 : Load-strain curve for SSG#1 and SSG# 2

5.1.3 Monotonic Test Result for SFRC-BCJ–S-12MM

SFRC-BCJ-S-12MM specimen has additional transverse reinforcement in the intersection area. Steel fibre concrete was used in casting the intersection area while the rest of the specimen was cast using normal concrete. The load vs. displacement curve shows that the ultimate load was 77 KN at displacement of 51 mm (Figure 5-7). The flexural cracks appeared in the beam at load of 25 KN and displacement of 2 mm. As the load increased the flexural cracks prolonged and became wider, while no cracks formed in the intersection area. The specimen failed due to the beam flexural damage at the beam column interface (Figure 5-8).

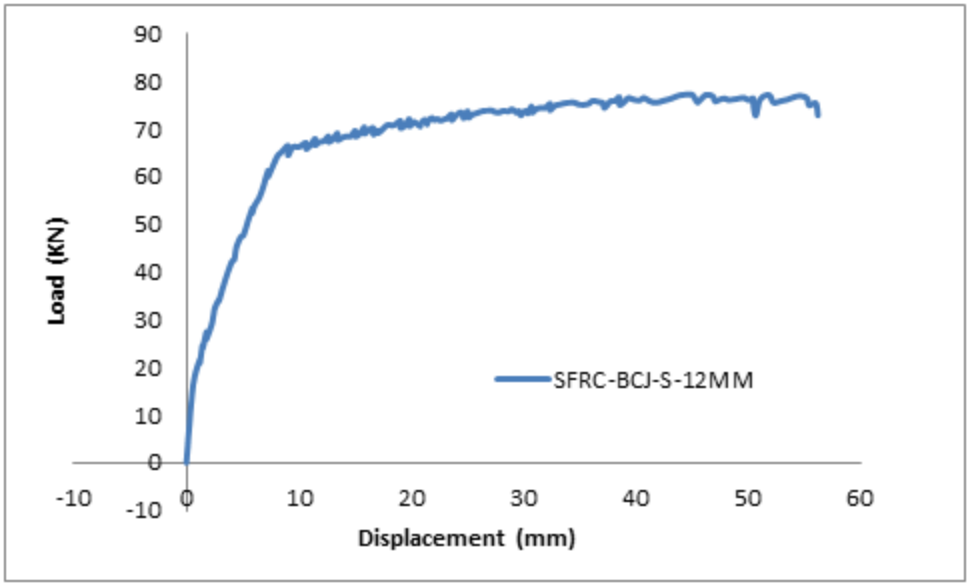

Figure 5-7 : Load-deflection response of SFRC-BCJ-S-12MM specimen

Figure 5-8: Crack pattern specimen SFRC-BCJ-S-12MM

Figure 5-9 shows the strain variation of beam steel reinforcement with the load applied on the tip of the beam.

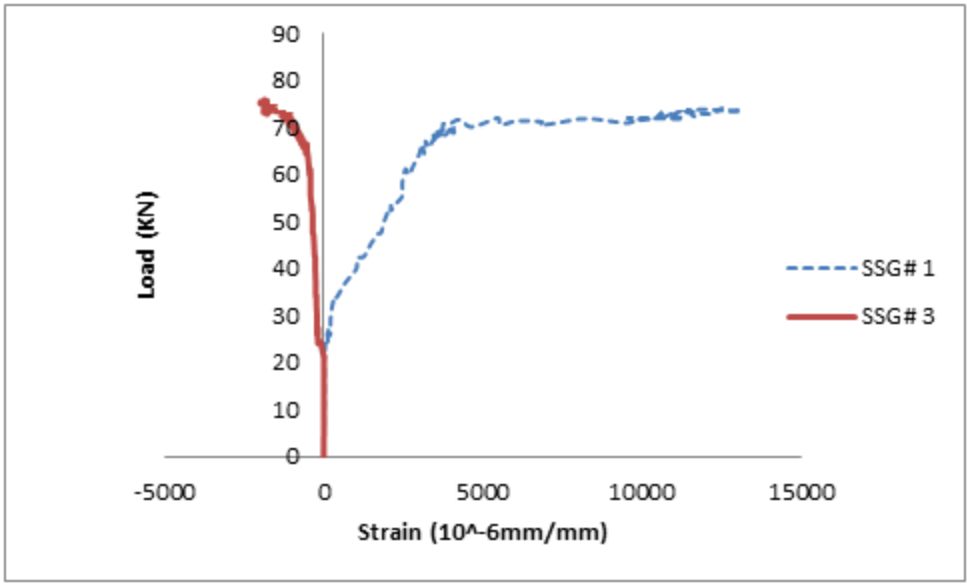

Figure 5-9: Load-strain curve for SSG #1 and SSG # 3

5.1.4 Comparison of Load Deflection Response of all BCJ-12MM Specimens

The load carrying capacity of NC-BCJ-12MM specimen reduced due to the flexural damage in the beam as well as the diagonal damage in the intersection area. Therefore, to improve the tensile capacity of the joint, steel fibre concrete (SFC) was used in casting the intersection area of SFRC-BCJ-12MM specimen. The presence of steel fibre in the joint prevented any cracks or damage to form in the intersection area. After the strengthening process the failure mode of SFRC-BCJ-12MM & SFRC-BCJ-S-12MM specimens became preferred flexural failure which is confirmed by the fact that the beam flexural strength was computed as 60 KN which is smaller than the ultimate load. Also, gauges installed on the 12 mm bars showed that the strain had exceeded the yield strain of the reinforcement. The load carrying capacity for SFRC-BCJ-12MM and SFRC-BCJ-S-12MM was same because the joint did not crack and the fail in both specimens were

due to the flexural damage in the beam. So the joint intersection stirrups of SFRC-BCJ-S-12MM specimen did not enhance the load carrying capacity of the joint (Figure 5-10).

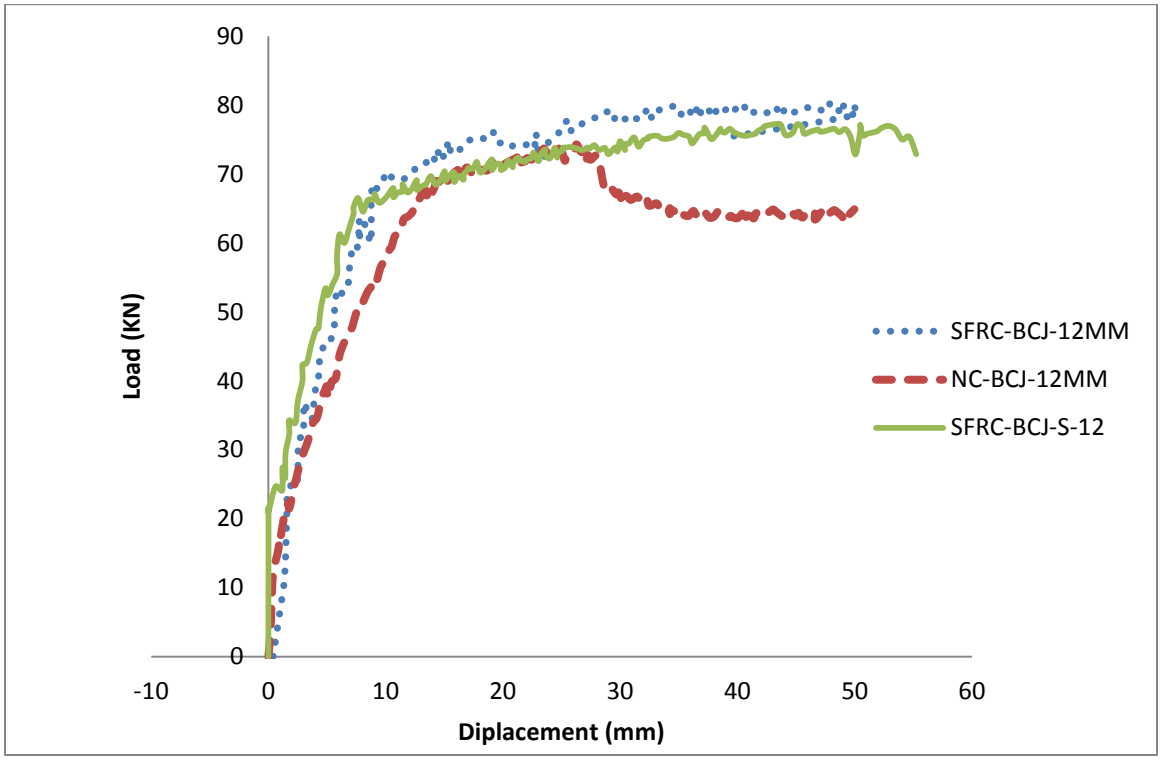

Figure 5-10: Comparison of load deflection response of all specimens reinforced with 12 mm flexural steel bars

Table 5-1: Ultimate load and mode of failure for BCJ-12MM specimens

Specimens #	Ultimate Load (KN)	Mode of Failure
NC-BCJ-12MM	74	Beam flexural with joint damage
SFRC-BCJ-12MM	79	Flexural failure
SFRC-BCJ-S-12MM	77	Flexural failure

5.2 Monotonic Test Result for BCJ-18MM

BCJ-18MM specimen reinforced with 18 mm longitudinal steel reinforcement and 8 mm transverse steel reinforcement in both beam and column.

5.2.1 Monotonic Test Result for NC-BCJ-18MM

NC-BCJ-18MM specimen was cast using normal concrete. The load vs. displacement curve shows that the ultimate load was 97.2 KN at displacement of 17.5 mm (Figure 5-11). At load of 37.1 KN and displacement of 3.5 mm the first flexural crack was occurred in the specimen near to the beam-column interface. At load of 50 KN and displacement of 5.5 mm the first shear crack formed in the intersection area. When the load increased the diagonal shear cracks extended and became wider. The joint failed due to the shear failure of the joint (Figure 5-12).

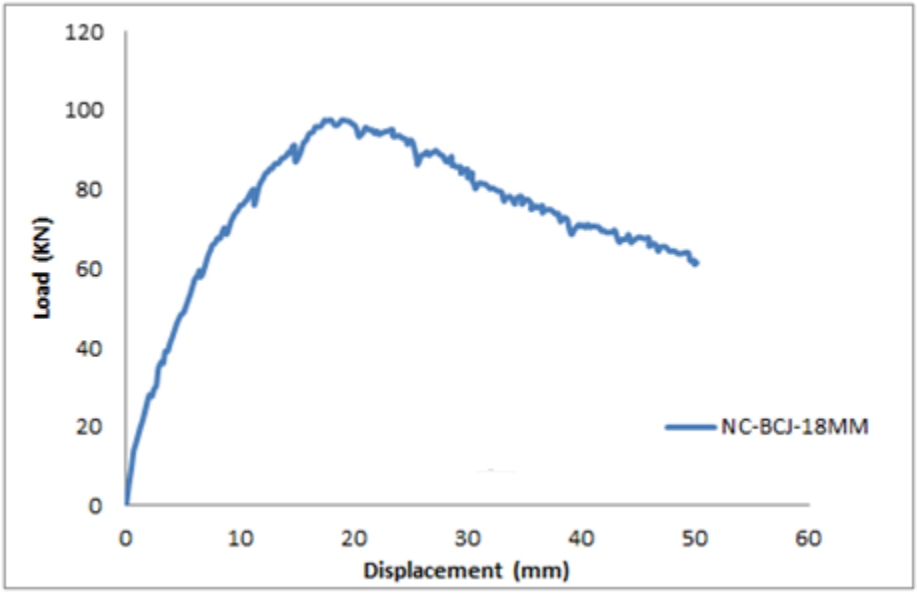

Figure 5-11: Load-deflection response of NC-BCJ-18MM specimen

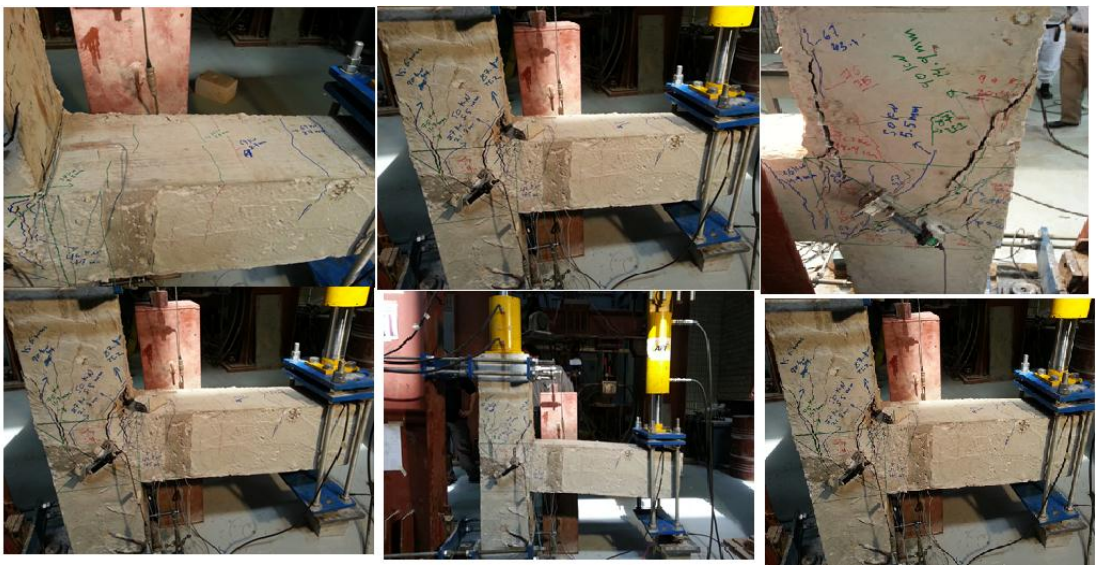

Figure 5-12: Crack pattern for specimen NC-BCJ-18MM

Steel strain gauges were fixed on the steel reinforcement to monitor the strain. Figure 5-13 shows the variation of the strain in different strain gauges vs. the applied load.

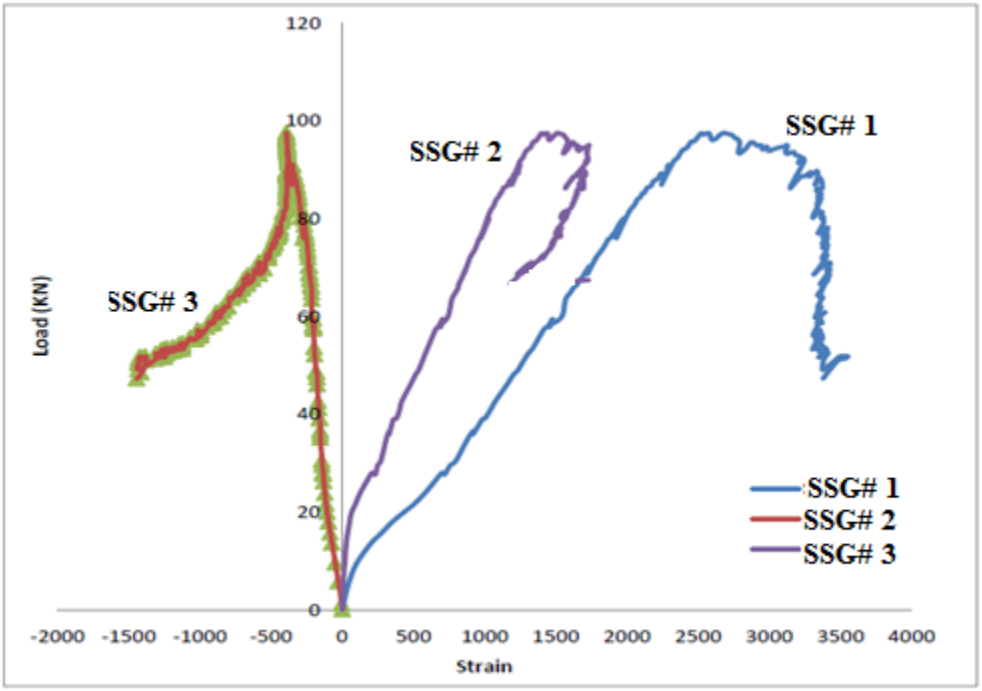

Figure 5-13: Load-strain curve for SSG# 1, SSG# 2, and SSG# 3

5.2.2 Monotonic Test Result for NC-BCJ-S-18MM

NC-BCJ-S-18MM specimen with additional stirrups in the intersection area. It was cast using normal concrete. As shown in the load vs. displacement curve, the ultimate load was 119.5 KN at displacement of 25.9 mm (Figure 5-14). At load of 34 KN and displacement of 3.4 mm the first flexural crack was formed in the specimen near the beam-column interface. At load of 53 KN and displacement of 6.3 mm the first shear crack formed in the joint intersection region. During the test the shear cracks extended and became wider. At the end of the test the specimen failed due to the joint shear failure (Figure 5-15).

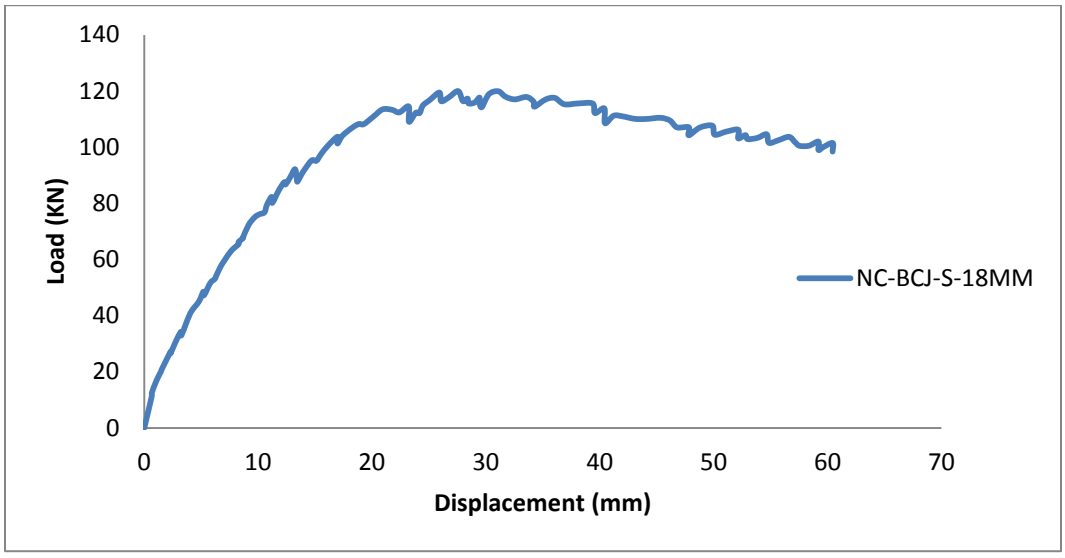

Figure 5-14: Load deflection response of NC-BCJ-S-18MM specimen

Figure 5-15: Crack pattern for specimen NC-BCJ-S-18MM

Several strain gauges were attached on the steel reinforcement to measure the strain. Figure 5-16 shows the strain in the top and bottom beam reinforcement.

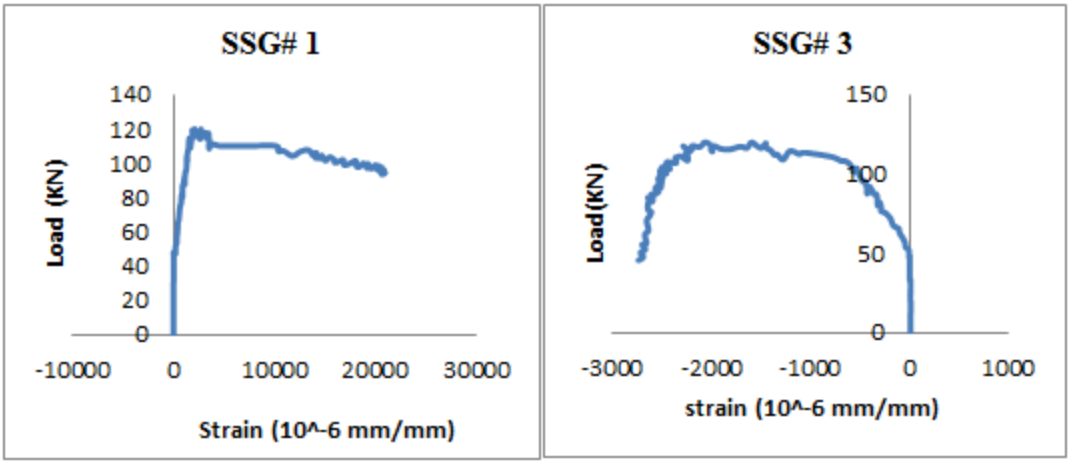

Figure 5-16: Load-strain curve for SSG# 1 and SSG# 3

5.2.3 Monotonic Test Result for SFRC-BCJ-18MM

SFRC-BCJ-18MM specimen with steel fibre concrete in the intersection region while the rest of the specimen was cast using normal concrete. The load vs. displacement curve shows that the ultimate load was 156 KN at corresponding displacement of 40 mm. (Figure 5-17). The first flexural crack formed in the specimen was at load of 40 KN and displacement of 2 mm, while the first diagonal crack formed at load of 104 KN and displacement of 10 mm. As the load increased the flexural crack width increased and other fine diagonal cracks appeared in the joint intersection region. Due to the presence of the steel fibre in the joint area, the shear cracks widths were very fine. The specimen failure was preferred flexural failure (Figure 5-18).

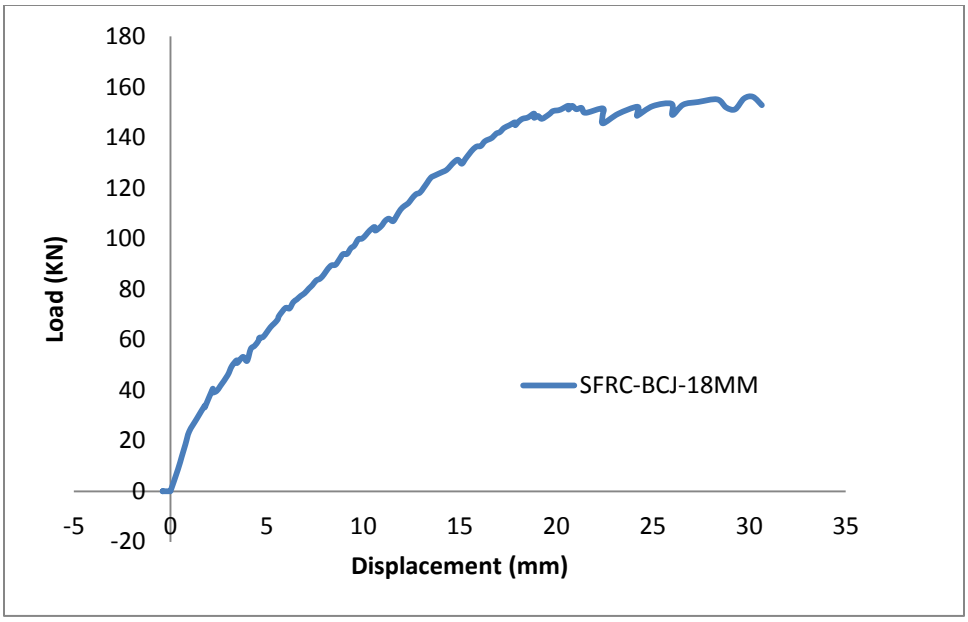

Figure 5-17: Load deflection response of SFRC-BCJ-18MM specimen

Figure 5-18: Crack pattern specimen SFRC-BCJ-18MM

Several strain gauges were attached on the reinforcement in different locations to monitor the strain in the steel (Figure 5-19).

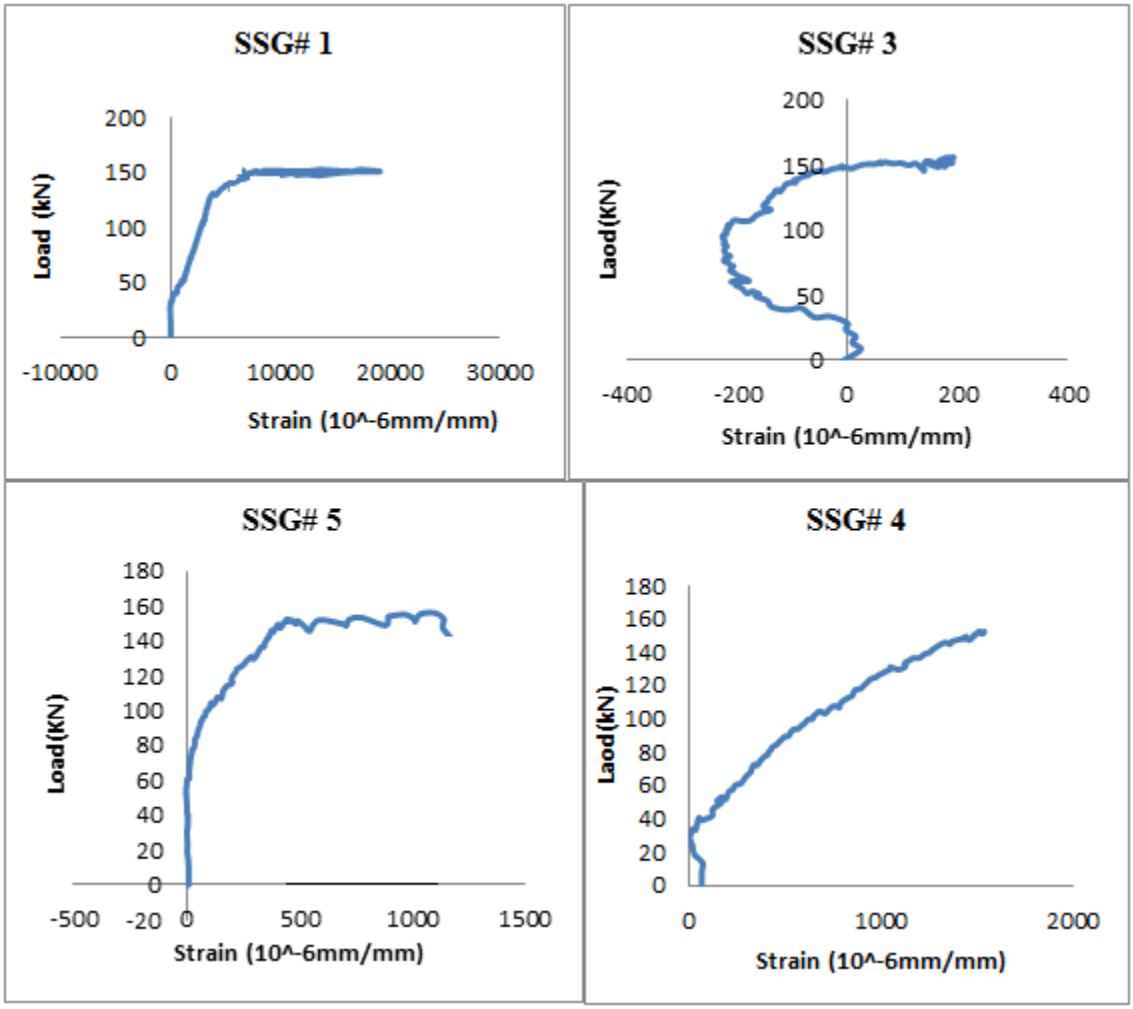

Figure 5-19: Load-strain curve for SSG# 1, SSG# 3, SSG# 4, and SSG# 5

5.2.4 Monotonic Test Result for SFRC-BCJ-S-18MM

SFRC-BCJ-S-18MM specimen has additional transverse reinforcement in the intersection area. It was strengthened with steel fibre concrete in the intersection area and the rest of the specimen was cast using normal concrete. The ultimate load was 151 KN at

corresponding displacement of 40 mm (Figure 5-20). The first flexural crack formed at load of 40 KN at displacement of 3 mm. The first diagonal crack formed at load of 95 KN at corresponding displacement of 12.3 mm. As the load increased the flexural crack width increased and other fine diagonal cracks appeared in the joint. The joint failure was beam flexural failure at the beam-column interface (Figure 5-21).

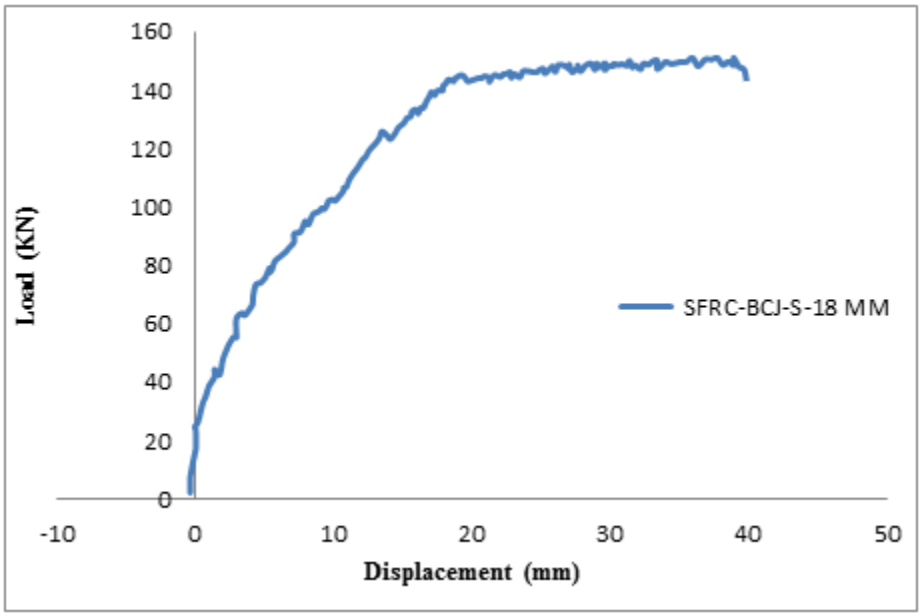

Figure 5-20: Load-deflection response of SFRC-BCJ-S-18MM specimen

Figure 5-21: Crack pattern specimen SFRC- BCJ-S-18MM

Different strain gauges were attached on the reinforcement in different locations to measure the strain in the steel. Figure 5-22 shows the strain in beam top and column reinforcement.

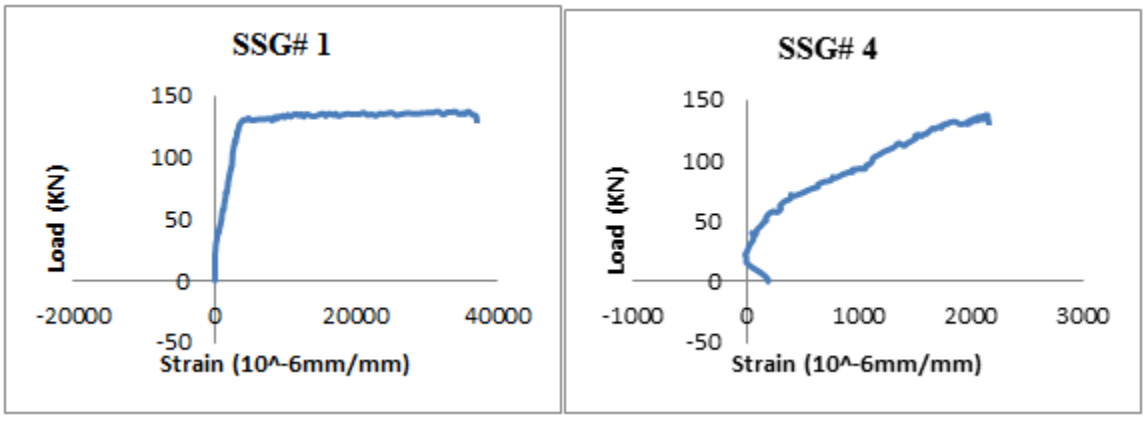

Figure 5-22: Load-strain curve for SSG# 1 and SSG# 4

5.2.5 Monotonic Test Result for UHPC-BCJ-18MM

UHPC-BCJ-18MM specimen with UHPC in the intersection region and the rest of the specimen was cast using normal concrete. The load vs. displacement curve shows that the ultimate load was 160 KN at displacement of 39 mm (Figure 5-23). The first crack in the specimen was flexural crack in the beam at load of 41 KN and displacement of 2.8 mm, while the first diagonal crack was at load of 146 KN and displacement of 19 mm. As the load increased the flexural crack width increased and extended through the beam while the shear crack was very fine and remained same up to the end of loading. The specimen failure was preferred flexural failure at the beam-column interface (Figure 5-24).

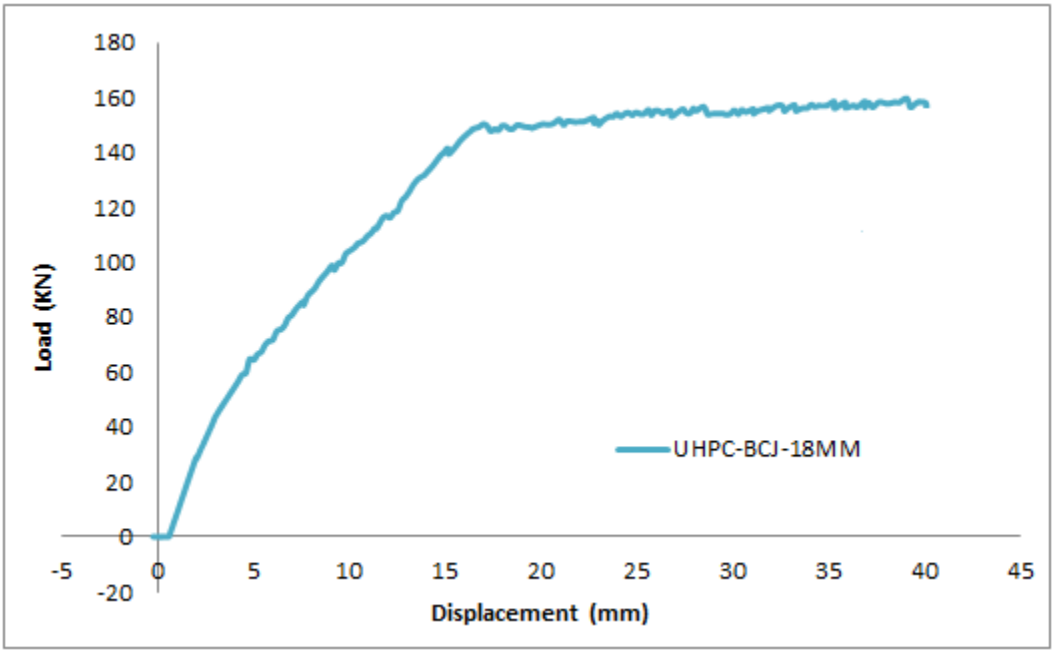

Figure 5-23: Load-deflection response of UHPC-BCJ-18MM specimen

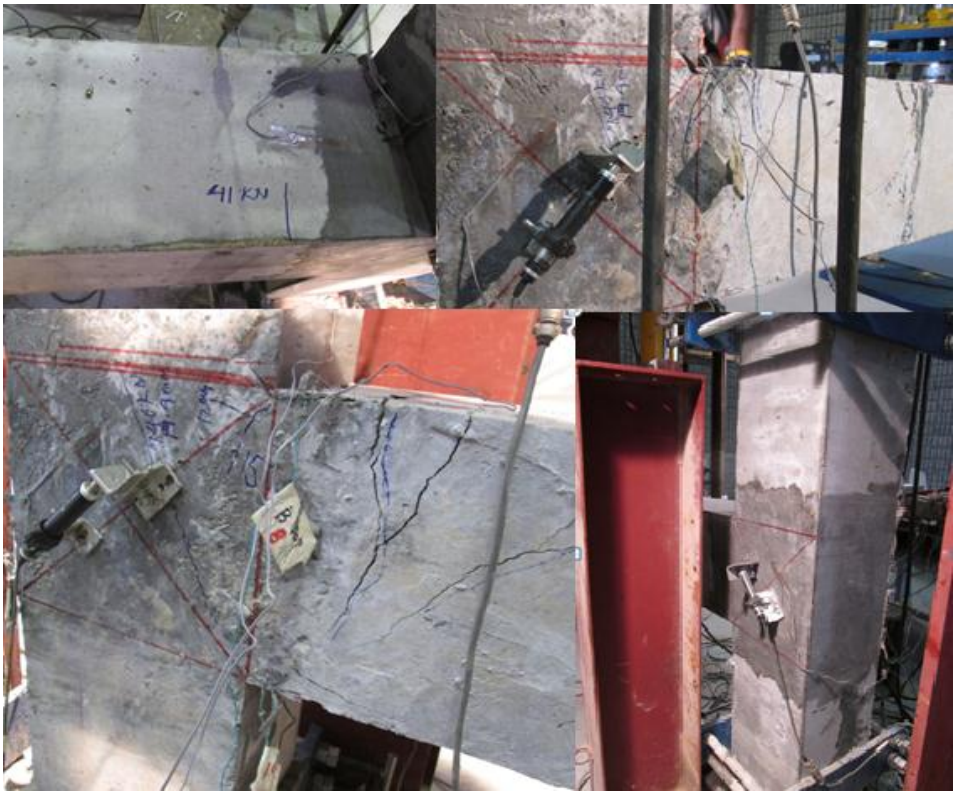

Figure 5-24: Crack pattern specimen UHPC- BCJ-18MM

The strains of top and bottom beam reinforcements are shown in Figure 5-25. The strain of top reinforcement shows that the strain had exceeded the yield strain.

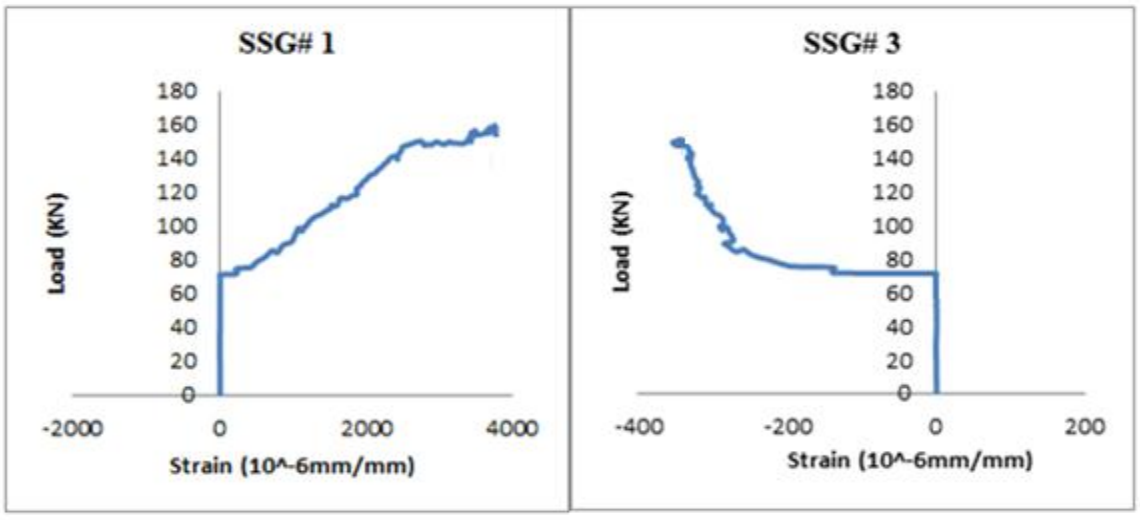

Figure 5-25 : Load-strain curve for SSG# 1 and SSG# 3

5.2.6 Comparison of Load Deflection Response of all Specimens Reinforced with 18 mm Flexural Steel Bars

The high strength concrete whether it is UHPC or SFC played a significant rule in shifting the plastic hinge from the joint intersection to the beam. The mode of failure changed from joint shear failure to preferred flexural beam failure. Since all the BCJ-18MM specimens reinforced with 18 mm steel bars, all the specimens has same beam flexural capacity which was computed as 137 KN which is smaller than the peak load of all specimens with high strength concrete (Figure 5-26). Also, gauges installed on the 18 mm steel bars showed that the strain had exceeded the yield strain of the reinforcement which is confirmed the flexural mode failure that got experimentally.

The steel fibre improved the shear and tensile strength of the high strength concrete, and hence the shear capacity of the joint. The load carrying capacity of the strengthened specimens was enhanced by more than 60% (Figure 5-26). Due to the high tensile strength of the UHPC in UHPC-BCJ-18MM specimen one fine crack occurred in the intersection area at load of 146 KN, while many fine cracks appeared in the intersection area of SFRC-BCJ-18MM specimen, it was started to appear at load of 104 KN. Since no wide shear cracks formed in the joint area of SFRC-BCJ-S-18MM specimen, the stirrups did not affect the load carrying capacity of the joint. While the stirrups in the NC-BCJ-S-18MM specimen improved the joint shear capacity by 23%. Table 5-2 shows the summery of the ultimate load, enhancement in the load carrying capacity, and the mode of failure of BCJ-18MM specimens.

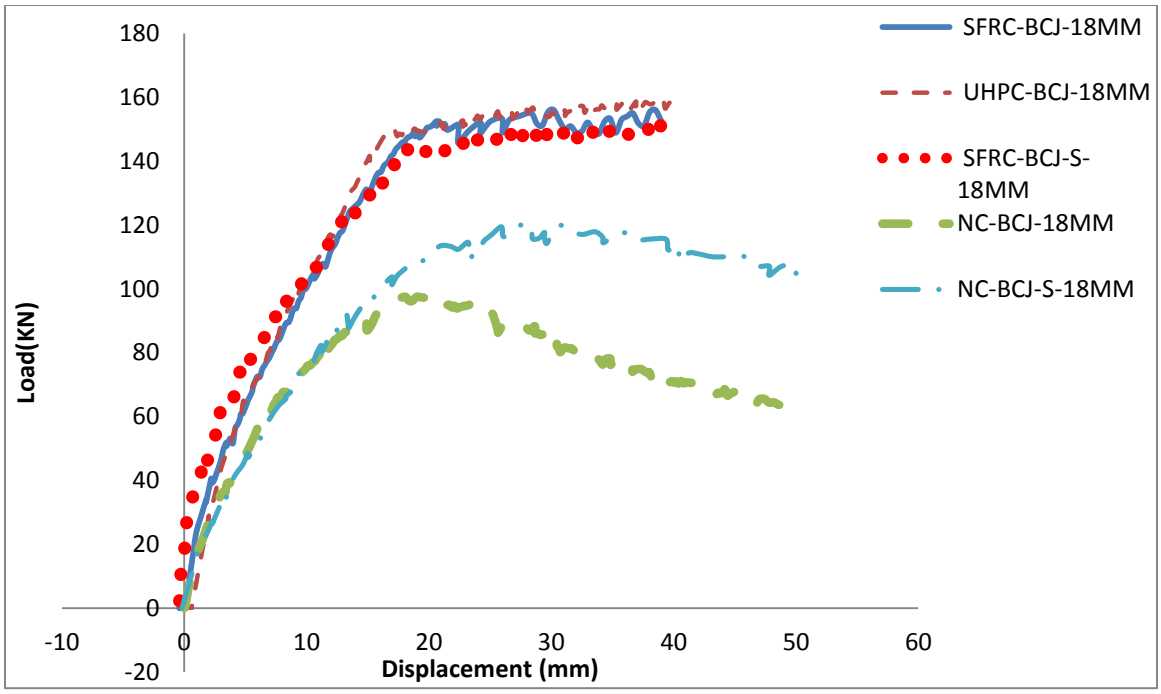

Figure 5-26: Comparison of load deflection response of all specimens reinforced with 18 mm longitudinal steel bars

Table 5-2: Ultimate load and mode of failure for BCJ-18MM specimens

Specimens #	Ultimate Load (KN)	Enhancement (%)	Test Type	Mode of Failure
NC-BCJ-18MM	97.2	Control	Monotonic	Joint shear failure
NC-BCJ-S-18MM	119.5	22.94	Monotonic	Joint shear failure
SFRC-BCJ-18MM	156	60.49	Monotonic	flexural failure
SFRC-BCJ-S-18MM	151	55.35	Monotonic	flexural failure
UHPC-BCJ-18MM	160	64.61	Monotonic	flexural failure

5.3 Cyclic Test Result for BCJ-12MM

5.3.1 Cyclic Test Result for NC-BCJ-12MM

The load versus displacement curve for NC-BCJ-12MM specimen is shown in Figure 5-27 . The ultimate load in pull direction was 67.8 KN and the maximum load in push direction was 69.4 KN. The first flexural crack occurred in the specimen was in the first cycle at load of 25 KN (push) and 20 KN (pull). The first shear crack in the joint intersection occurred in the third push cycle was at load of 53 KN. The beam column interface of the specimen was totally damaged and the reinforcement of the joint intersection was visible (Figure 5-28).

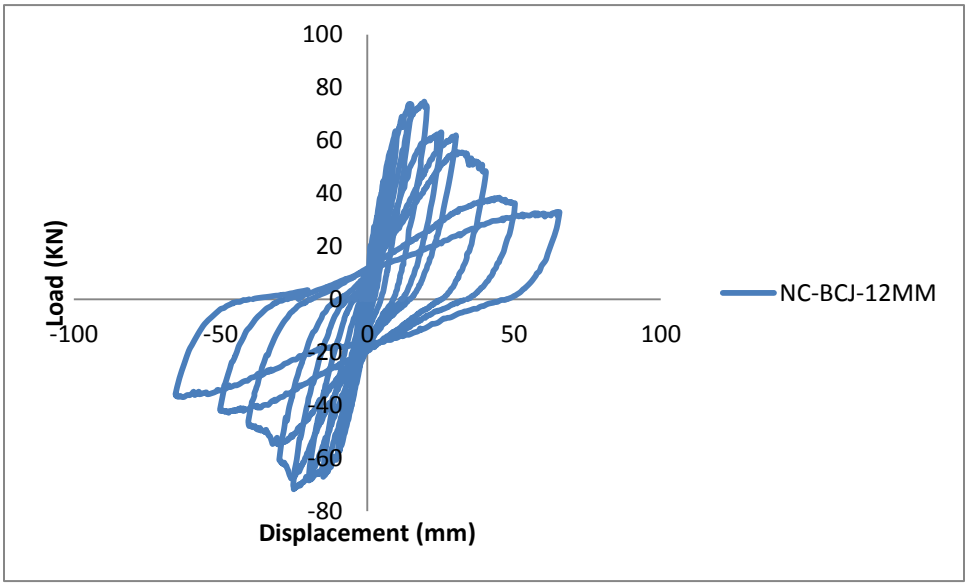

Figure 5-27: Hysteresis loop of NC-BCJ-12MM specimen

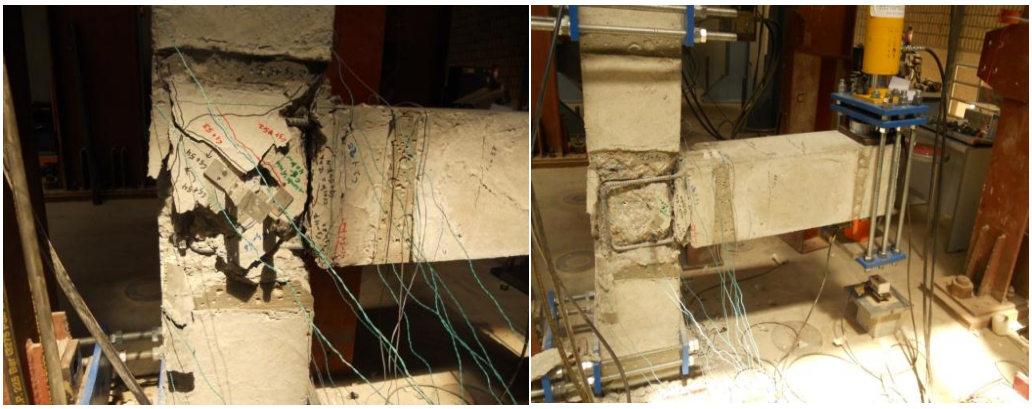

Figure 5-28: Joint damage for specimen NC- BCJ-12MM

Strain gauges were fixed in several locations on the surface of the reinforcement to measure the strains. Figure 5-29 and 5-30 show the load- strain curve of the top and bottom beam reinforcements.

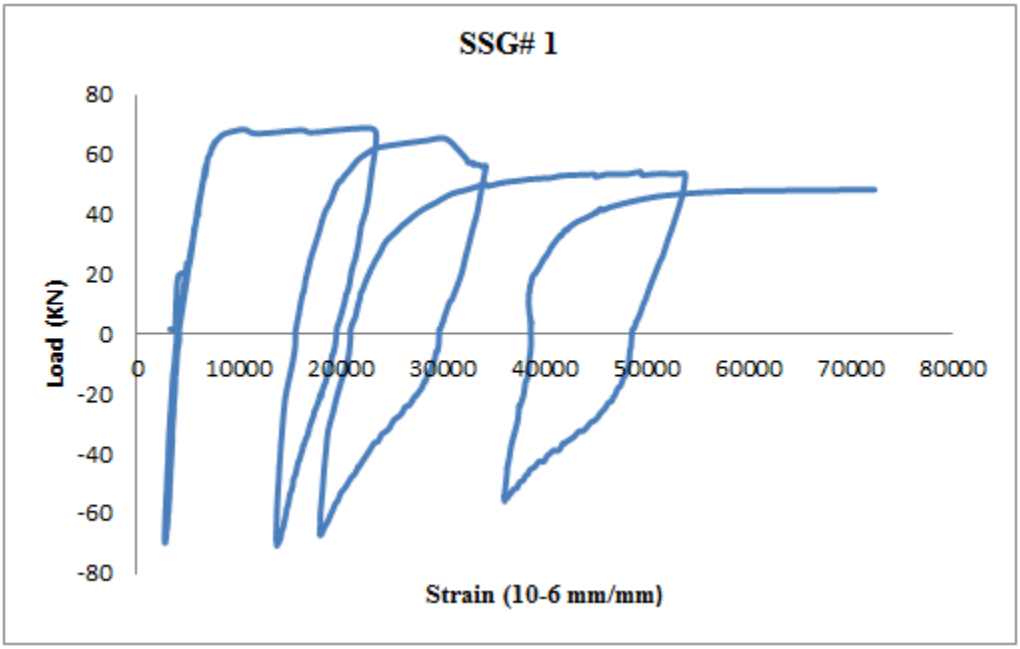

Figure 5-29: Load-strain curve for SSG# 1

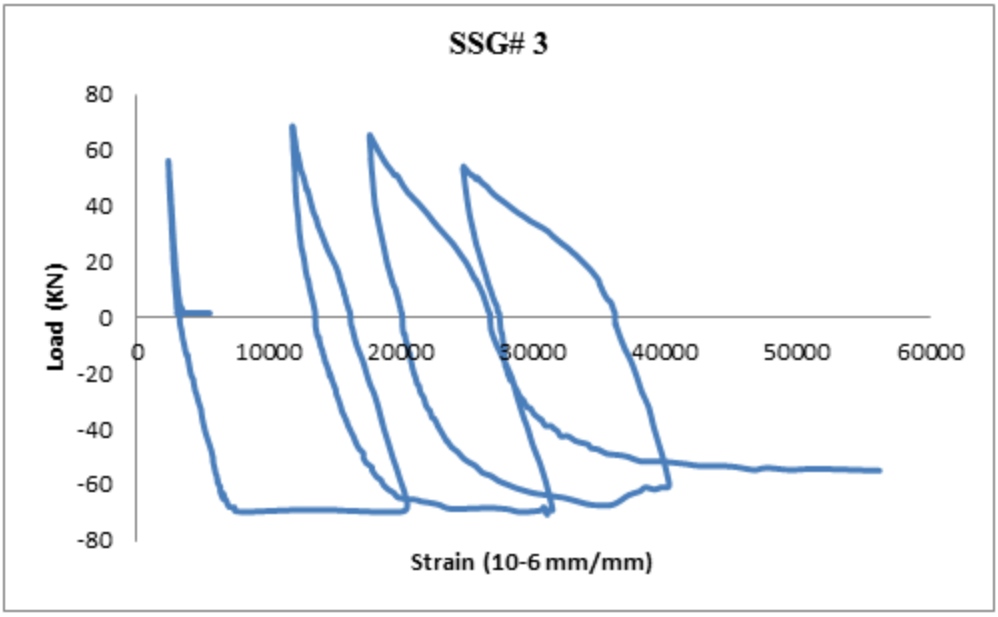

Figure 5-30: Load-strain curve for SSG# 3

5.3.2 Cyclic Test Result for SFRC-BCJ-12MM

The load-displacement graph of SFC-BCJ-12MM specimen shows that the maximum load was 62 KN in pull direction and the maximum load in push direction was 70 KN (Figure 5-31). The first flexural crack occurred in the specimen was in the first cycle at load of 26 KN (push) at the beam column interface. The first shear crack in the joint intersection formed in the third push cycle at load of 62 KN (Figure 5-32). The flexural cracks width increased as the load increased and extended in the beam. During the test other fine cracks appeared in the intersection area. The joint failure was preferred flexural failure (Figure 5-33).

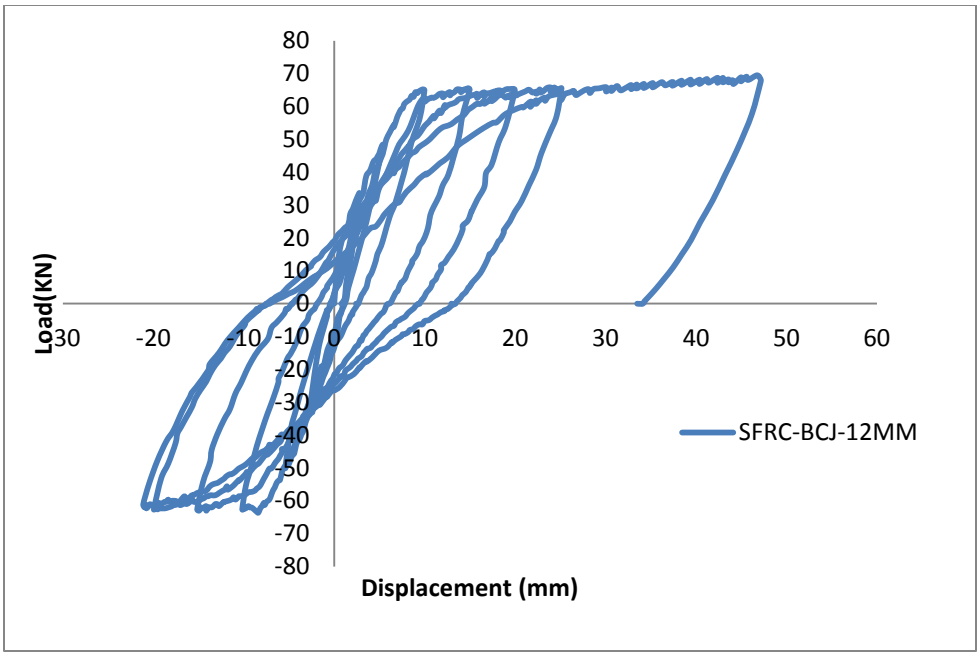

Figure 5-31: Hysteresis loop of SFRC-BCJ-12MM specimen

Figure 5-32: Crack pattern specimen SFRC-BCJ-12MM

Figure 5-33: Flexural damage of specimen SFRC-BCJ-12MM

Strain gauges were attached on the steel reinforcement in different locations to measure the strain in the steel. Figure 5-34 and 5-35 show the load versus strain of the top and bottom beam reinforcements.

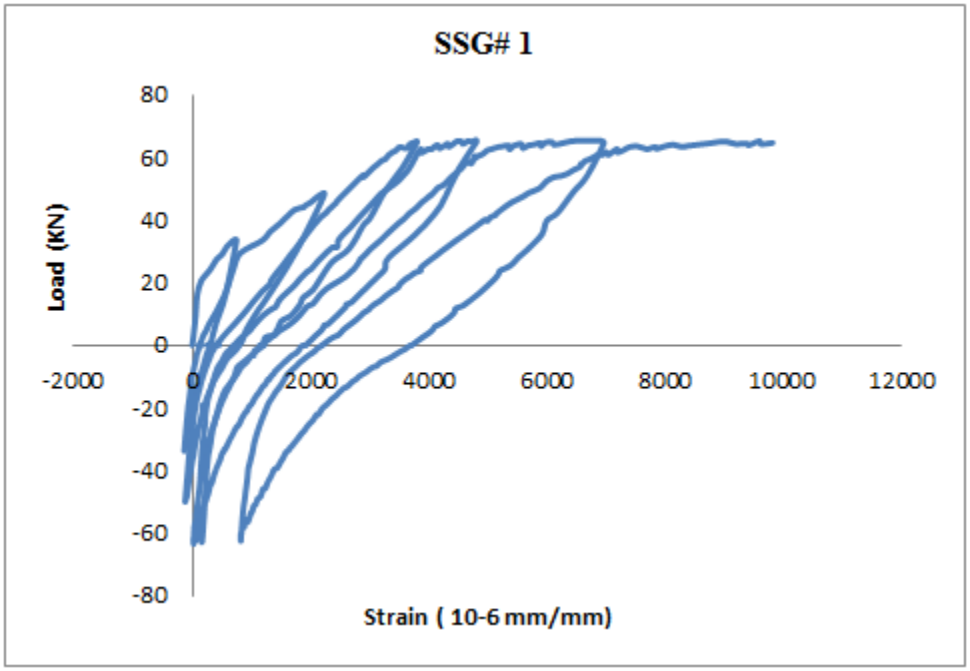

Figure 5-34: Load-strain curve for SSG# 1

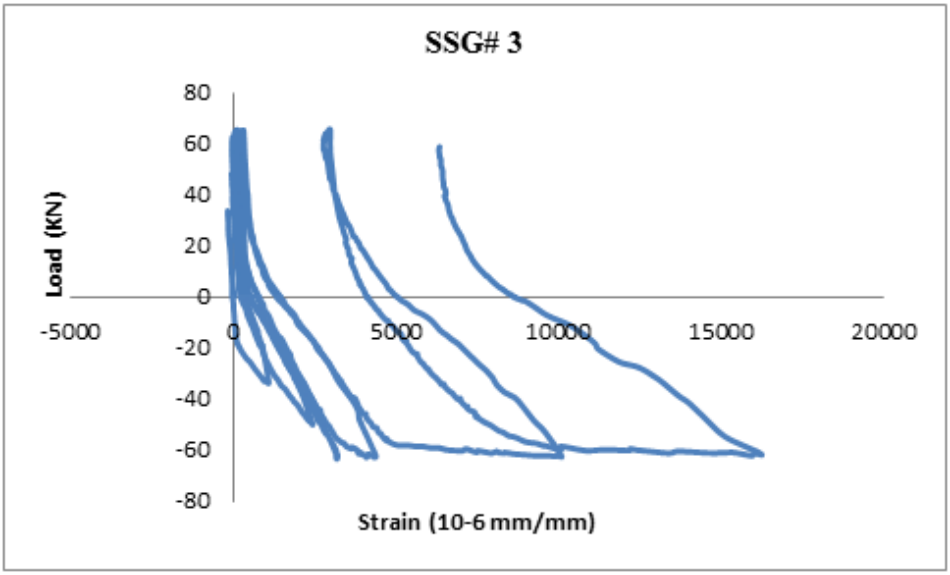

Figure 5-35: Load-strain curve for SSG# 3

5.3.3 Cyclic Test Result for SFRC-BCJ-S-12MM

The load-displacement graph for SFRC-BCJ-S-12MM specimen shows that the ultimate load in pull direction was 62 KN and the ultimate load in push direction was 69 KN (Figure 5-36). The first flexural crack occurred in the specimen was in the first push cycle at load of 25 KN at the beam column interface. The first diagonal crack in the joint intersection formed in the fourth pull cycle at load of 56 KN (Figure 5-37). The flexural cracks width increased as the load increased and extended in the beam. During the test several fine cracks appeared in the intersection area. The joint failure was preferred flexural failure (Figure 5-38).

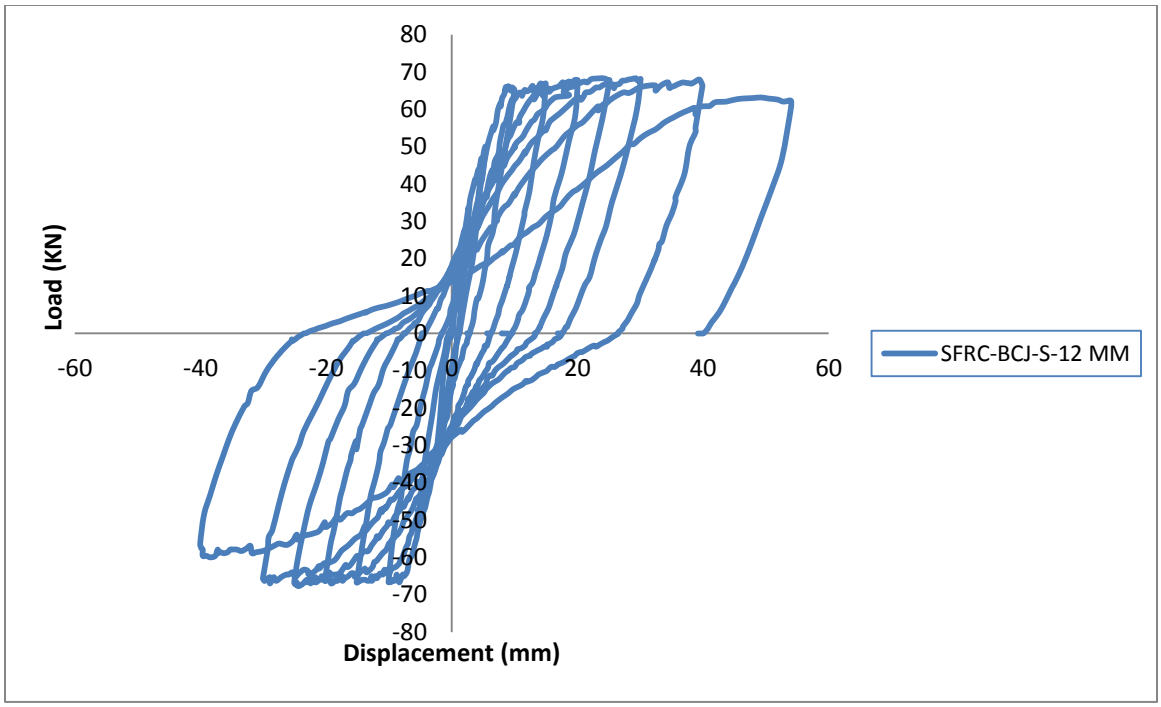

Figure 5-36: Hysteresis loop of SFRC-BCJ-S-12MM specimen

Figure 5-37: Crack pattern specimen SFRC-BCJ-S-12MM

Figure 5-38: Flexural damage of specimen SFRC-BCJ-S-12MM

Figure 5-39 and 5-40 show the load vs. strain of the top and bottom beam reinforcements.

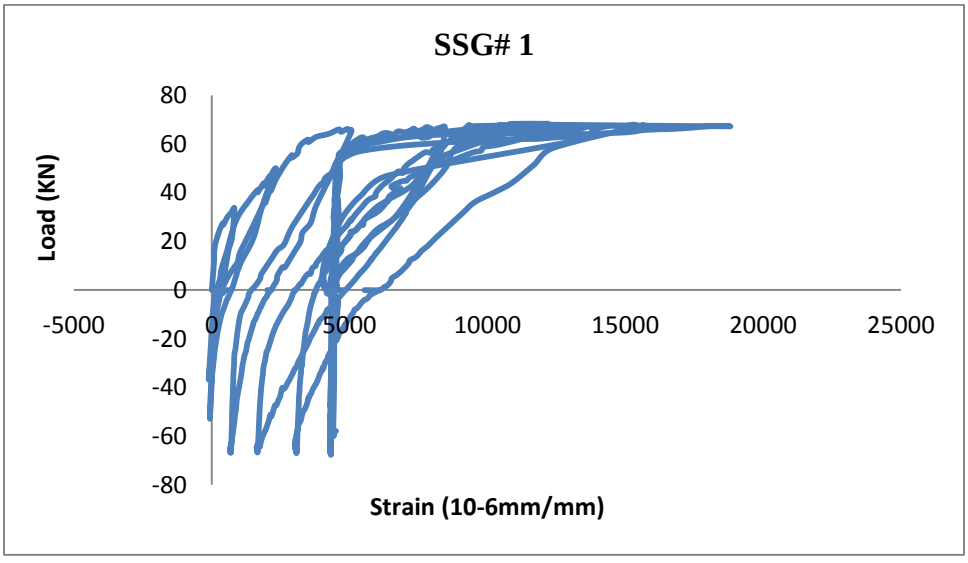

Figure 5-39: Load-strain curve for SSG# 1

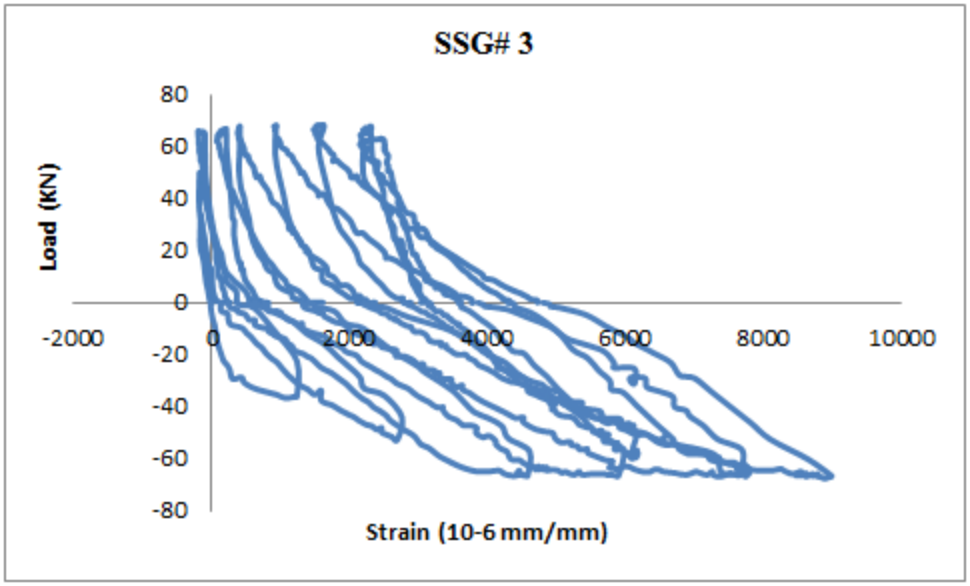

Figure 5-40: Load-strain curve for SSG# 1 and SSG# 3

5.3.4 Cyclic Comparison of Hysteresis of BCJ-12MM Specimens

The damage of NC-BCJ-12MM specimen was due to beam flexural damage with some damage in the joint intersection region, While the damage in the strengthened specimens was totally flexural damage. The stiffness of the strengthened specimens enhanced after strengthening with SFC and it did not decrease up to the end of the test. That was due to the limited hydraulic jack capacity. The additional stirrups in SFRC-BCJ-S-12MM did not enhance the capacity of the joint because the joint region did not crack. Since the plastic hinge occurred in the beam the capacity of all specimens were same (Figure 5-41).

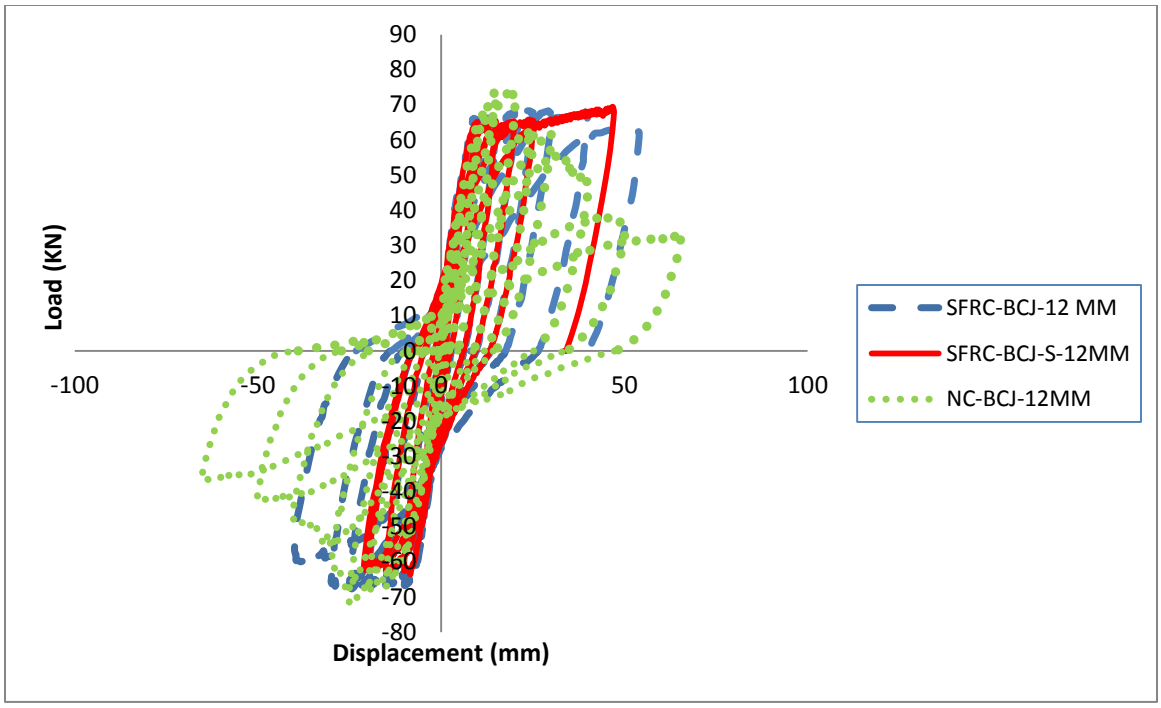

Figure 5-41: Hysteresis loops of all BCJ-12MM specimens

5.4 Cyclic Test Result for BCJ-18MM

5.4.1 Cyclic Test Result for NC-BCJ-18MM

The load vs. displacement curve for NC-BCJ-18MM specimen is shown in Figure 5-42. The ultimate load in the push and pull directions were 99 KN and 100.3KN respectively. At load of 45KN in the first push cycle, the first flexural crack was formed near the beam column interface. The diagonal crack in the joint region formed at load of 60 KN and displacement of 5.59 mm in the second push cycle. As the load and displacement increased the diagonal cracks extended toward the center of the joint. In the last two cycles, concrete in the beam-column interface was crushed and spalled off on both sides of the joint (Figure 5-43). The specimen failed due to the joint damage.

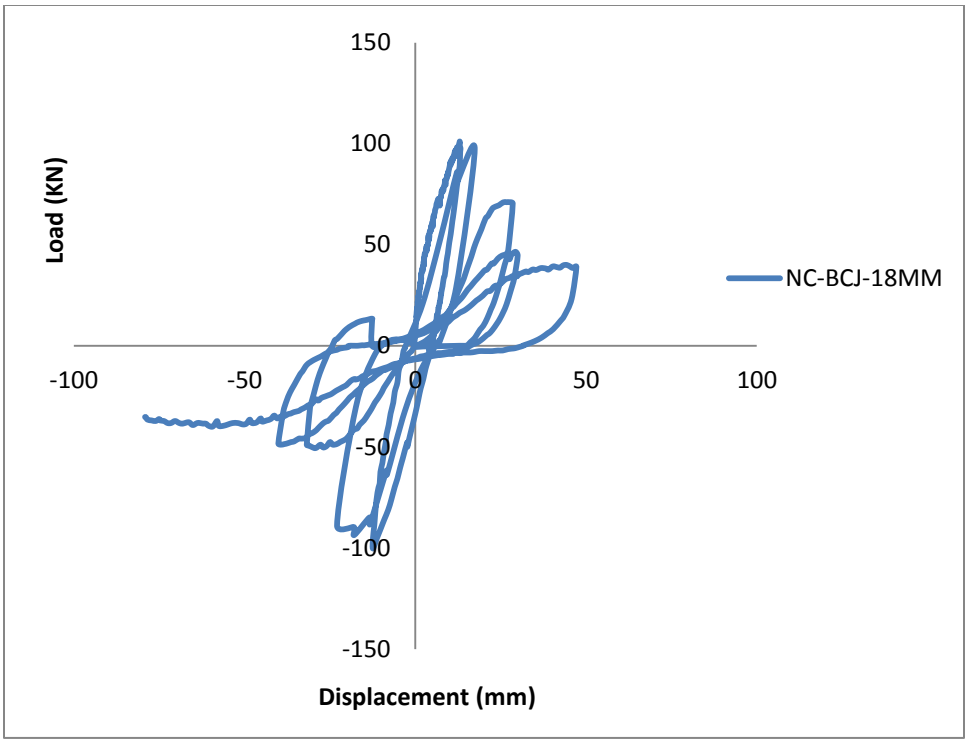

Figure 5-42: Hysteresis loop of NC-BCJ--18MM specimen

Figure 5-43: Crack pattern specimen NC-BCJ-18MM

Strain gauges were attached to the reinforcement to monitor the strain in the steel. Figure 5-44 and 5-45 show the variation of the strain in top and bottom beam reinforcement with the applied cyclic load.

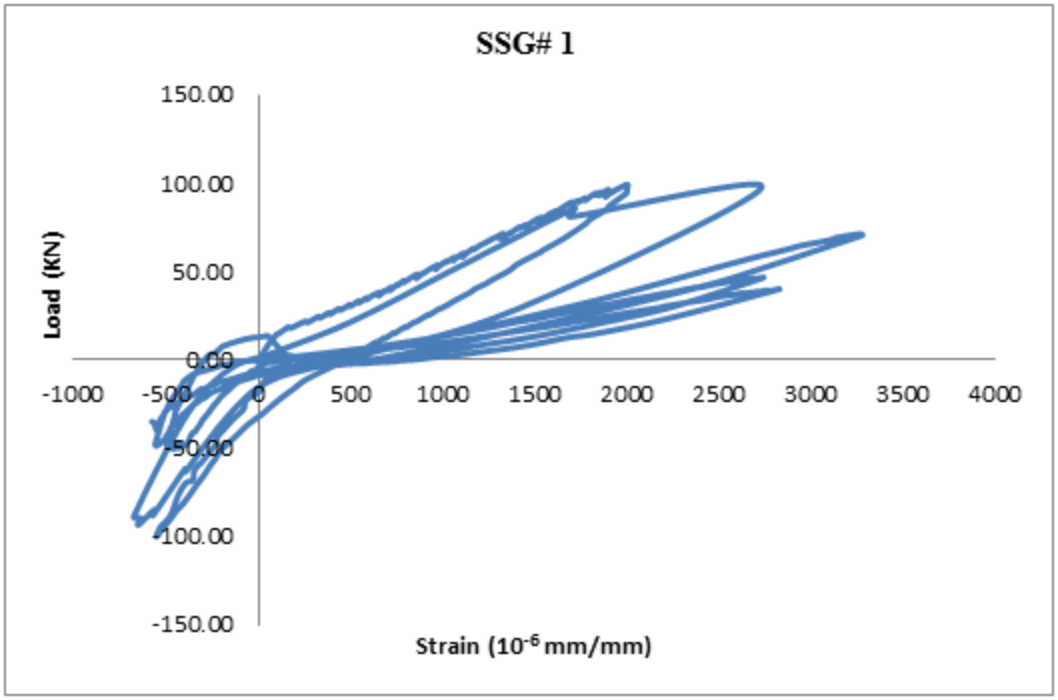

Figure 5-44: Load-strain curve for SSG# 1

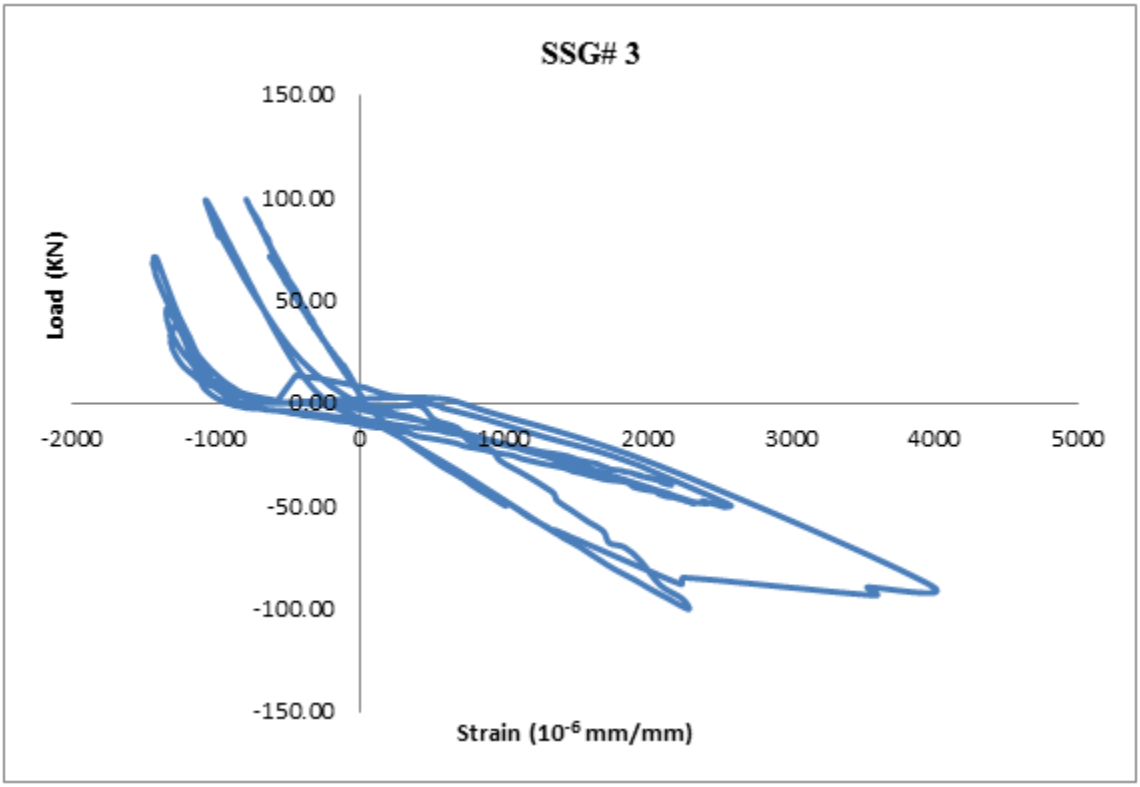

Figure 5-45: Load-strain curve for SSG# 3

5.4.2 Cyclic Test Result for NC-BCJ-S-18MM

Figure 5-46 shows the load-displacement graph of NC-BCJ-S-18MM specimen. The maximum loads in the push and pull cycles were 123.4 KN and 114.6 KN respectively. The first flexural crack formed in the beam at load of 31 KN in the first push cycle. The diagonal crack appeared in the joint area at load of 54 KN in the second push cycle (Figure 5-47). As the load increased the flexural cracks extended in the beam and became wider, while the diagonal cracks prolonged in the intersection area. The joint failure was joint shear failure (Figure 5-47).

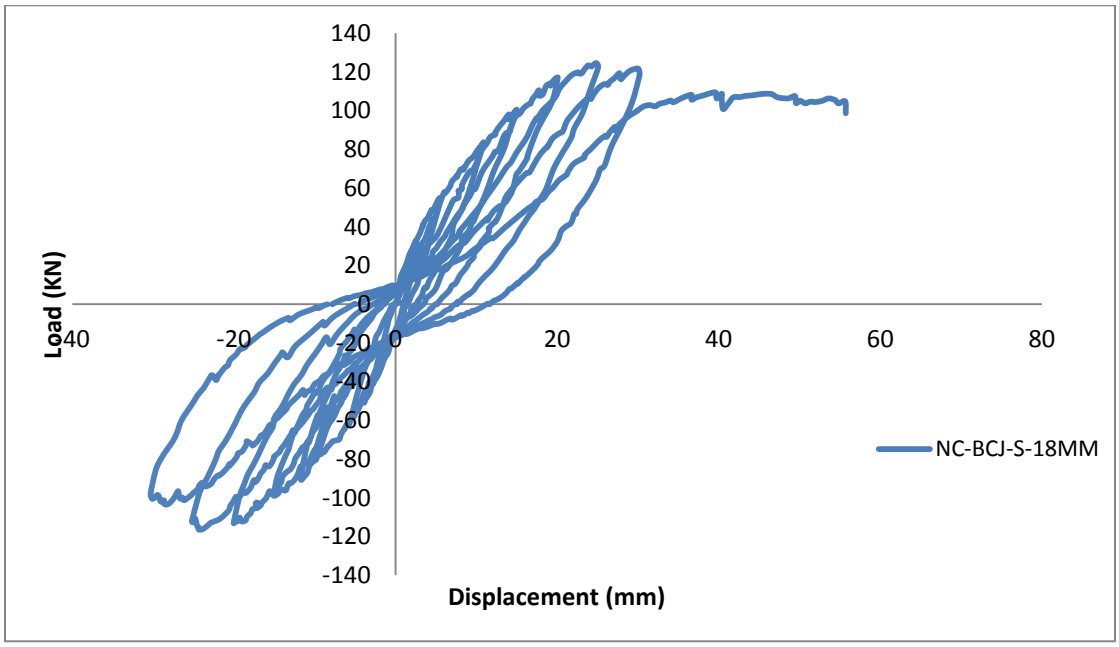

Figure 5-46: Hysteresis loop of NC-BCJ-18MM specimen

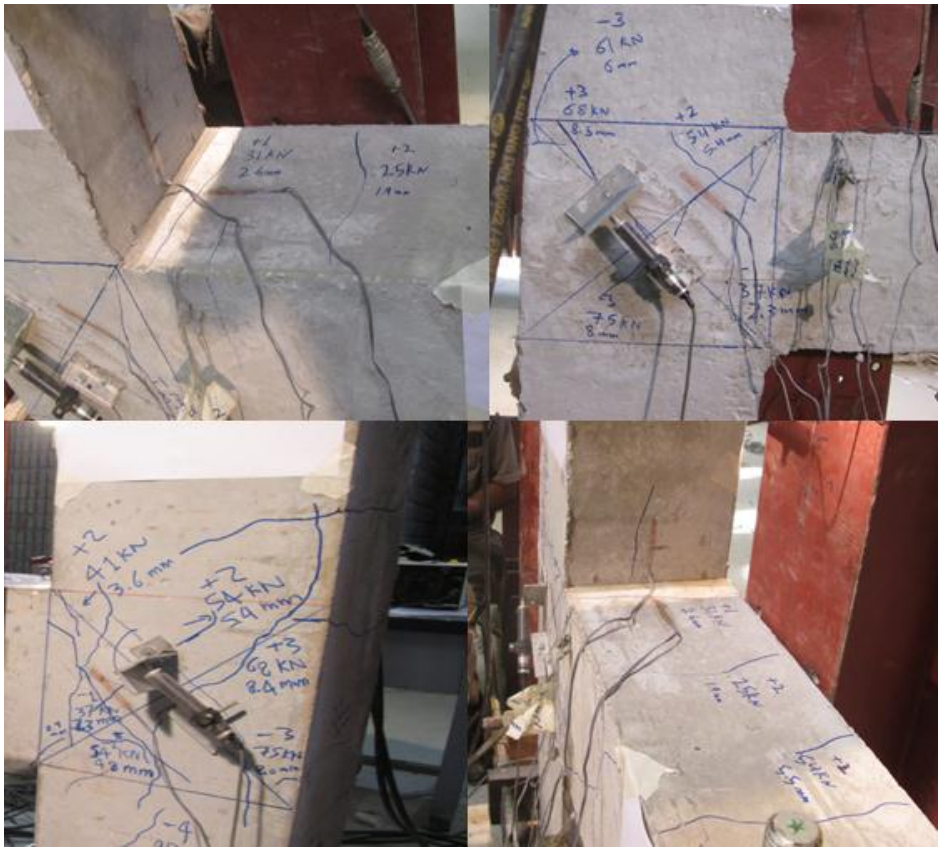

Figure 5-47: Crack pattern specimen NC-BCJ-S-18MM

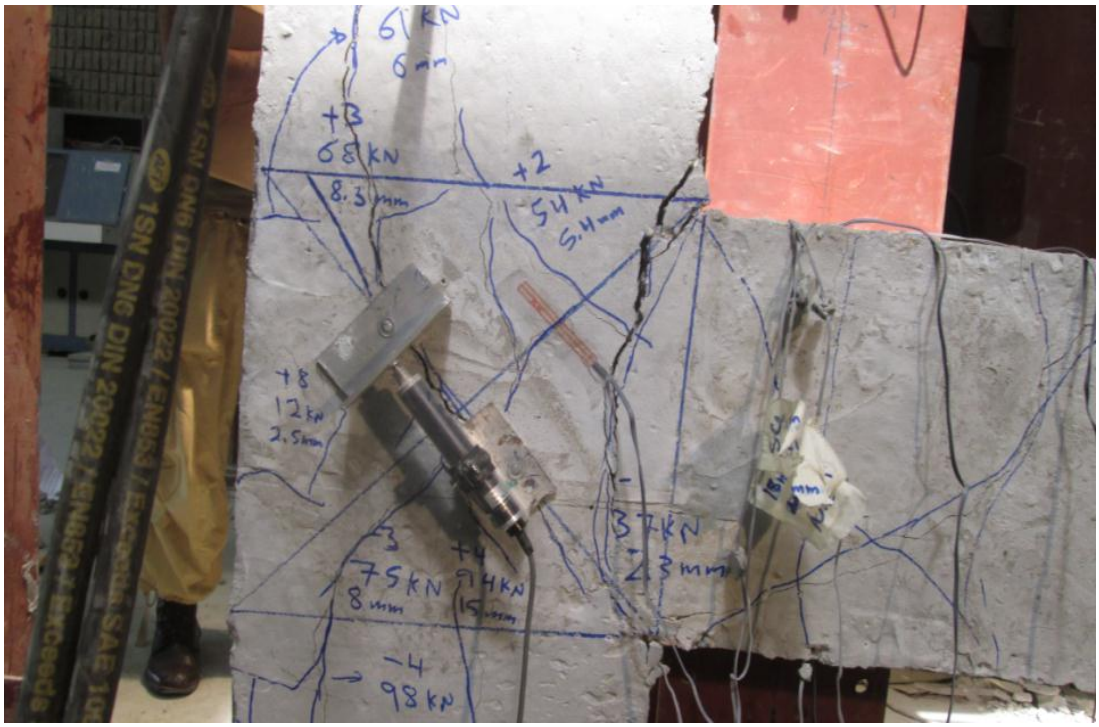

Figure 5-48: Joint damage of specimen NC-BCJ-S-18MM

Steel strain gauges were attached on the steel reinforcement to measure the strain in the steel bars. Figure 5-49 and 5-50 show the variation of strain of the top and bottom beam reinforcement.

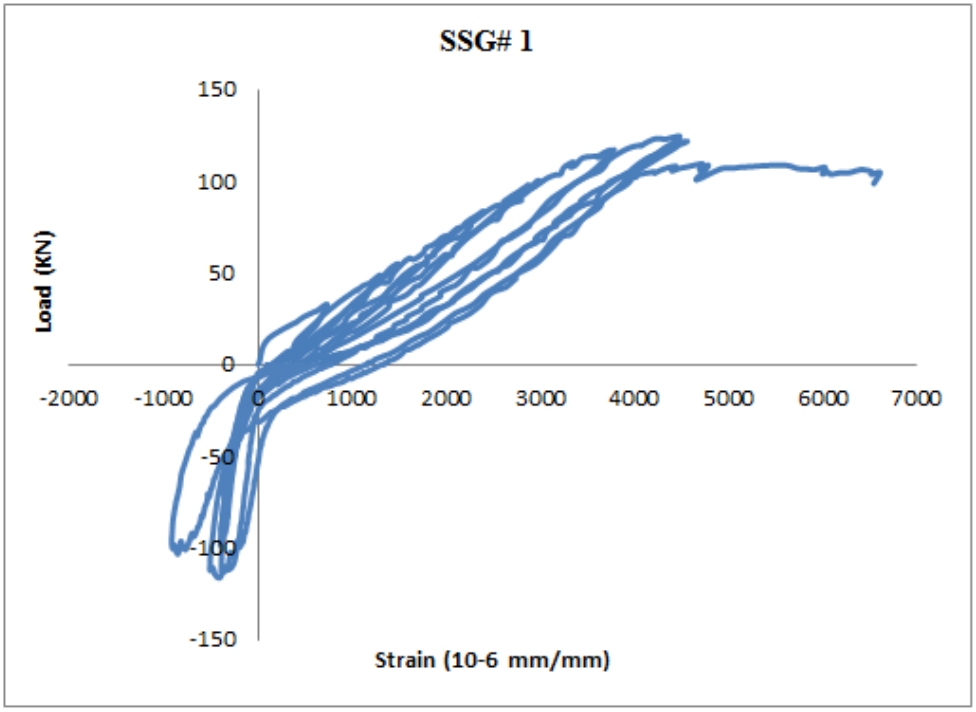

Figure 5-49 Load-strain curve for SSG# 1

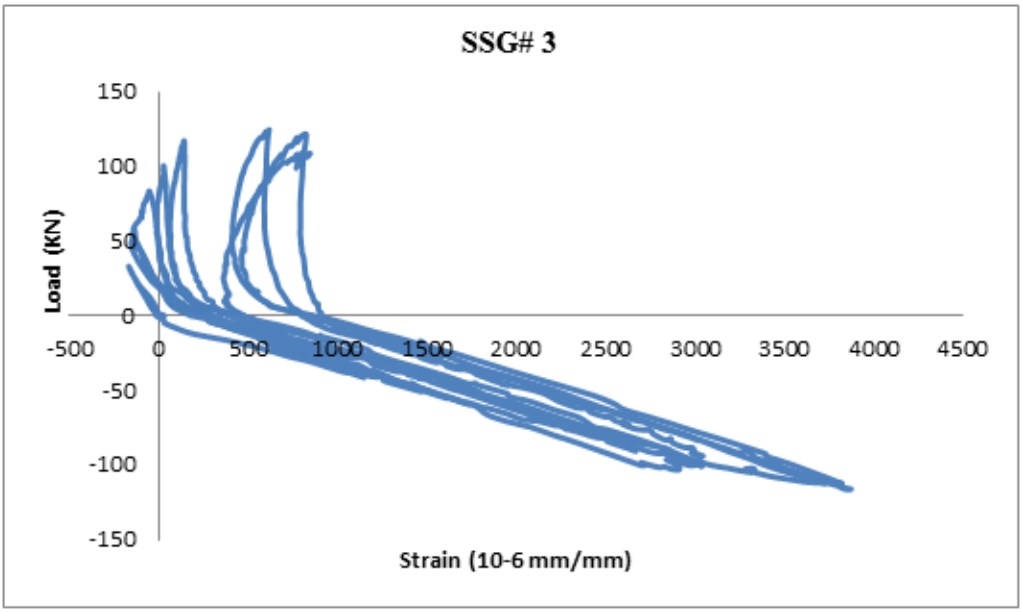

Figure 5-50: Load-strain curve for SSG# 3

5.4.3 Cyclic Test Result for SFRC-BCJ-18MM

The load-displacement graph for SFRC-BCJ-18MM specimen shows that the maximum load in the push and pull cycles were 150 KN and 133 KN respectively (Figure 5-51). The first flexural crack was formed in the beam at load of 38 KN in the first push cycle, while the first shear crack was appeared in the joint area at load of 100 KN in the third push cycle. As the load increased the flexural cracks extends in the beam and many shear cracks formed in the joint region with a small width. The specimen failed due to the flexural damage in the beam (Figure 5-52).

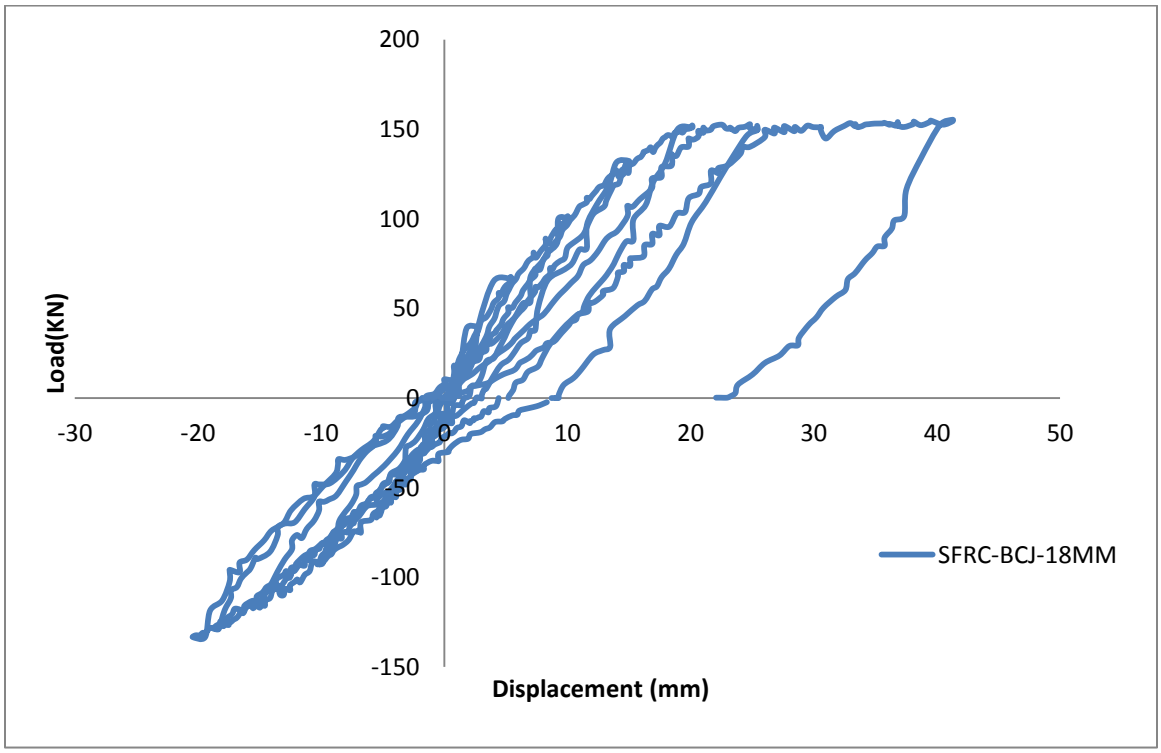

Figure 5-51: Hysteresis loop of SFRC-BCJ--18MM specimen

Figure 5-52: Crack pattern specimen SFRC-BCJ--18MM

Steel strain gauges were used to measure the strain in the steel bars. Figure 5-53 and 5-45 show the variation of steel strain of top and bottom reinforcement of the beam, with the applied load.

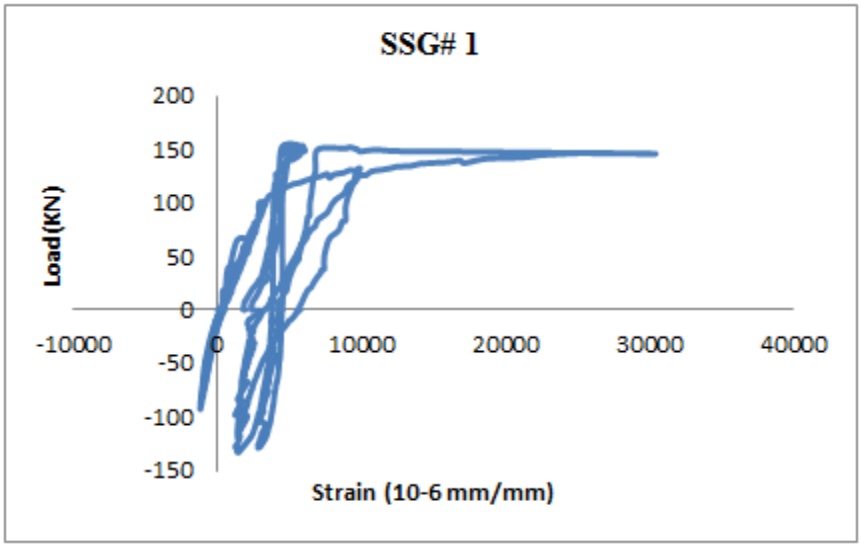

Figure 5-53: Load-strain curve for SSG #1

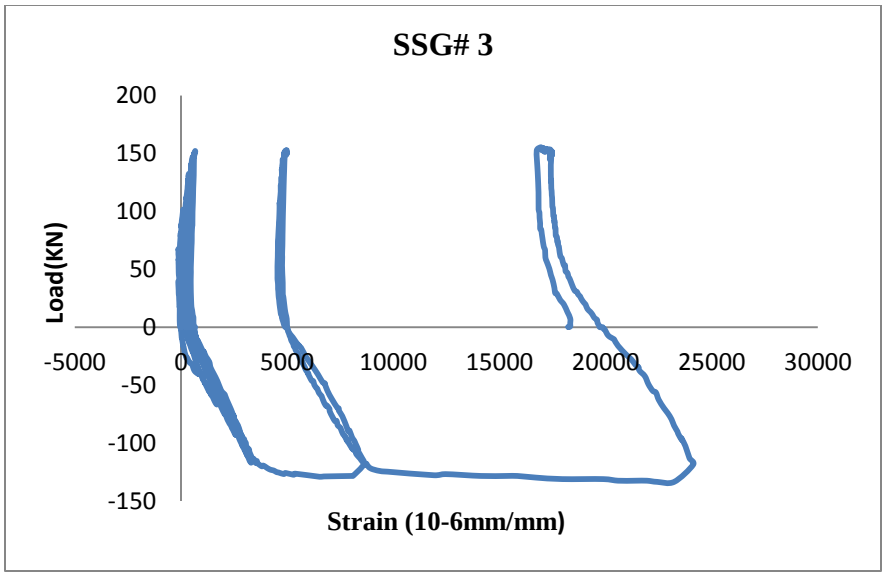

Figure 5-54: Load-strain curve for SSG# 3

5.4.4 Cyclic Test Result for SFRC-BCJ-S-18MM

The load vs. displacement curve for SFRC-BCJ-S-18MM specimen is shown in Figure 5-55. The ultimate loads in pull and push directions were 130 KN and 155 KN respectively. The first flexural crack was occurred in the specimen was in the first push cycle at load of 39 KN. The first shear crack in the joint intersection was occurred in the third push cycle at load of 76 KN. During the test the flexural cracks were extended in the beam and became wider while many fine cracks were formed in the joint (Figure 5-56). The specimen failed due to the flexural damage of the beam.

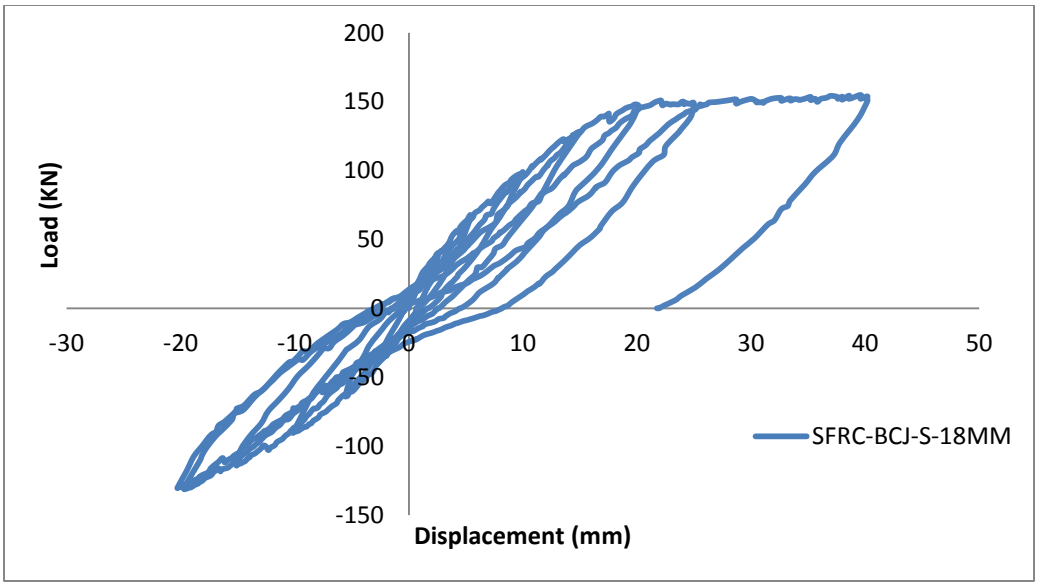

Figure 5-55: Hysteresis loop of SFRC-BCJ-S-18MM specimen

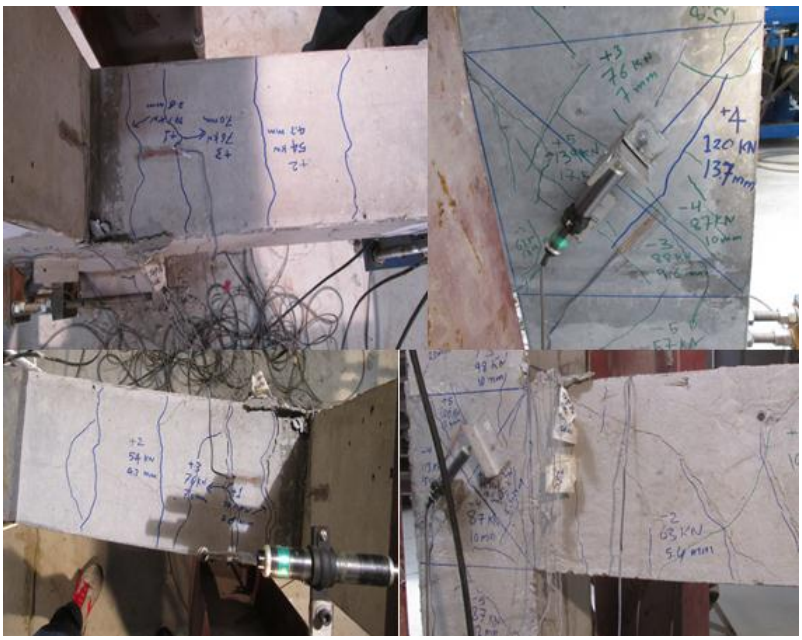

Figure 5-56: Crack pattern specimen SFRC-BCJ-S-18MM

Figure 5-57 and 5-58 show the strain in top and bottom beam reinforcement with the cyclic load which was applied on the tip of the beam.

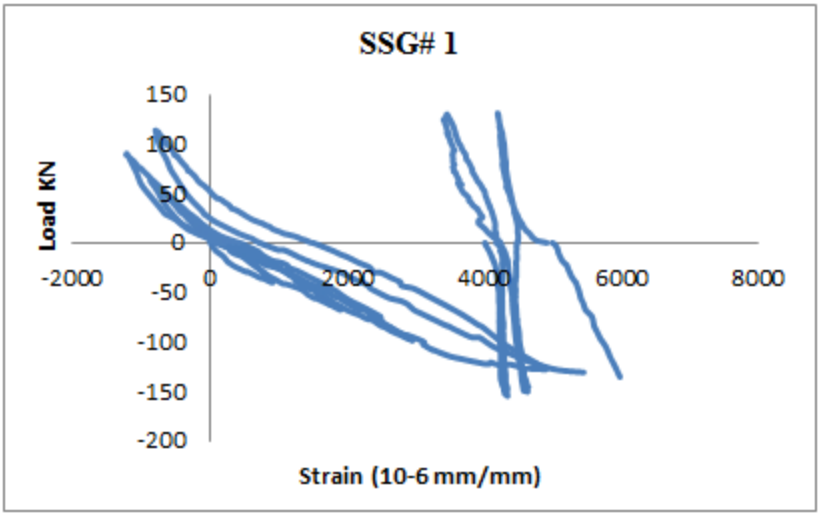

Figure 5-57: Load-strain curve for SSG# 1

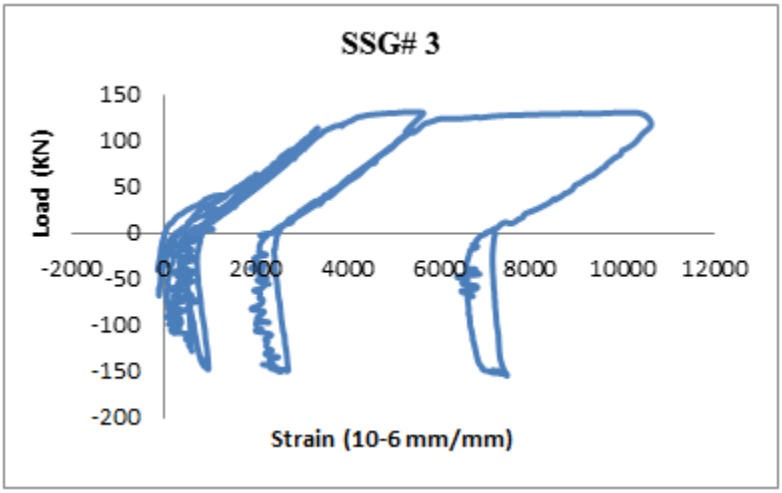

Figure 5-58: Load-strain curve for SSG# 3

5.4.5 Cyclic Test Result for UHPC-BCJ-18MM

The maximum loads in the push and pull directions of the strengthened specimen (UHPC-BCJ-18MM) were 157 KN and 115 KN respectively (Figure 5-59). At load of 44 KN the first flexural crack was formed, while no diagonal cracks appeared in the joint

area during the test. As the load increased the flexural cracks extended in the beam. The specimen failed due to the flexural damage in the beam (Figure 5-60).

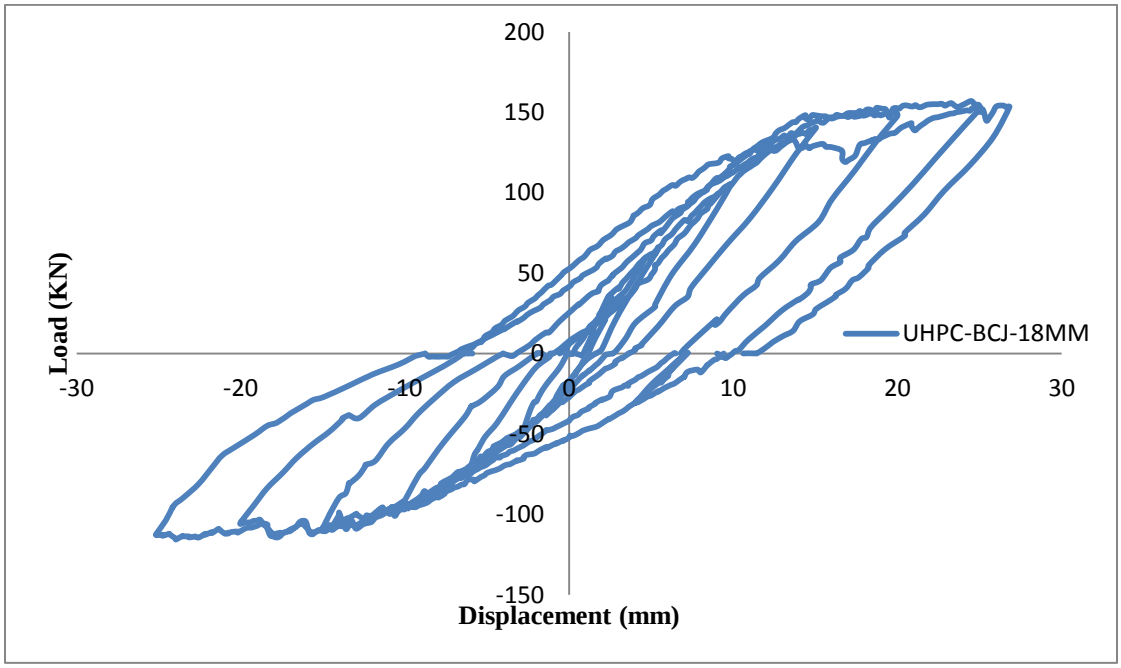

Figure 5-59: SFRC-BCJ-S-18MM specimen

Figure 5-60: Crack pattern specimen UHPC-BCJ-18MM

Several steel strain gauges were installed on the steel cage of the specimen Figure 5-61 and 5-62 show the strain of top and bottom beam reinforcement.

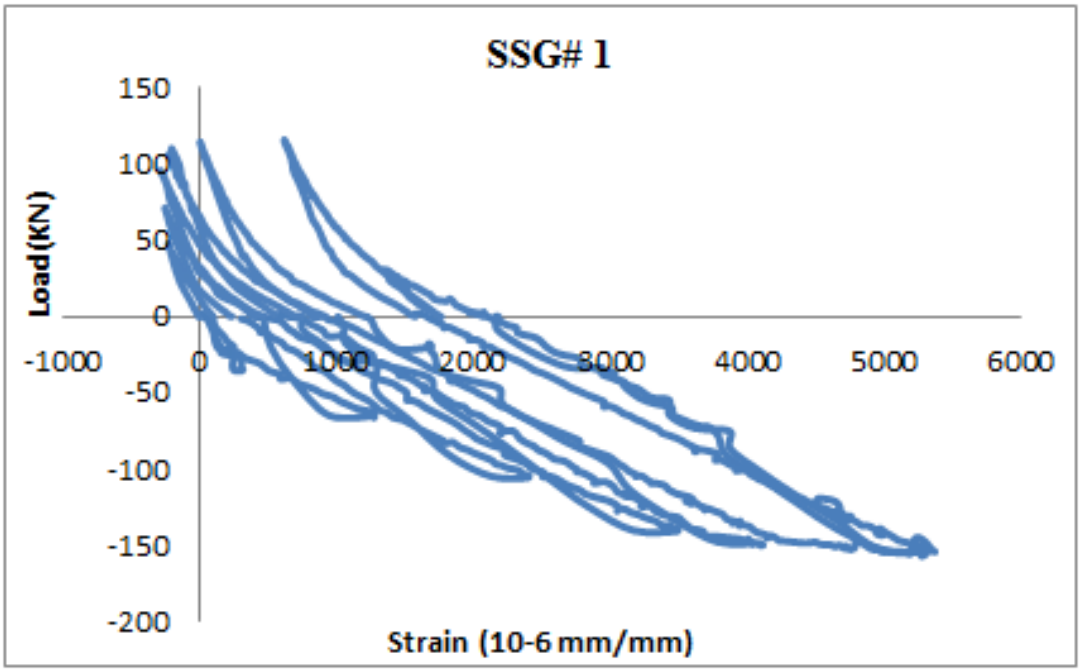

Figure 5-61: Load-strain curve for SSG# 1

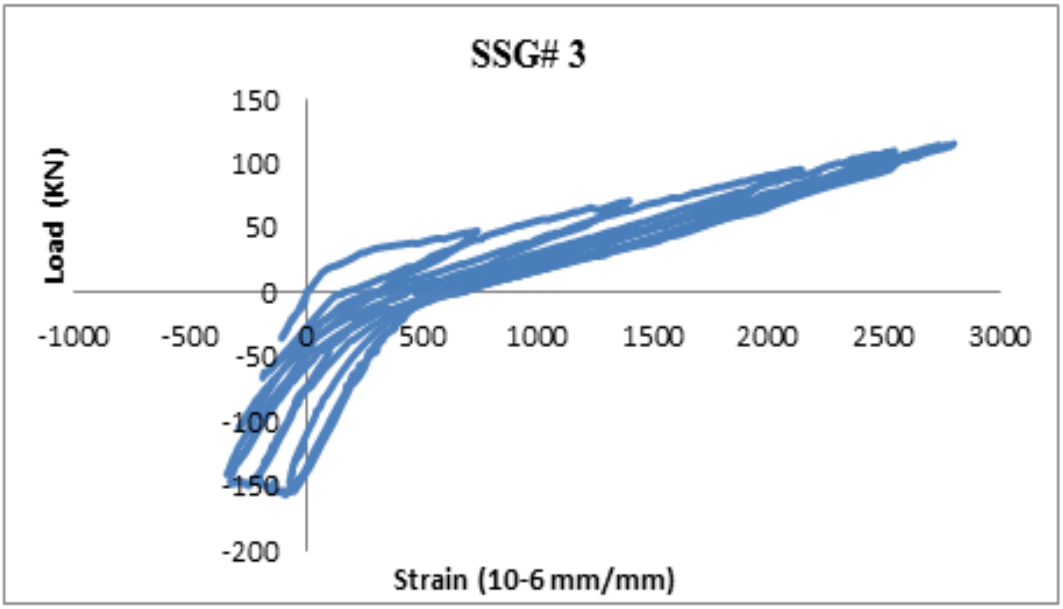

Figure 5-62: Load-strain curve for SSG# 3

5.4.6 Cyclic Comparison of Hysteresis of BCJ-18MM Specimens

The damage of the NC-BCJ-18MM specimen was started in the beam at the beam-column interface, then the cracks formed in the joint as the load increased. The specimen failed due to the joint shear damage. The presence of the UHPC and SFC in the strengthened specimens changed the mode of failure from joint shear failure to the preferred flexural failure. Since the tensile strength of the SFC is less than the tensile strength of the UHPC several fine cracks appeared in the SFC joints. The presence of the stirrups in the SFC joint region did not affect the load carrying of the specimen because the main crack was formed in the beam. But the joint region stirrups played a significant role in improving the capacity of NC-BCJ-S-18MM specimen. The stiffness of the strengthened specimens improved and it did not decrease due to the limited capacity of the hydraulic jack (Figure 5-63). Table 5-3 shows the ultimate load and the enhancement of load carrying capacity for BCJ-18MM specimens.

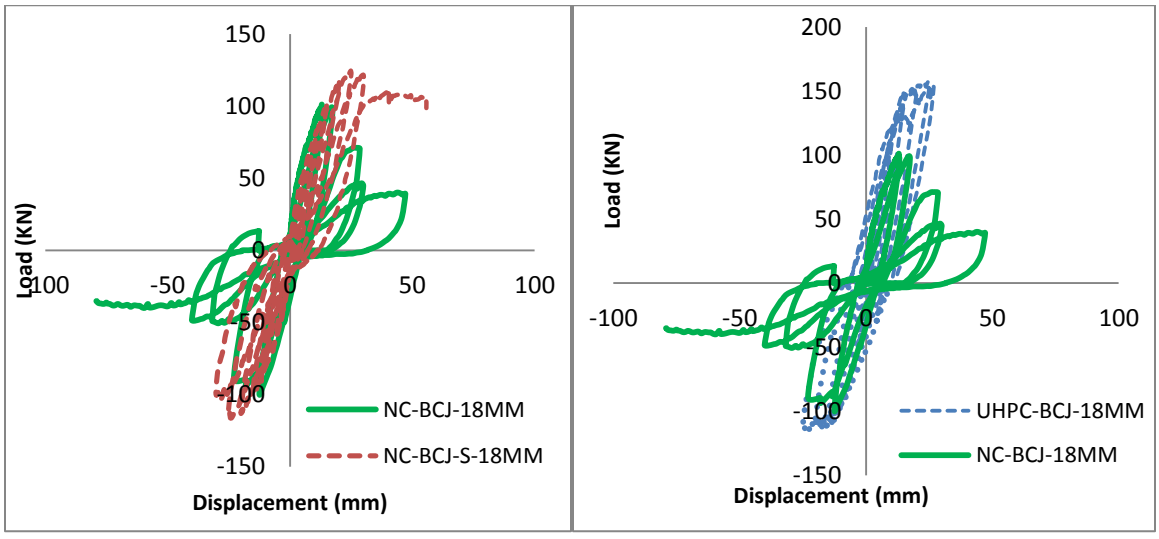

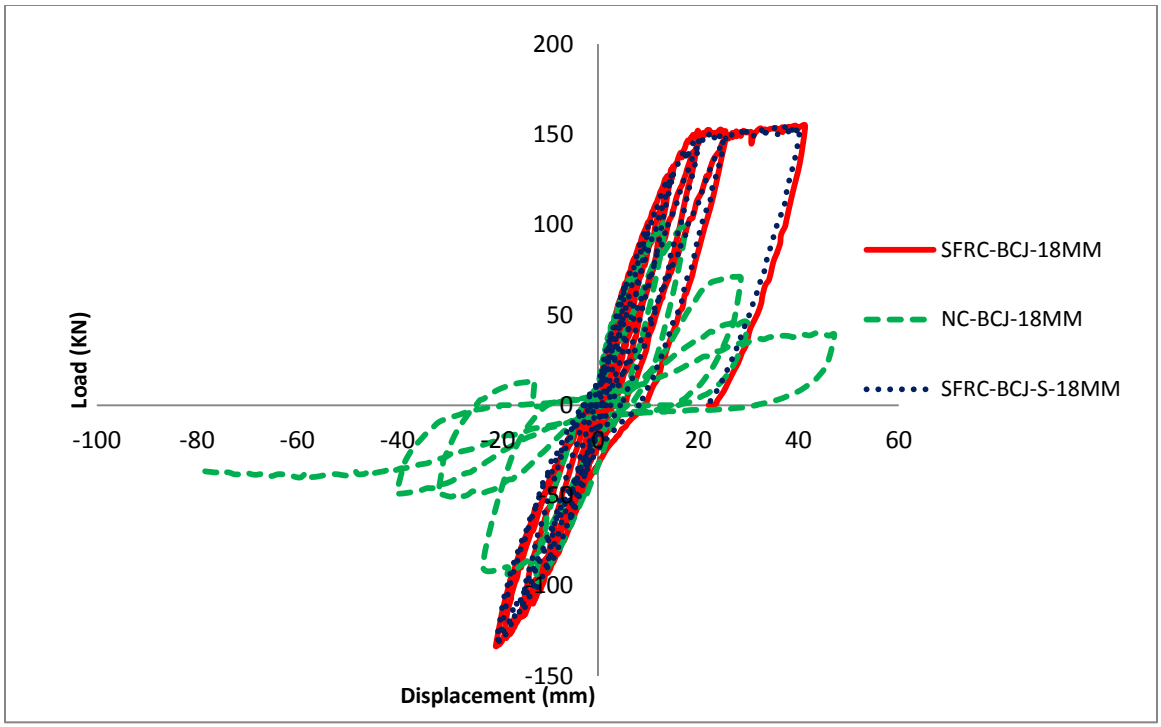

Figure 5-63: Comparison of load-deflection response of all BCJ-12MM specimens

Table 5-3: Ultimate load and mode of failure for BCJ-18MM specimens

Specimens #	Ultimate Load (KN)	Enhancement (%)	Test Type
NC-BCJ-18MM	99	Control	Cyclic
NC-BCJ-S-18MM	123.4	24.65	Cyclic
SFRC-BCJ-18MM	150	51.52	Cyclic
SFRC-BCJ-S-18MM	155	56.57	Cyclic
UHPC-BCJ-18MM	157	58.59	Cyclic

5.5 Equivalent Viscous Damping

Viscous damping coefficient has two components as represented by Blandon and Priestly [2005]:

$EVD = \varepsilon_0 + \varepsilon_{hyst}$

where

ε_0 is the initial damping in the elastic range while ε_{hyst} is the energy dissipation due to the nonlinear behavior of the structure (hysteric). Blandon and Preistly [2005] neglected the elastic value.

The hysteresis equivalent damping corresponding to the nonlinear response ε_{hyst} can be calculated using the following formula:

$\varepsilon_{hyst} = E_D / (4 \pi E_{s0})$

where, E_D is the dissipated energy within a given cycle and E_{s0} is the elastic strain energy.

The equivalent viscous damping (EVD) was calculated for all specimens of beam column joint (Figure 5-64).

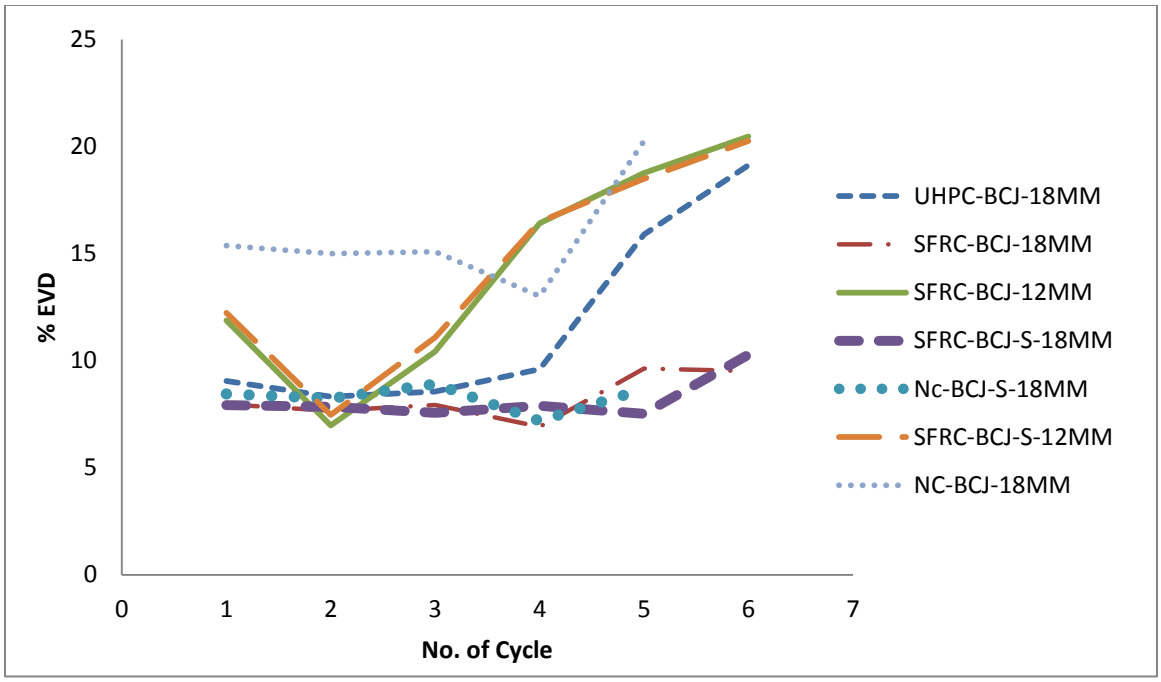

Figure 5-64: Equivalent viscous damping of hysteresis envelope of BCJ specimens

CHAPTER 6

Discussions Of Results Using Experimental Results And Mechanistic

6.1 Experimental Joint Shear Capacity of NC-BCJ-18MM

Two loads were applied on the BCJ specimen, one load was applied on the tip of the beam and the other load was applied on the top of the column. As a result of the applied loads, principal stresses will be developed in the joint intersection region (Figure 6-1).

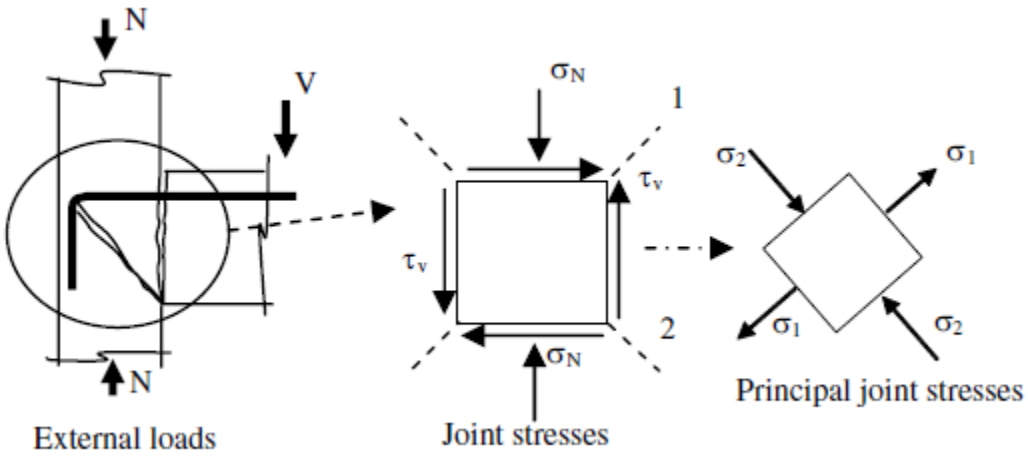

Figure 6-1: External loads, joint stresses, and principal stresses [35]

Using steel strain readings which were recorded experimentally, the joint shear force for NC-BCJ-18MM can be calculated from the following equilibrium equation:

$$V_j = T - V_c \qquad [6.1]$$

where:

Vc: Shear force in the column which is equal to $\frac{P\ lb}{lc}$ (Figure 6-2)

T : The force in the main steel reinforcement of the beam which is equal to $\varepsilon_s \times E_s \times A_s$

ε_s: Strain of beam top reinforcement which is equal to 0.0011 (Figure 5-13) at cracking load of 60 KN.

E_s: Modulus of elasticity.

A_s: Top reinforcement area of the beam.

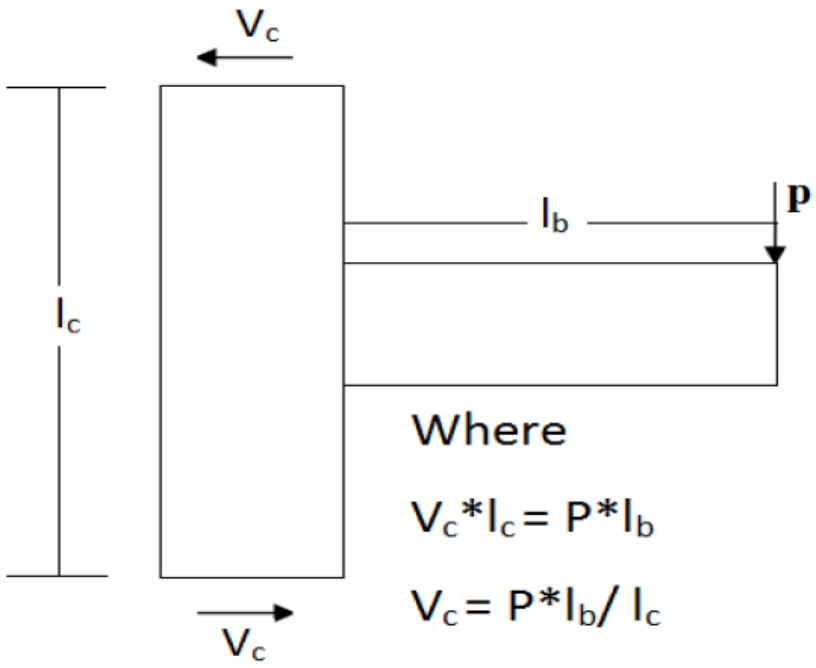

Figure 6-2: Shear in column

Substitute in equation [6.1], the joint shear force can be computed as:

$$Vj = \varepsilon_s \times E_s \times A_s - \frac{P\ lb}{lc}$$

$$= 0.0011 \times 200 \times 763.02 - \frac{60 \times 900}{1400}$$

= 129.3 KN

So the average shear stress $v_{jh} = \frac{Vj}{Aj} = \frac{129.3}{250 \times 300}$ = 1.72 MPa

The experimental tensile principal stress can be calculated as:

$$\sigma_{1\,(exp)} = \frac{-\sigma_N}{2} + \sqrt{\left(\frac{-\sigma_N}{2}\right)^2 + v_{jh}^2} \qquad [6.2]$$

$\sigma_{N\,=}$ column axial stress $\left(\frac{N}{Ag}\right) = \frac{150000}{300 \times 250}$ = 2 MPa

$\sigma_{1\,(exp)}$ = 0.99 MPa

$\sigma_{1\,(exp)}$ can be expressed in terms of $\sqrt{fc'}$ as follows:

$\sigma_{1\,(exp)} = k\sqrt{fc'}$ = 0.99

k = 0.18 (fc'= 30 MPa)

The joint shear force at the ultimate load which was 99.2 KN can be calculated as

Vj = T – Vc [6.1]

Substituting in equation [6.1] the shear force can be computed as follows:

$Vj = \varepsilon_s \times E_s \times A_s - \frac{P\ lb}{lc}$

= $0.002 \times 200 \times 763.02 - \frac{99.2 \times 900}{1400}$

= 241.44 KN

So the shear stress $v_{jh} = \frac{Vj}{Aj} = \frac{241.44}{250 \times 300} = 3.21$ MPa

The experimental principal tensile stress $\sigma_{1\,(exp)} = \frac{-\sigma_N}{2} + \sqrt{(\frac{-\sigma_N}{2})^2 + v_{jh}^2}$

σ_N = column axial stress $(\frac{N}{Ag}) = \frac{150000}{300 \times 250} = 2$ MPa

$\sigma_{1\,(exp)} = 2.36$ MPa

$\sigma_{1\,(exp)}$ can be expressed in terms of $\sqrt{fc'}$ as follows:

$\sigma_{1\,(exp)} = k\sqrt{fc'} = 2.36$

$k = 0.43$ (fc' = 30 MPa)

For specimen NC-18D the failure was joint shear failure, in this case substituting of v_{jh} in equation [6.2] would yield the magnitude of the principal stress σ_1 associated with the shear failure of the joint. Table 6-1 shows $\sigma_1 = 0.43\sqrt{fc'}$ for this specimen. Similarly, for specimen NC-12D where substantial joint damage was noted concomitant with yield of beam steel in flexure, the same computation led to $\sigma_1 = 0.4\sqrt{fc'}$.

However, for the other specimens reported in Table 6-1 the failure load was clearly flexural for these cases. In this case, the component v_{jh} is just a measure of the average shear stress (and not joint shear strength), leading to the in equality statement regarding the major principal stress, σ_1.

Table 6-1: Tensile principal stresses at the ultimate load

Specimen #	NC-BCJ-18MM	SFRC-BCJ-18MM	UHPC-BCJ-18MM	NC-BCJ-12MM	SFRC-BCJ-12MM
Ultimate Load (KN)	97.2	156	160	74	79
Mode of Failure	Joint shear failure	Flexure beam failure	Flexure beam failure	Flexure beam failure	Flexure beam failure
Ɛ	0.002	0.005569	0.003839	0.003225	0.004437
T (KN)	305.21	529	507.1	211.17	219.75
V (KN)	241.44	428.71	404.24	163.6	168.96
v_{jh} (MPa)	3.22	5.72	5.39	2.18	2.25
$\sigma_{1\,(exp)}$ (MPa)	$0.43\sqrt{f'c}$ f'c for NC = 30MPa	$\lessdot 0.79\sqrt{f'c}$ f'c for SFRC = 53 MPa	$\lessdot 0.52\sqrt{f'c}$ f'c for UHPC = 108MPa	$0.4\sqrt{f'c}$ f'c for NC = 30 MPa	$\lessdot 0.41\sqrt{f'c}$ f'c for SFRC = 53 MPa

6.2 Shear Strength of the Joints

Several models are available for prediction of the joint shear strength, Tsonos et al. [42] predicted the joint shear strength based on strut and tie model. The joint shear strength can be computed using the following equation:

$$\left[\frac{\alpha\gamma}{2\sqrt{f_c}}\left(1+\sqrt{1+\frac{4}{\alpha^2}}\right)\right]^5+\frac{5\alpha\gamma}{\sqrt{f_c}}\left(\sqrt{1+\frac{4}{\alpha^2}}-1\right)=1 \qquad [6.4]$$

where

γ= joint shear stress expressed as a multiple of $\sqrt{f'c}$

$\alpha = h_b / h_c$

h_b = Total depth of beam

hc = Total depth of column

Jiuru et al. [41] created a model to predict the ultimate joint shear strength of fibre reinforced concrete joints based on the assumption that the concrete can resist tensile stress after cracks occurred. The ultimate shear strength has three contributions, Shear strength resisted by concrete (V_c), Shear strength resisted by steel fibre (V_f), and Shear strength resisted by joint region stirrups (V_s).These are expressed as:

$$V_c = 0.1\left(1+\frac{N}{b_c h_c f_{ac}}\right) b_j h_j f_{ac} \qquad [6.5]$$

$$V_f = 2\frac{l_f}{d_f} v_f b_j h_j \qquad [6.6]$$

$$V_s = f_{ys}\frac{A_{sh}}{S}\left(d - a_s^{'}\right) \qquad [6.7]$$

Ilki et al. [35] reported that the joint shear failure is assumed to correspond to the formation of a diagonal crack in the joint. A diagonal crack is assumed to form when principal tensile stress reaches the tensile strength of concrete. The joint shear strength can be expressed as:

$$\tau_{vc} = 0.5\sqrt{f_c'}\sqrt{1-\frac{N}{0.5\sqrt{f_c'}A_g}} \qquad [6.8]$$

where

$0.5\sqrt{f'c}$ is the concrete tensile strength while Park et al. [43] expressed the tensile strength of the concrete as $0.4\sqrt{f'c}$.

The empirical equation [6.3] is given by ACI to calculate the maximum joint shear strength capacity for properly detailed exterior reinforced concrete beam column joints with the γ=15. Using the above equations the values of ultimate shear strength were computed and compared with the experimental values (Table 6-2).

Table 6-2: Comparison of ultimate shear strength

Specimen	$\mathbf{V_{exp}}$	$\mathbf{V_{th}}$				
		Ilki	**Park**	**ACI**	**Tsonos et al. (1992)**	**Jiuru et al. (1992)**
NC-BCJ-18MM	241	270	227	512	363	210
NC-BCJ-S-18MM	304	381	338	622	474	321
SFRC-BCJ-18MM	429	340	284	680	642	480
SFRC-BCJ-S-18MM	417	450	394	791	753	591
UHPC-BCJ-18MM	404	459	379	971	1302	795
NC-BCJ-12MM	164	270	227	512	363	210
SFRC-BCJ-12MM	169	340	284	680	642	480
SFRC-BCJ-S-12MM	168	450	394	791	753	591

CHAPTER 7

NUMERICAL SIMULATION OF HIGH STRENGTH CONCRETE BCJ

7.1 INTRODUCTION

In recent years, many researchers studied the behavior of reinforced concrete beam column joint numerically using different softwares like ANSYS, Vector 2, ABAQUS, and DIANA, as mentioned in the previous studies in Chapter 2. ABAQUS6.13, (Hibbit, Karlsson et al. 1998) was used in this study in modeling different models of BCJ under monotonic load, which are:

- 3D model for NC-BCJ-18MM.
- 3D model for NC-BCJ-S-18MM.
- 3D model for SFRC-BCJ-18MM.
- 3D model for SFRC-BCJ-S-18MM.
- 3D model for UHPC-BCJ-18MM.
- 3D model for NC-BCJ-12MM.
- 3D model for SFRC-BCJ-12MM.

- 3D model for SFRC-BCJ-S-12MM.

3D nonlinear finite element model was created for different scenarios of strengthening of beam–column joint specimens using ABAQUS 6.13. Concrete in plastic range was defined using concrete damage plasticity model (CDP) while The Longitudinal and transverse steel reinforcement was defined as an elastic-plastic material.

7.2 Material Models

7.2.1 Concrete Damage Plasticity Model

ABAQUS software predicts the concrete behavior by two methods, concrete smeared cracking model and concrete damage plasticity (CDP) model. In this research, CDP was used in defining concrete material. The CDP model needs the elastic modulus, Poisson's ratio, and parameters of the plastic damage which are shown in Table 7-1. CDP model also need the compressive and tensile behavior of concrete.

Table 7-1: Plastic damage parameters

Ψ	Dilatation angle
ε	Flow potential eccentricity
f_{bo}/f_{co}	The ratio of initial equilibrium compressive yield stress to initial uniaxial compressive yield stress
K	The ratio of second stress invariant

v	Viscosity parameter

This model needs the concept of isotropic elastic damage in combination with isotropic tensile and compressive plasticity to define the plastic response of concrete. Tensile cracking and compressive crushing are two main mechanisms of the concrete failure in CDP model. Concrete stress-strain behavior under uniaxial compression after elastic range was represented in terms of stress vs. inelastic strain (crushing strain) and the concrete tension behavior was represented in terms of stress vs. inelastic strain (cracking strain).

Different parameters were used in defining concrete material in ABAQUS. Some parameters were used in defining concrete in the elastic range and others were used to define the concrete in the plastic range. Table 7-2 shows the values which were used in defining the concrete materials in BCJ models. Uniaxial stress-inelastic strain for concrete materials in compression and tension was used in defining concrete material in the plastic range.

Table 7-2: Concrete parameters used in plastic damage model

Concrete Type	**Mass Density (Tone/mm3)**	**Young's Modulus (MPa)**	**Poisson's Ratio**	**Dilation Angle Ψ (Degree)**	**Eccentricity ε**	f_{bo}/f_{co}	**K**
NC	2.39E-9	29000	0.2	36	0.1	1.16	0.67
SFC	2.44E-9	35173	0.2	36	0.1	1.16	0.67
UHPC	2.44E-9	40000	0.2	36	0.1	1.16	0.67

7.2.2 Steel Reinforcement

The Longitudinal and transverse steel reinforcement behavior was defined as an elastic - plastic material (Figure 7-1). Modulus of elasticity, Poisson's ration, and mass density were used in defining the steel reinforcement material in the elastic range Table 7-3.

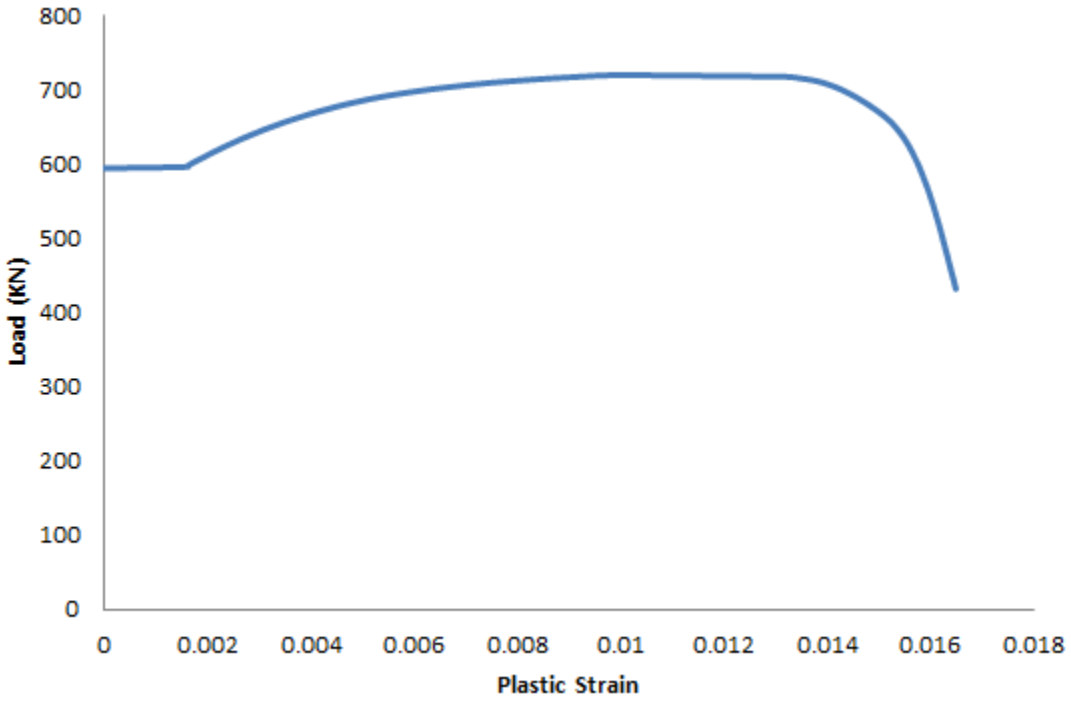

Figure 7-1: Stress-plastic strain for steel

Table 7-3: Parameters used in defining steel reinforcement in the elastic range

Elastic Modulus (MPa)	200000
Poisson's ration	0.3
Mass Density (Tone/mm3)	7.5E-9

7.3 Element Type and Meshing

Several parts were created to model the exterior BCJs. The different parts and their element types are shown in Table 7-4 . The boundary conditions of the column were pin at the bottom of the column while the top of the column was constrained in x and z direction. The column axial load was applied as pressure with value of 2 MPa while the load was applied at one node on the tip of the beam. The model was divided into small elements through meshing (Figure 7-2). The steel cage was created as shown in Figure 7-3 .

Table 7-4: Element properties

Part	Element	Element description
Concrete	C3D8R	8 node linear brick, reduced integration
Steel plate	C3D8R	8 node linear brick, reduced integration
Steel bar	T3D2	2 node truss element

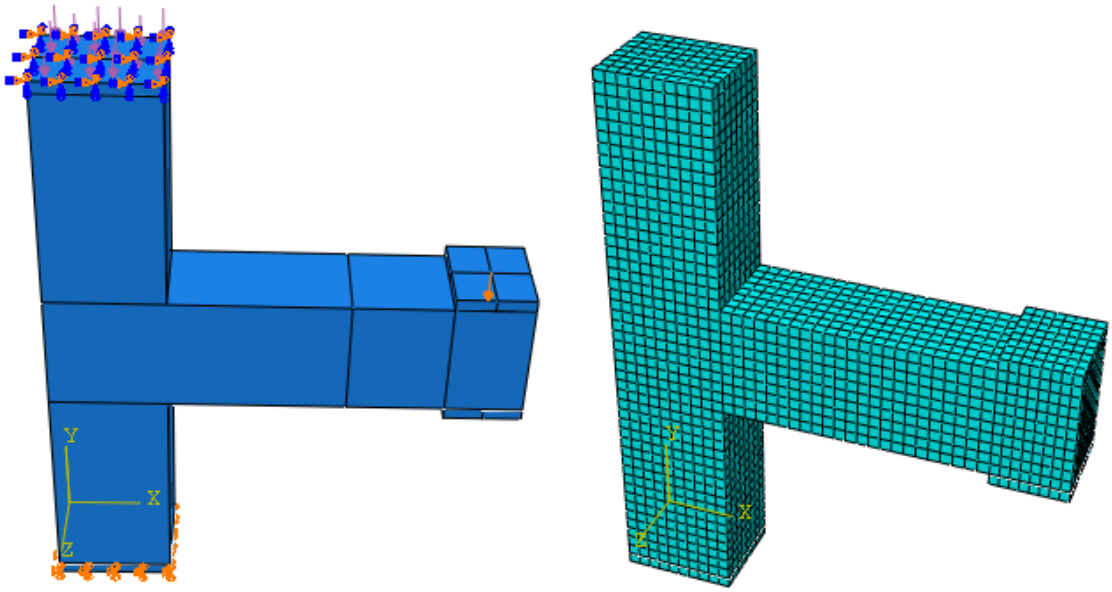

a b

Figure 7-2: (b) Applied loads and boundary condition and (b) 3-D FE model of BCJ Specimen and meshing

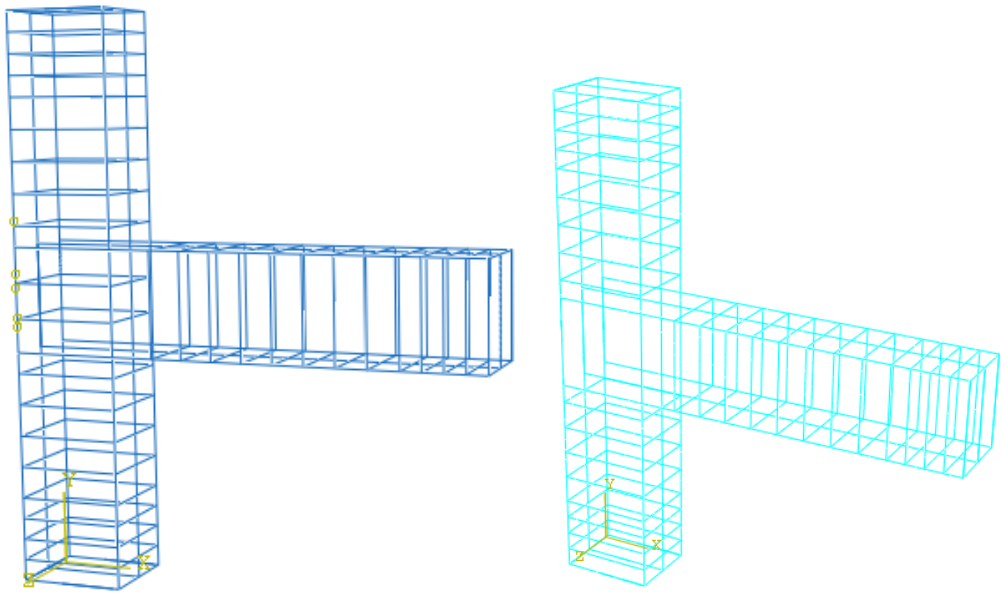

Figure 7-3: Steel cage with and without stirrups in the joint intersection region

7.4 Numerical Simulation of BCJs

7.4.1 Numerical Simulation of NC-BCJ-12MM

The load deflection response for NC-BCJ-12MM is shown in Figure 7-4. The numerical result is closely matching with the experimental result. The steel stress at the yielding load is shown in Figure 7-5. The concrete stresses S11, S22 and S12 is shown in Figure 7-6 to 7-8. The cracks pattern in the specimen was closely correlated with the specimen damage (Figure 7-9).

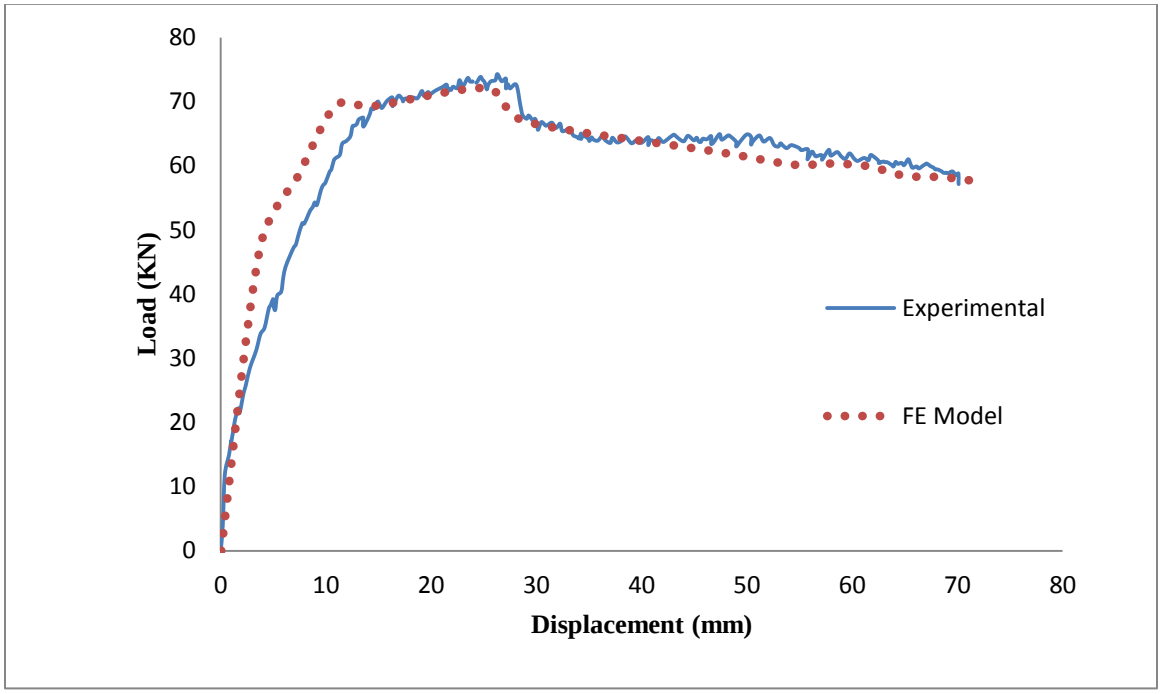

Figure 7-4: Load displacement response for NC-BCJ-12MM

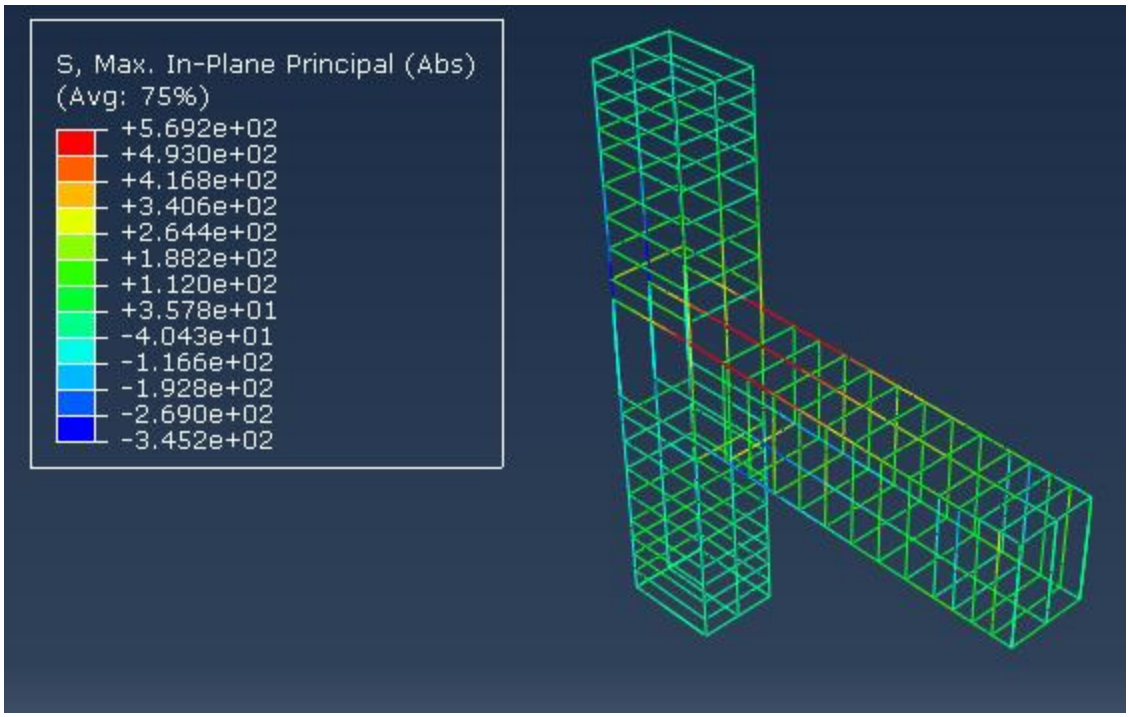

Figure 7-5: Steel stress at yielding load (Δ = 16.7 mm) for NC-BCJ-12MM

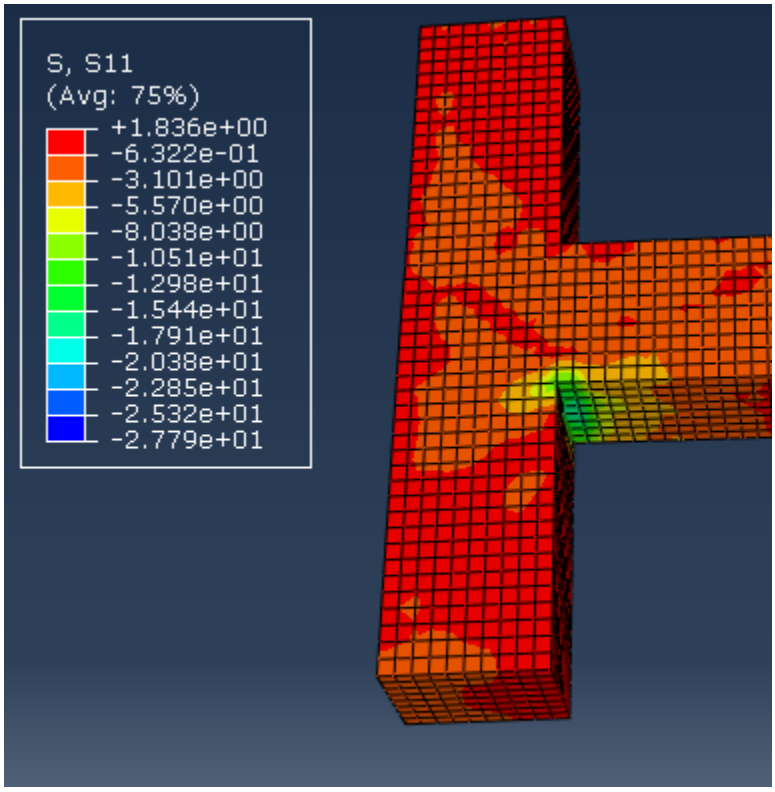

Figure 7-6: Stress S11 in concrete at yielding load (Δ = 16.7 mm) for NC-BCJ-12MM

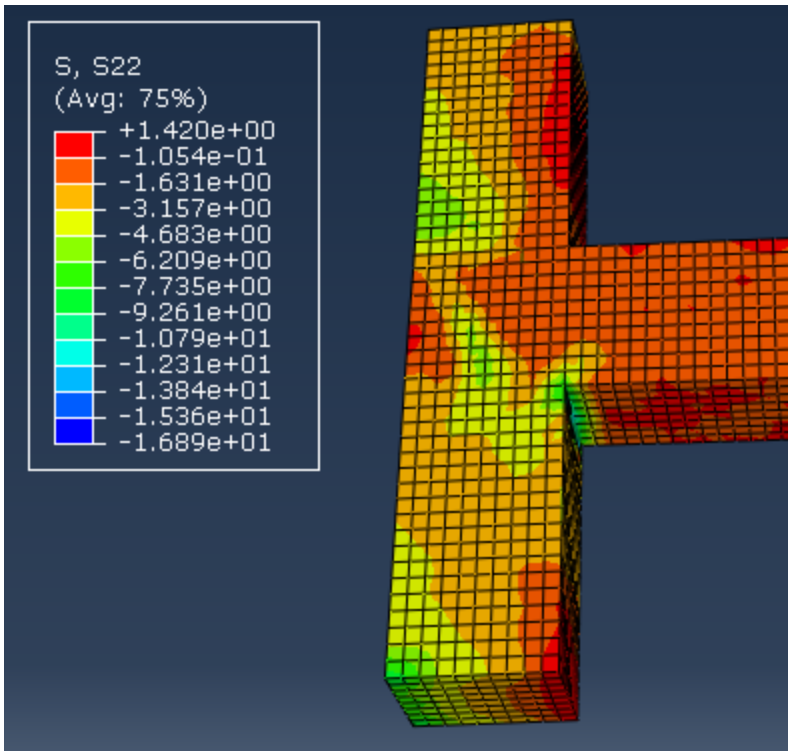

Figure 7-7: Stress S22 in concrete at yielding load (Δ = 16.7 mm) for NC-BCJ-12MM

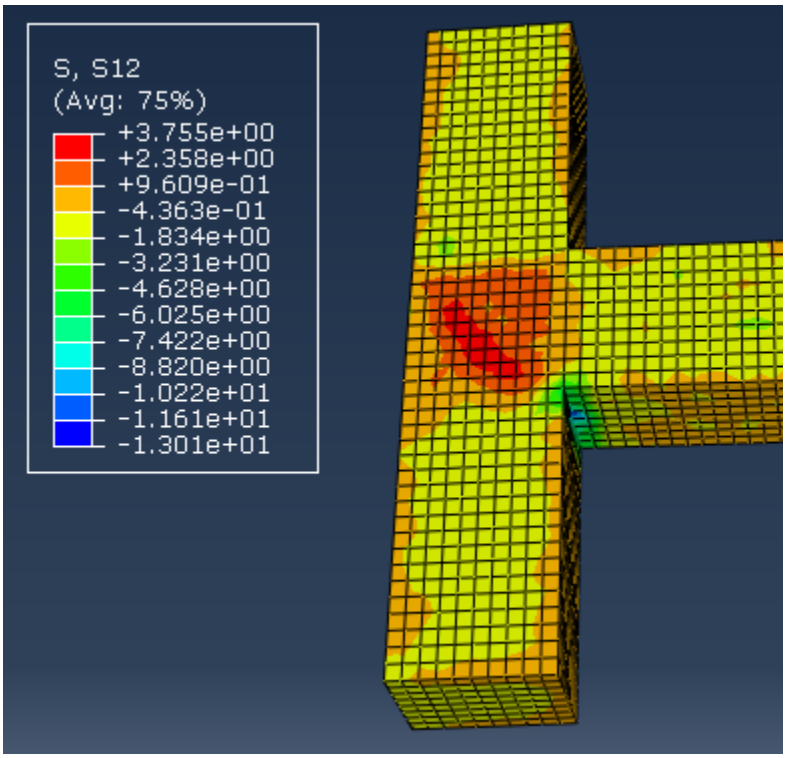

Figure 7-8: Stress S12 in concrete at yielding load (Δ = 16.7 mm) for NC-BCJ-12MM

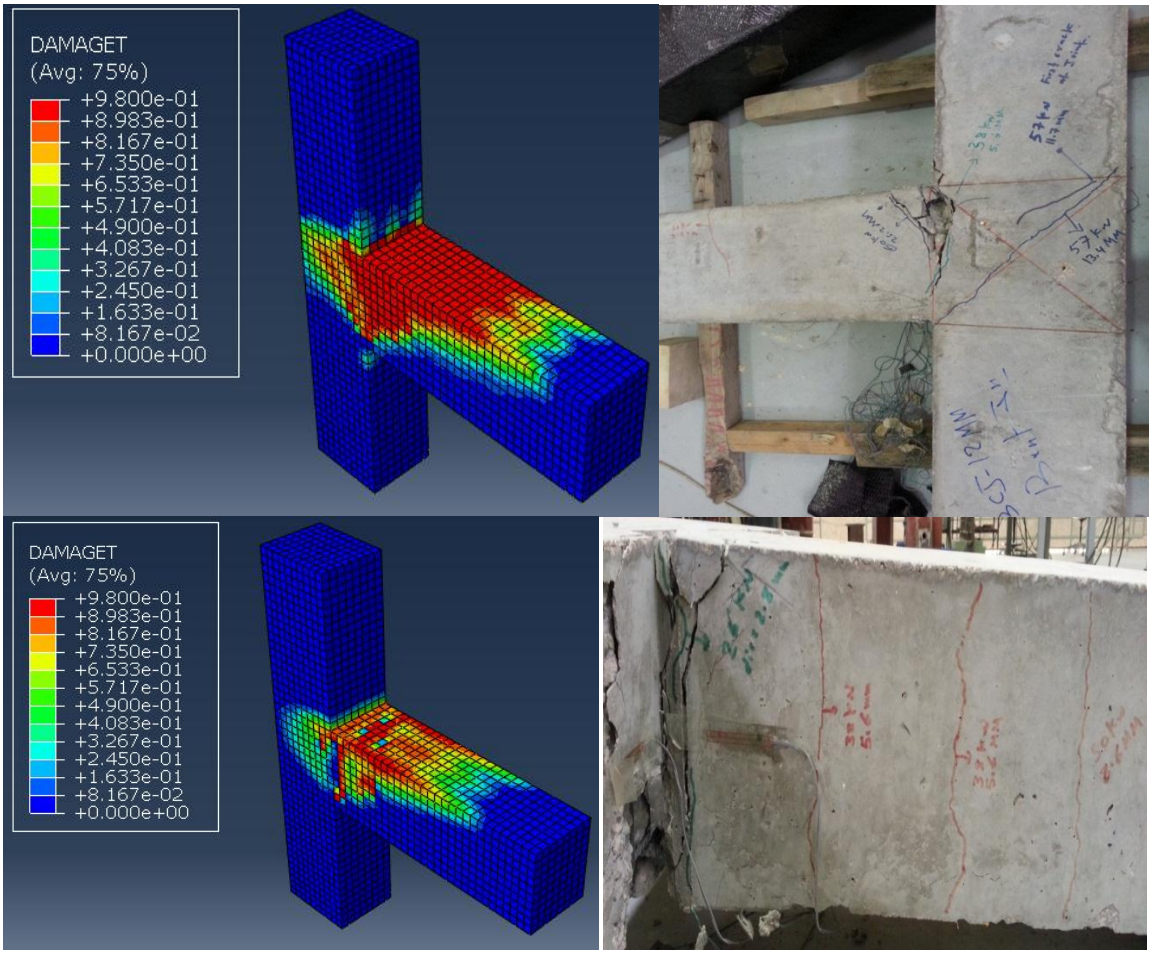

Figure 7-9: Damage propagation and crack pattern from experimental test for NC-BCJ-12MM

7.4.2 Numerical Simulation of SFRC-BCJ-12MM

The load deflection response for SFRC-BCJ-12MM is shown in Figure 7-10. The numerical result is closely matched with the experimental result. The steel stress at the yielding load is shown in Figure 7-11. The concrete stresses S11, S22 and S12 is shown in Figure 7-12 to 7-14. The cracks pattern in the specimen was correlated with the specimen damage (Figure 7-15).

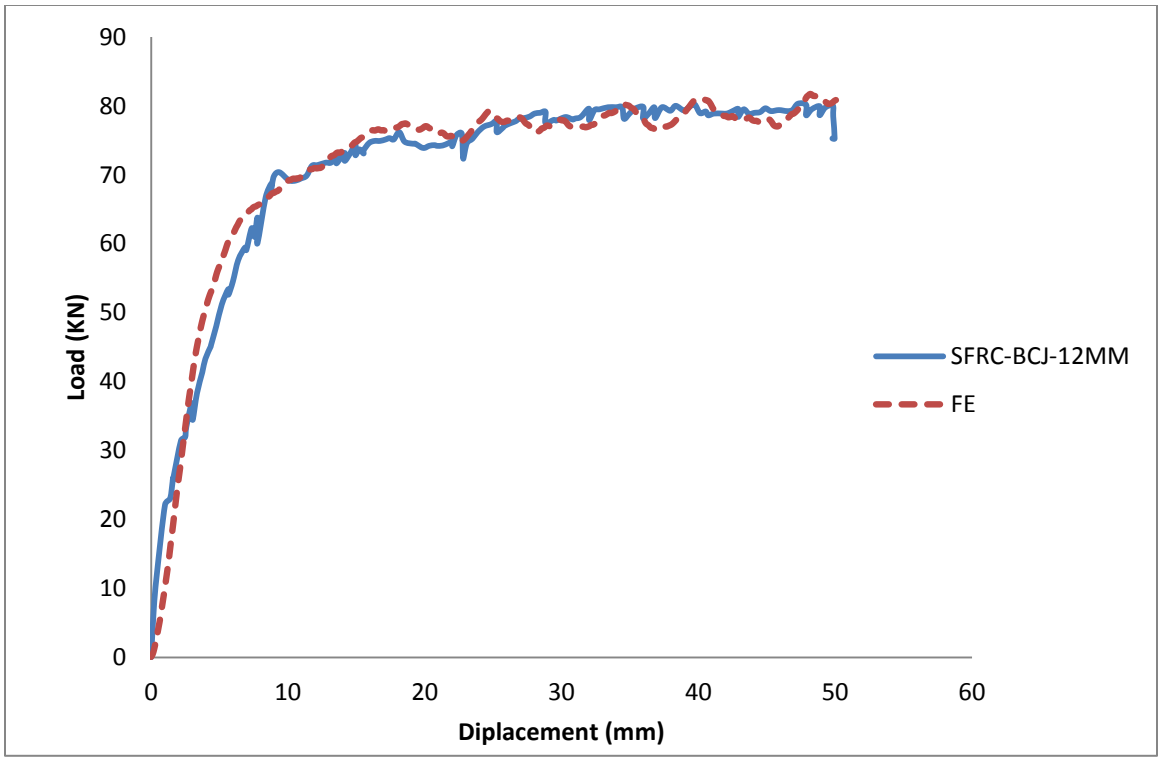

Figure 7-10: Load displacement response for NC-BCJ-12MM

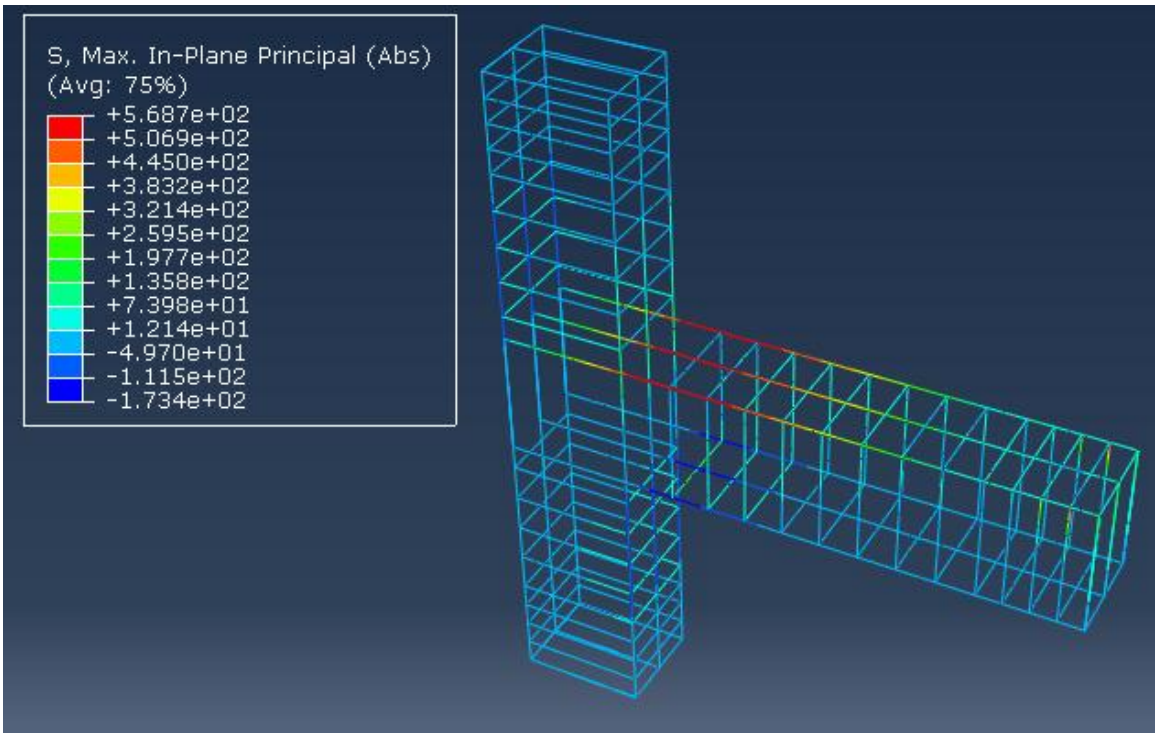

Figure 7-11: Steel stress at yielding load (Δ = 7.63 mm) for SFRC-BCJ-12MM

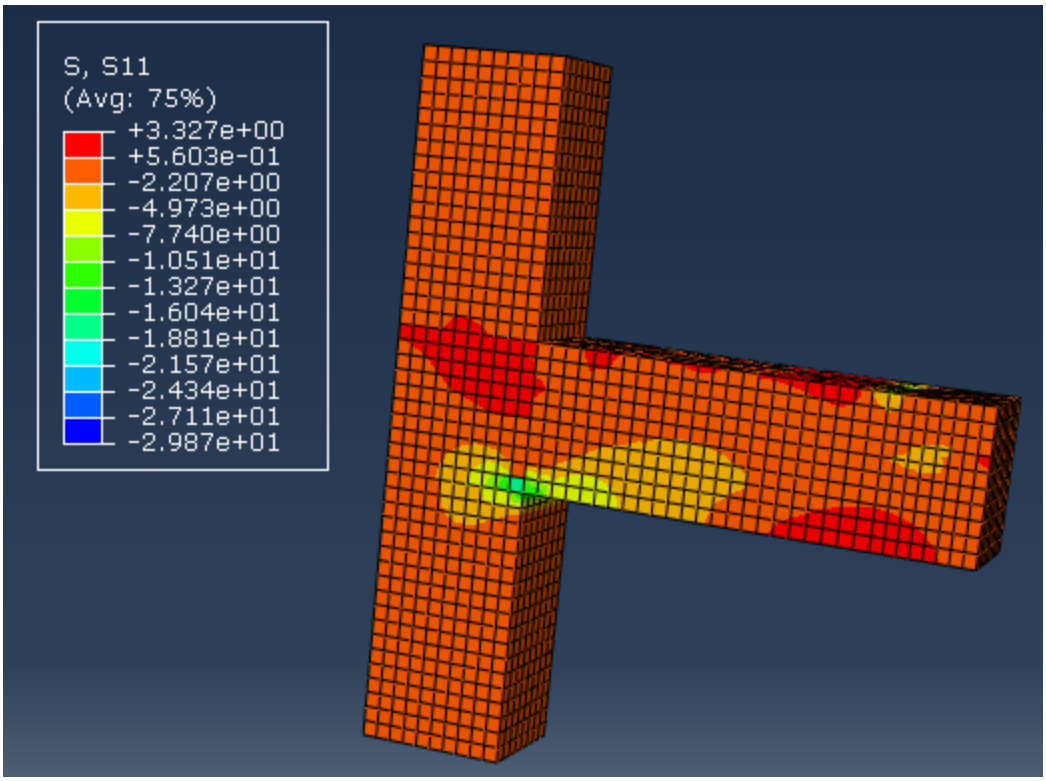

Figure 7-12: Stress S11 in concrete at yielding load (Δ = 7.63 mm) for SFRC-BCJ-12MM

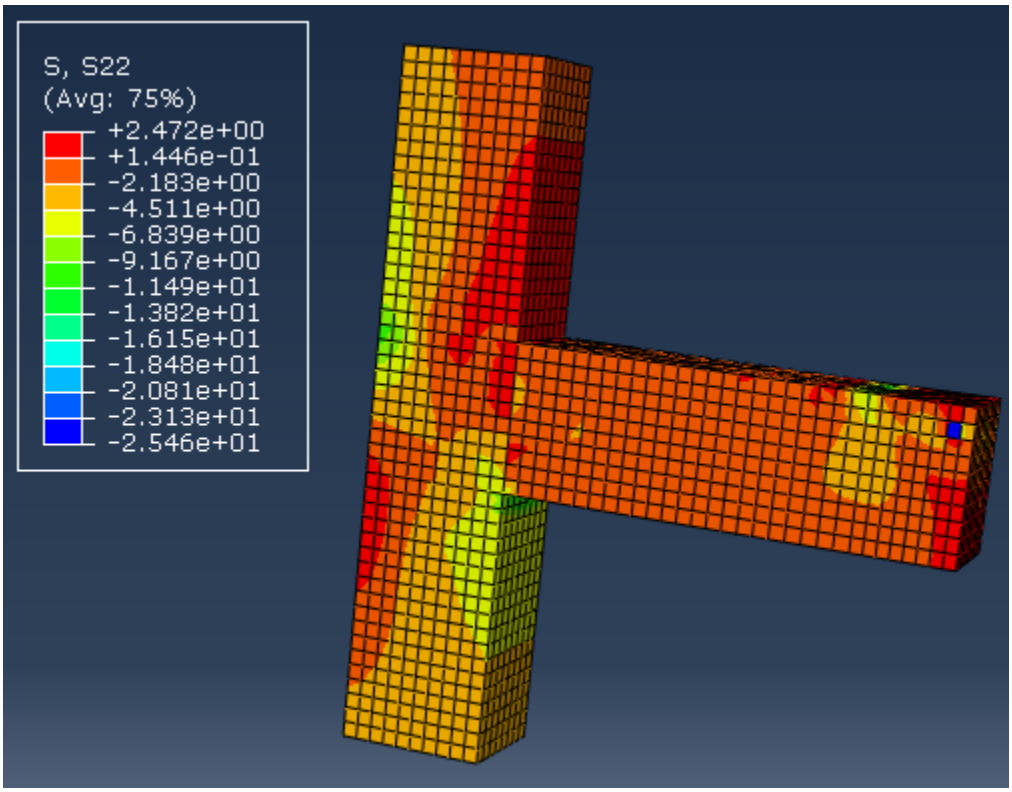

Figure 7-13: Stress S22 in concrete at yielding load (Δ = 7.63 mm) for SFRC-BCJ-12MM

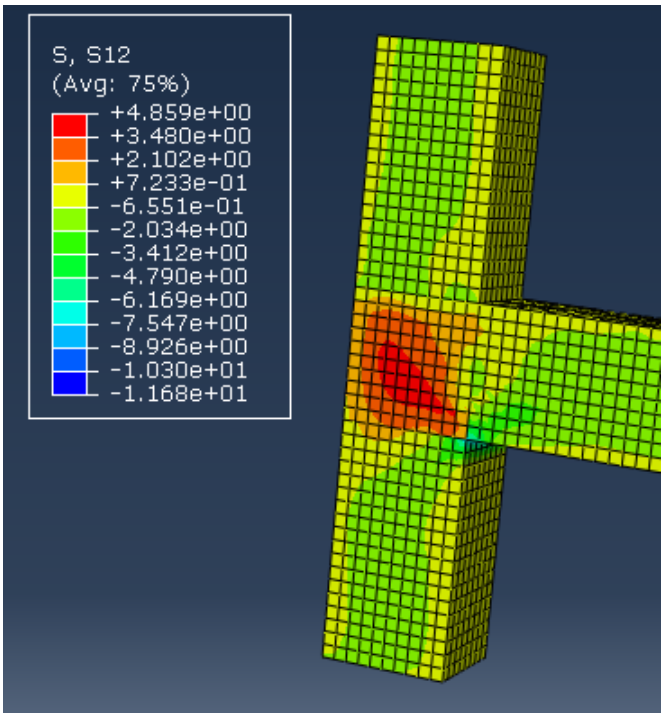

Figure 7-14: Stress S12 in concrete at yielding load (Δ = 7.63 mm) for NC-BCJ-12MM

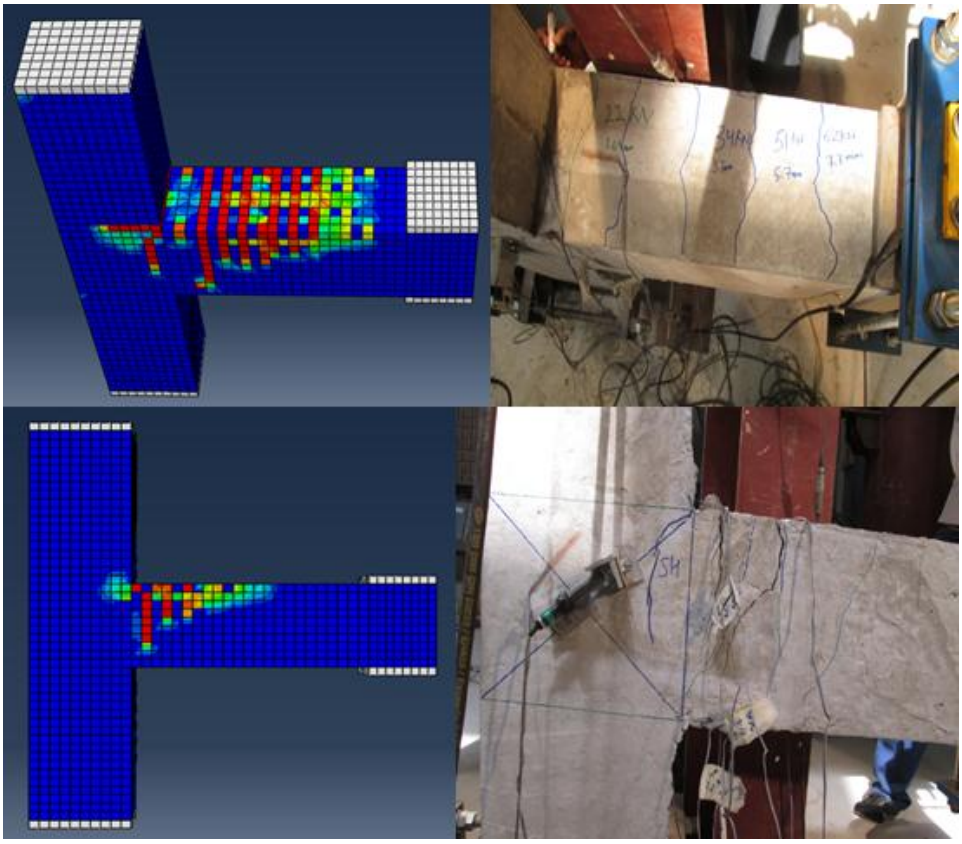

Figure 7-15: Damage propagation and crack pattern SFRC-BCJ-12MM

7.4.3 Numerical Simulation of SFRC-BCJ-S-12MM

The load-deflection curve for SFRC-BCJ-S-12MM is shown in Figure 7-16. The finite element result is closely matched with the experimental result. The steel stress at the yielding load is shown in Figure 7-17. The concrete stresses S11, S22 and S12 is shown in Figure 7-18 to 7-20. The damage in the specimen was same as in the SFRC-BCJ-12MM.

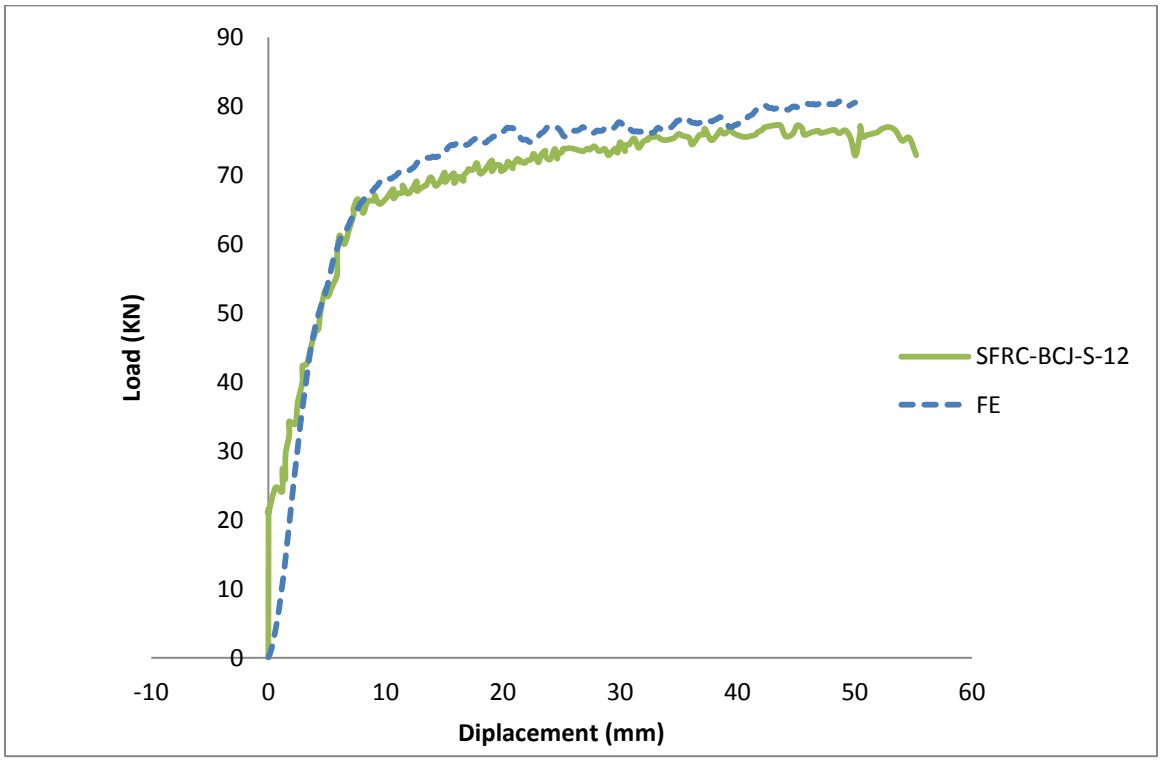

Figure 7-16: Load displacement response for SFRC-BCJ-S-12MM

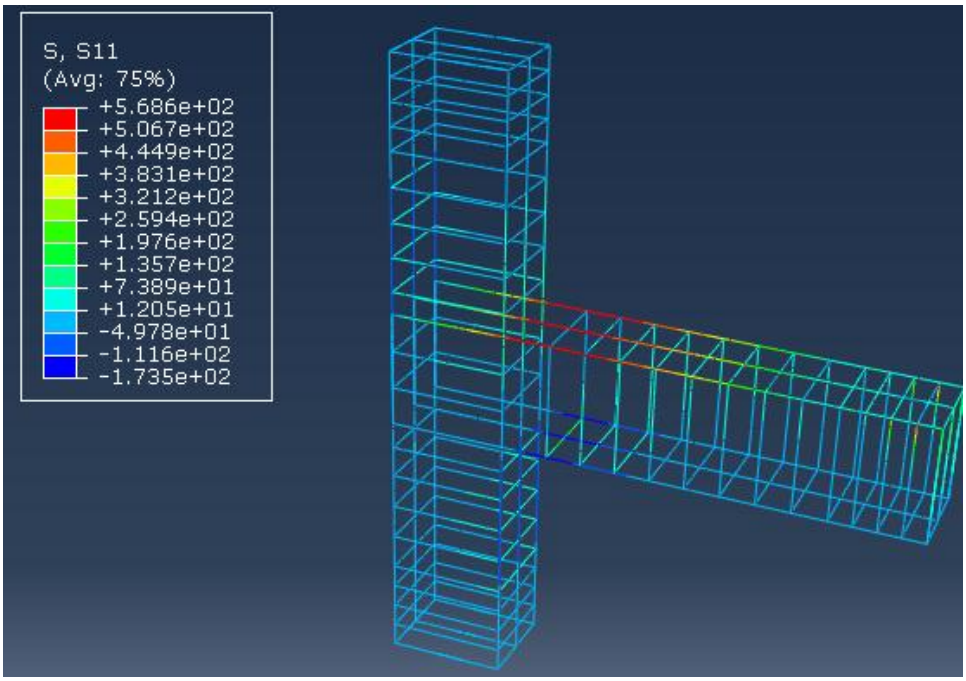

Figure 7-17: Steel stress at yielding load (Δ = 7.63 mm) for SFRC-BCJ-S-12MM

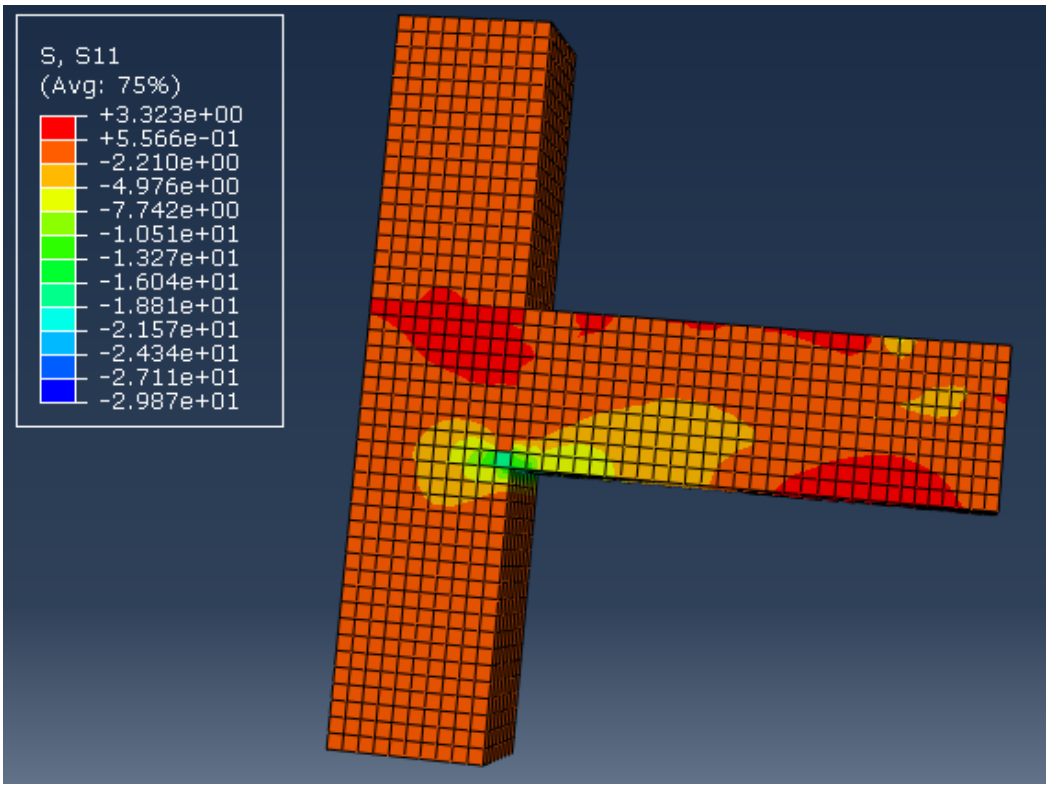

Figure 7-18: Stress S11 in concrete at yielding load (Δ = 7.63 mm) for SFRC-BCJ-S-12MM

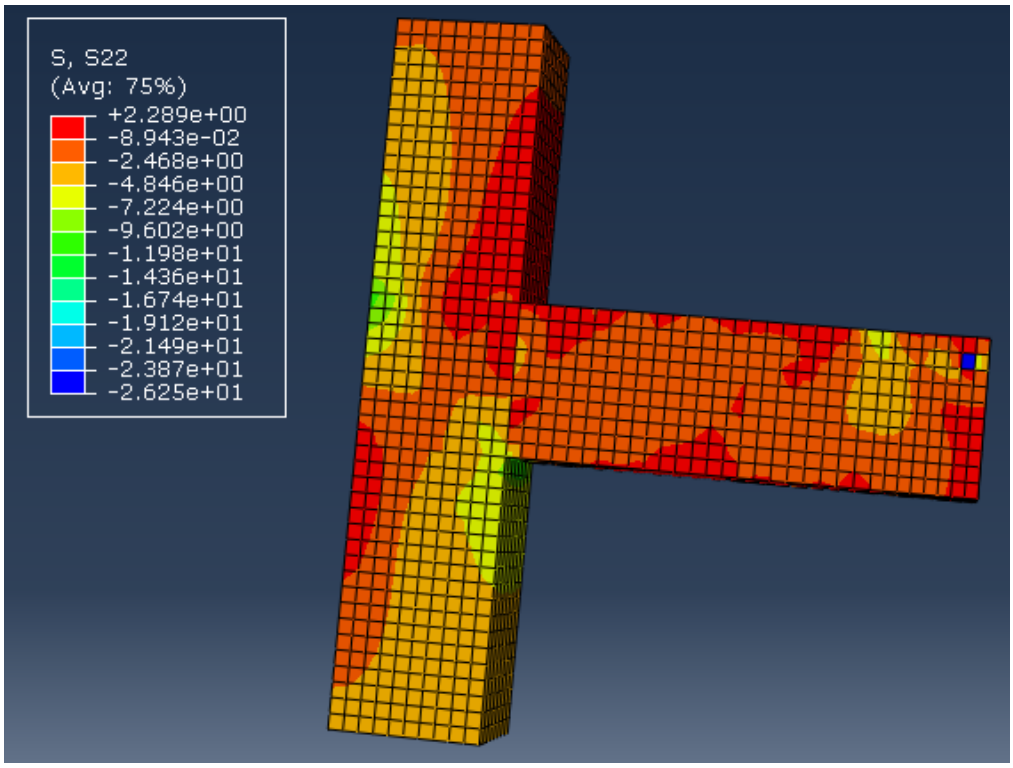

Figure 7-19: Stress S11 in concrete at yielding load (Δ = 7.63 mm) for SFRC-BCJ-S-12MM

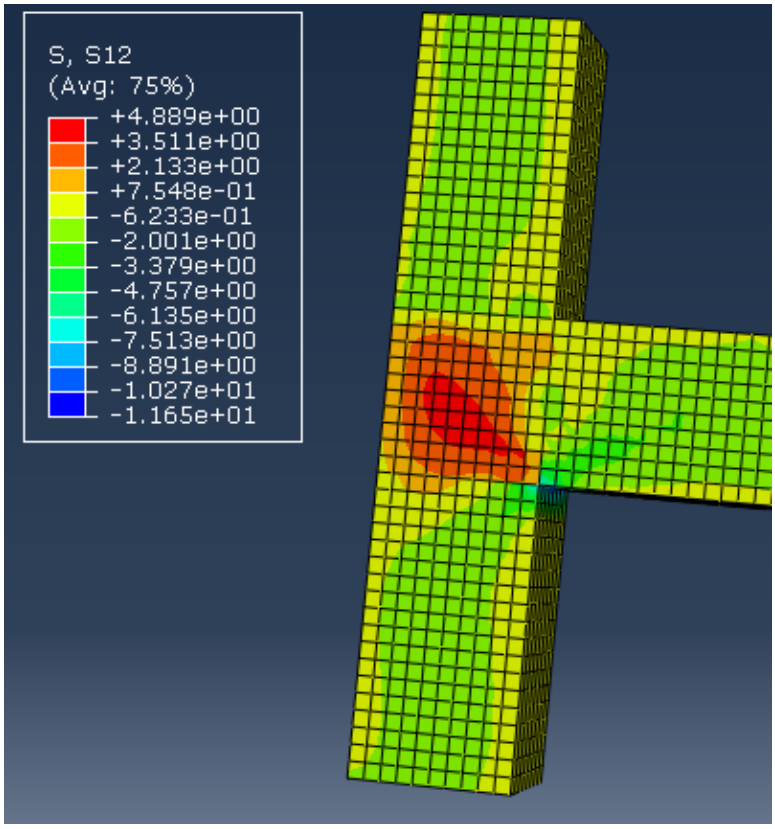

Figure 7-20: Stress S12 in concrete at yielding load (Δ = 7.63 mm) for SFRC-BCJ-S-12MM

7.4.4 Numerical Simulation of NC-BCJ-18MM

The experimental and numerical load-deflection curves of the NC-BCJ-18MM specimen, under monotonic load up to failure are shown in Figure 7-21. The result of finite element simulation matches closely with the experimental results.

The reinforcement stress at ultimate load and displacement of 28.7 mm is shown in Figure 7-22. The stresses S11, S22 and S12 at yielding load are shown in Figure 7-23 to 7-25. The damage in the specimen is closely correlated with the crack pattern (Figure 7-26).

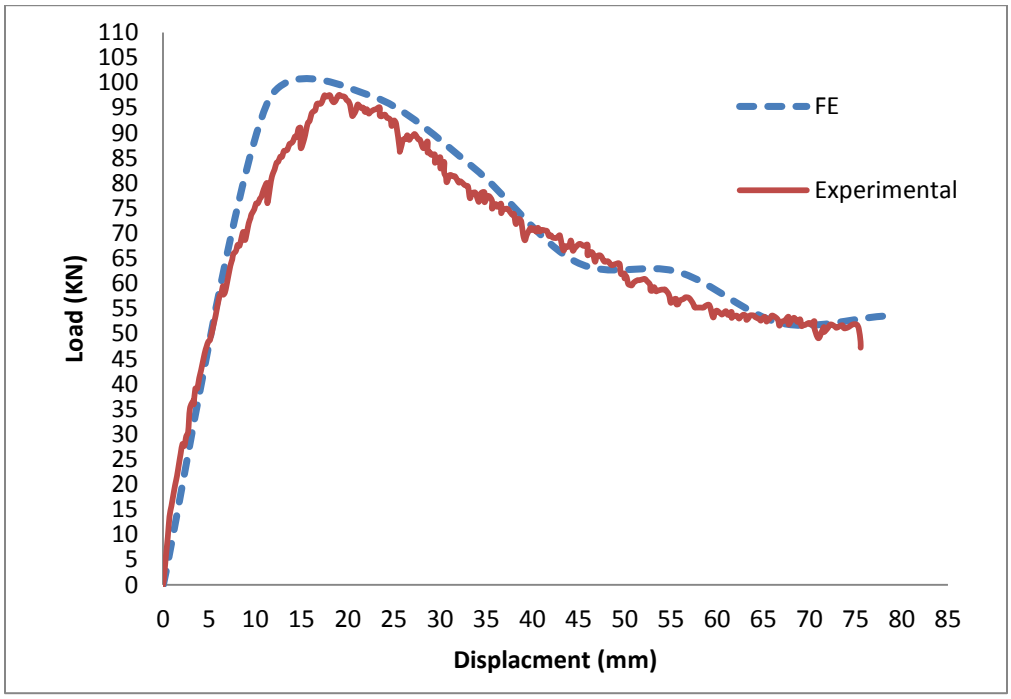

Figure 7-21: Load displacement response for NC-BCJ-18MM

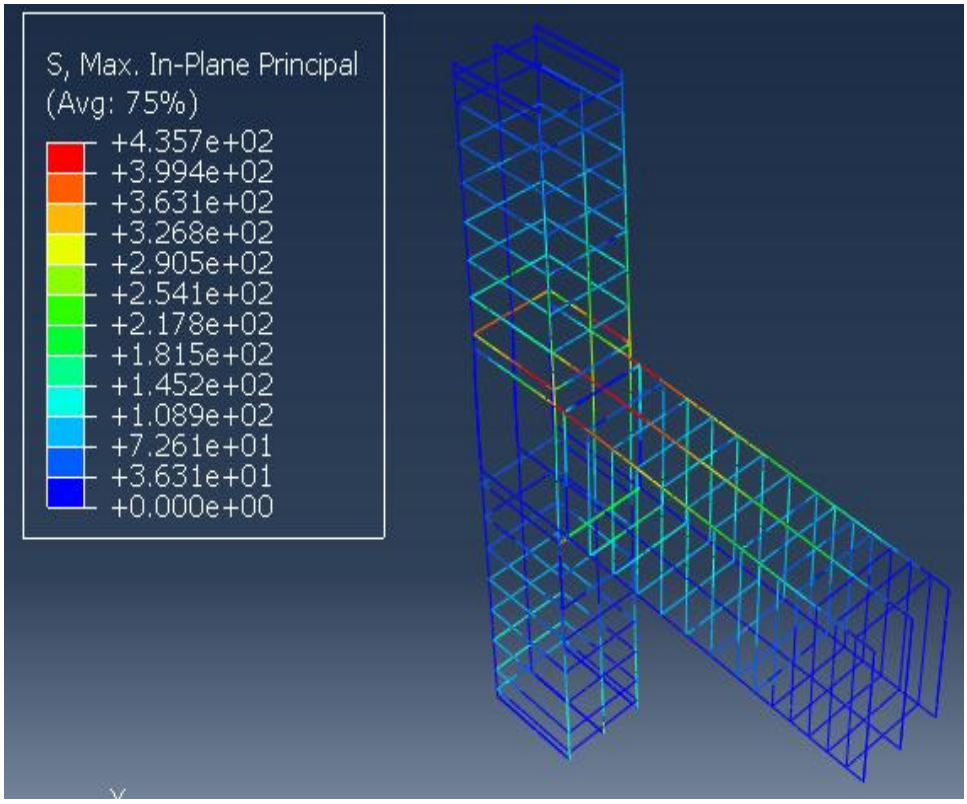

Figure 7-22: Steel stress at ultimate load (Δ = 28.7 mm) for NC-BCJ-18MM

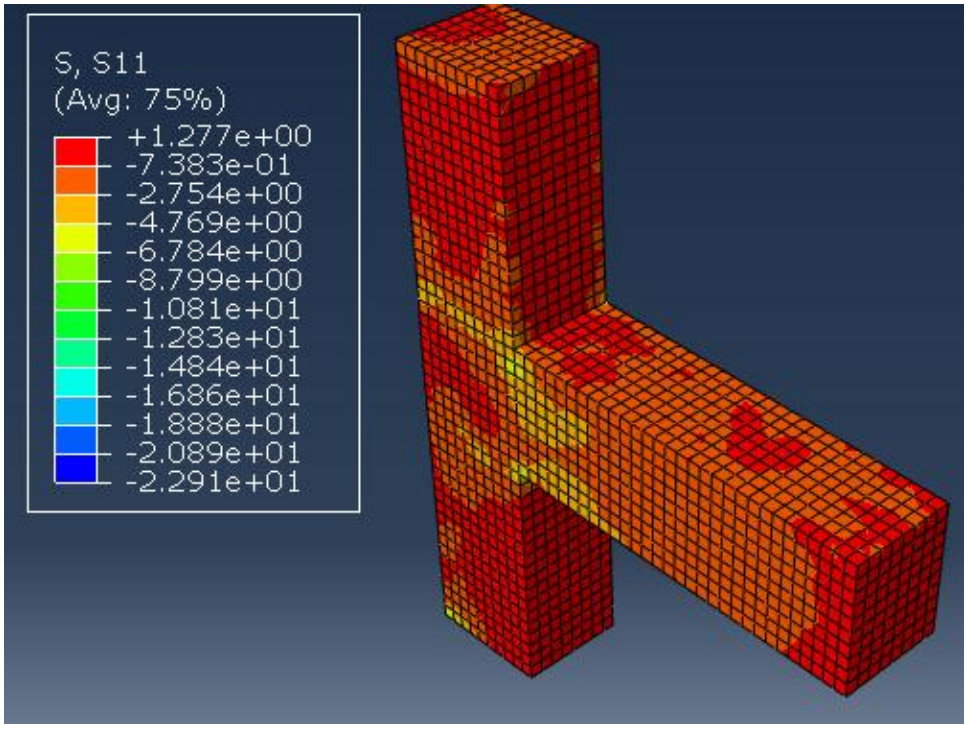

Figure 7-23: Stress S11 in concrete at yielding load (Δ = 21 mm) for NC-BCJ-18MM

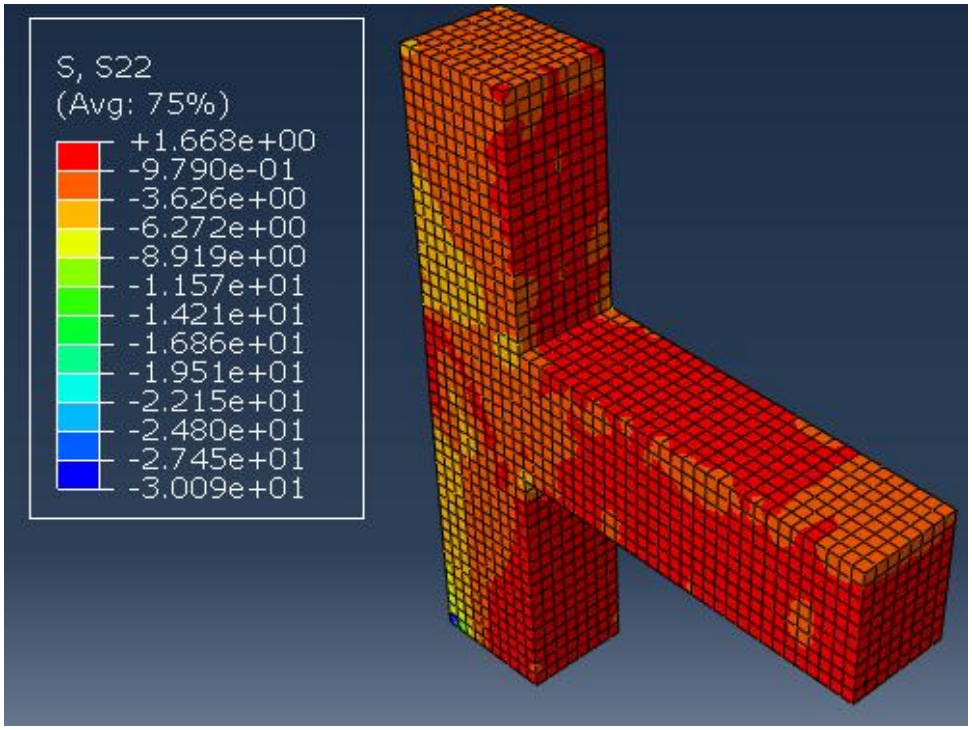

Figure 7-24: Stress S22 in concrete at yielding load (Δ = 21 mm) for NC-BCJ-18MM

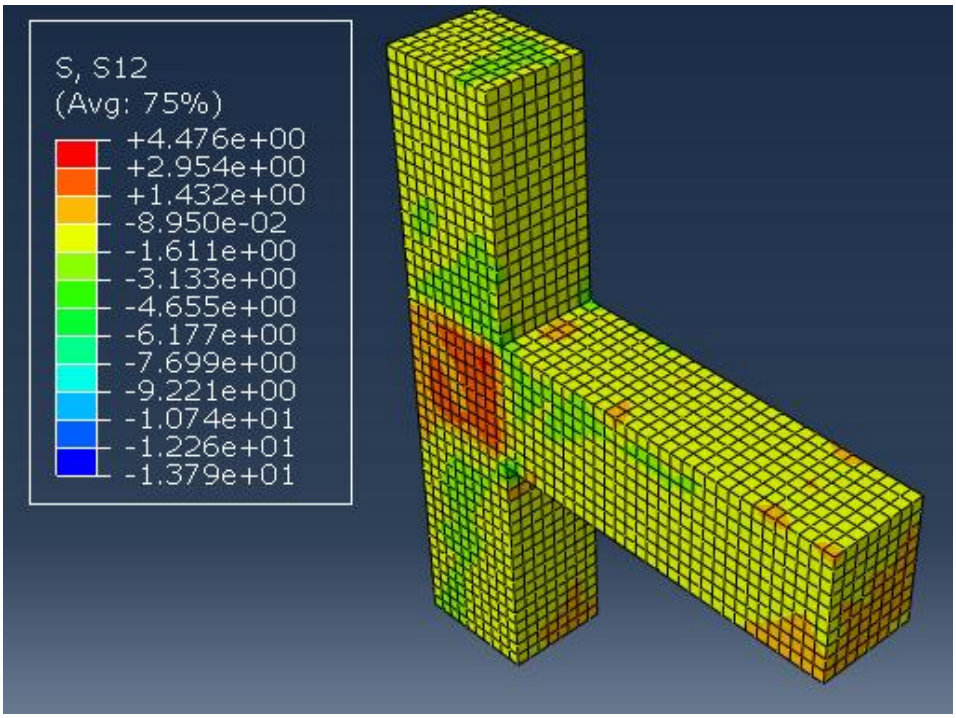

Figure 7-25: Stress S12 in concrete at yielding load (Δ = 21 mm) for NC-BCJ-12MM

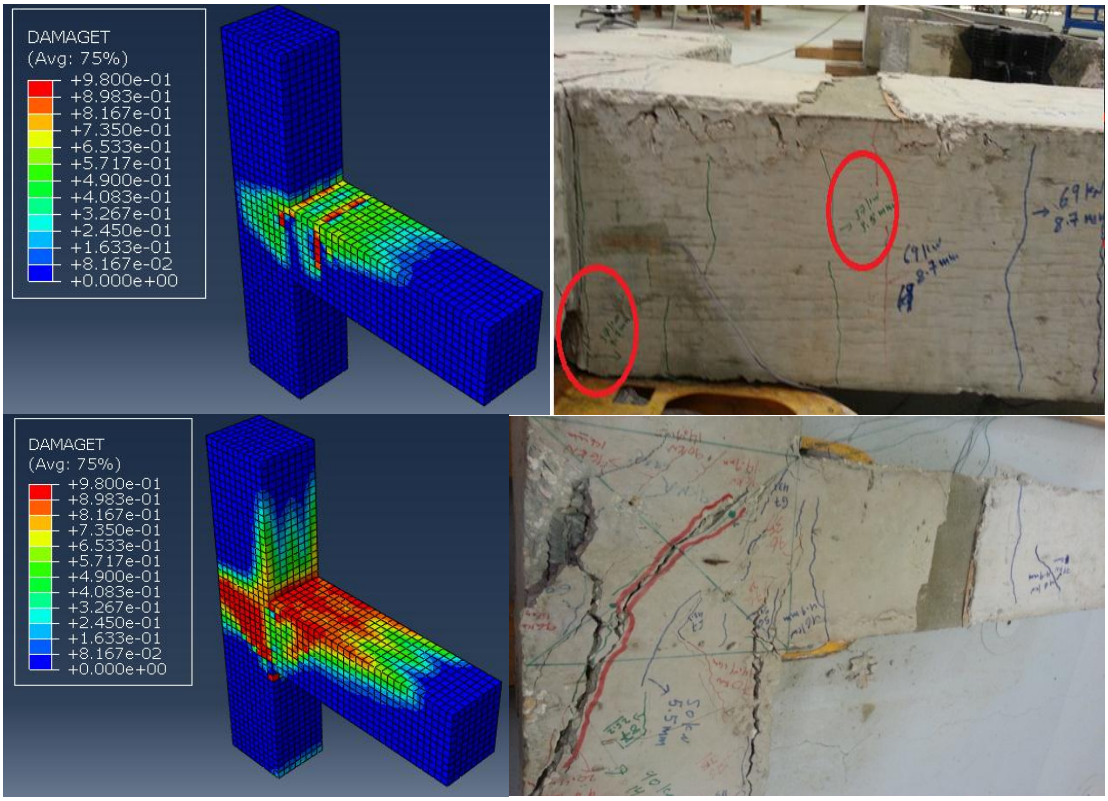

Figure 7-26: Damage propagation and crack pattern for NC-BCJ-18MM specimen

7.4.5 Numerical Simulation of SFRC-BCJ-18MM

The experimental and numerical load-deflection curves of the SFRC-BCJ-18MM specimen, under monotonic load up to failure are shown in Figure 7-27. The result of finite element simulation matches closely with the experimental results.

The reinforcement stress at ultimate load and displacement of 28.7 mm is shown in Figure 7-28. The stresses S11, S22 and S12 at yielding load are shown in Figure 7-29 to 7-31. The damage is correlated with the crack pattern which is noted in the experimental program (Figure 7-32).

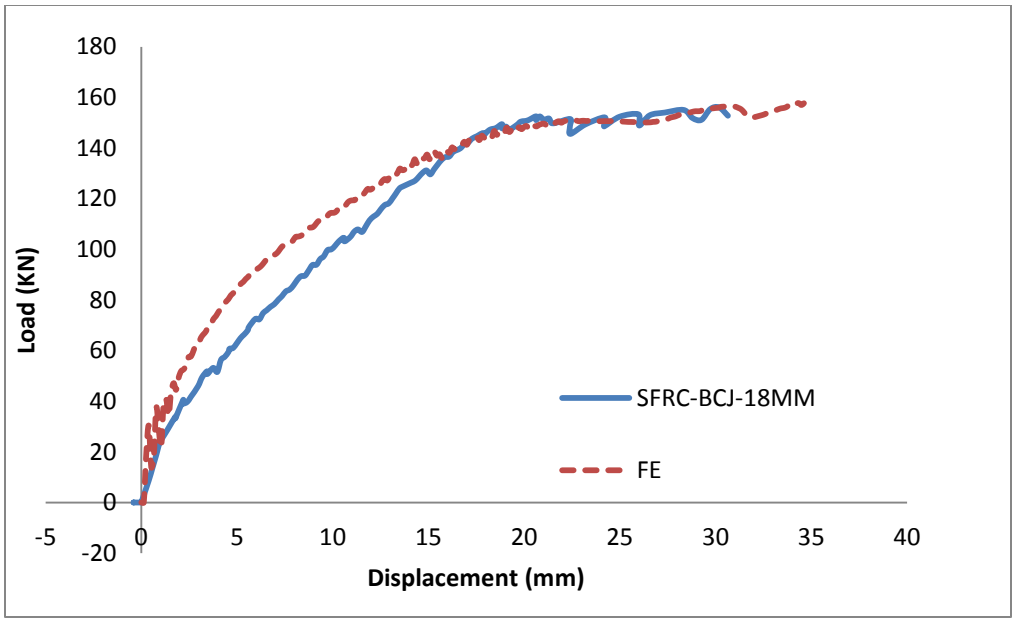

Figure 7-27: Load displacement response for SFRC-BCJ-12MM

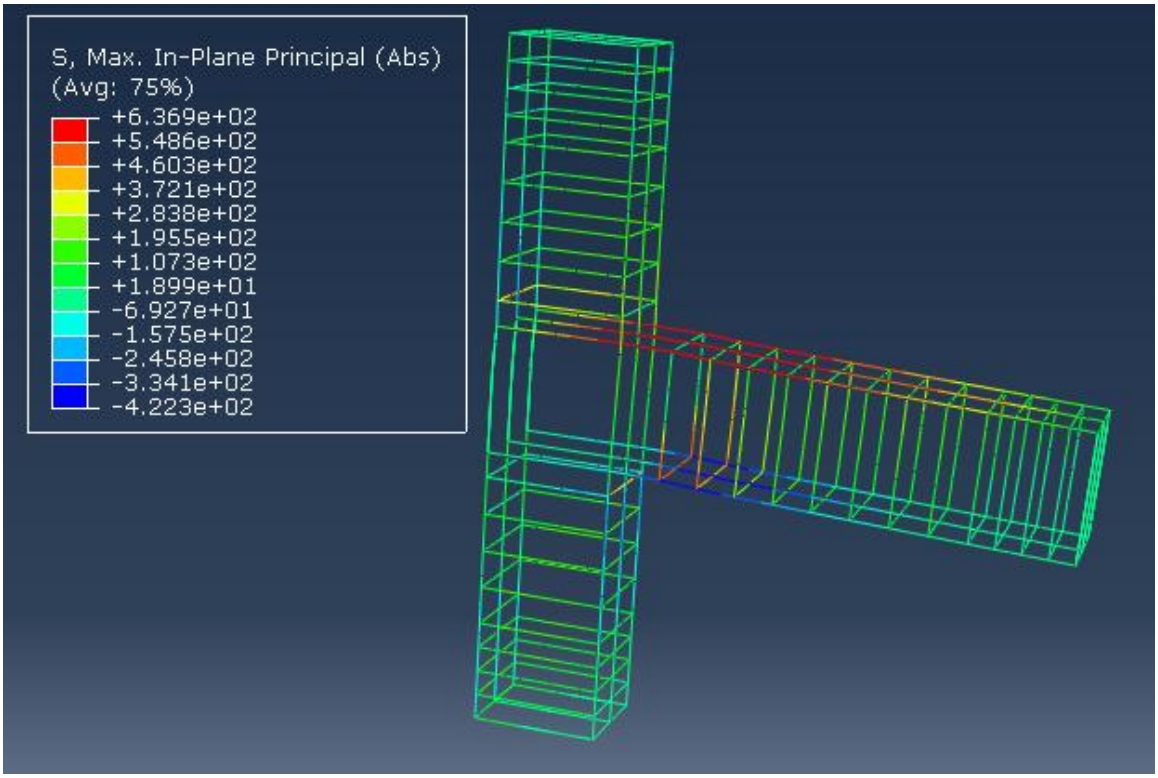

Figure 7-28: Steel stress at ultimate load for SFRC-BCJ-18MM

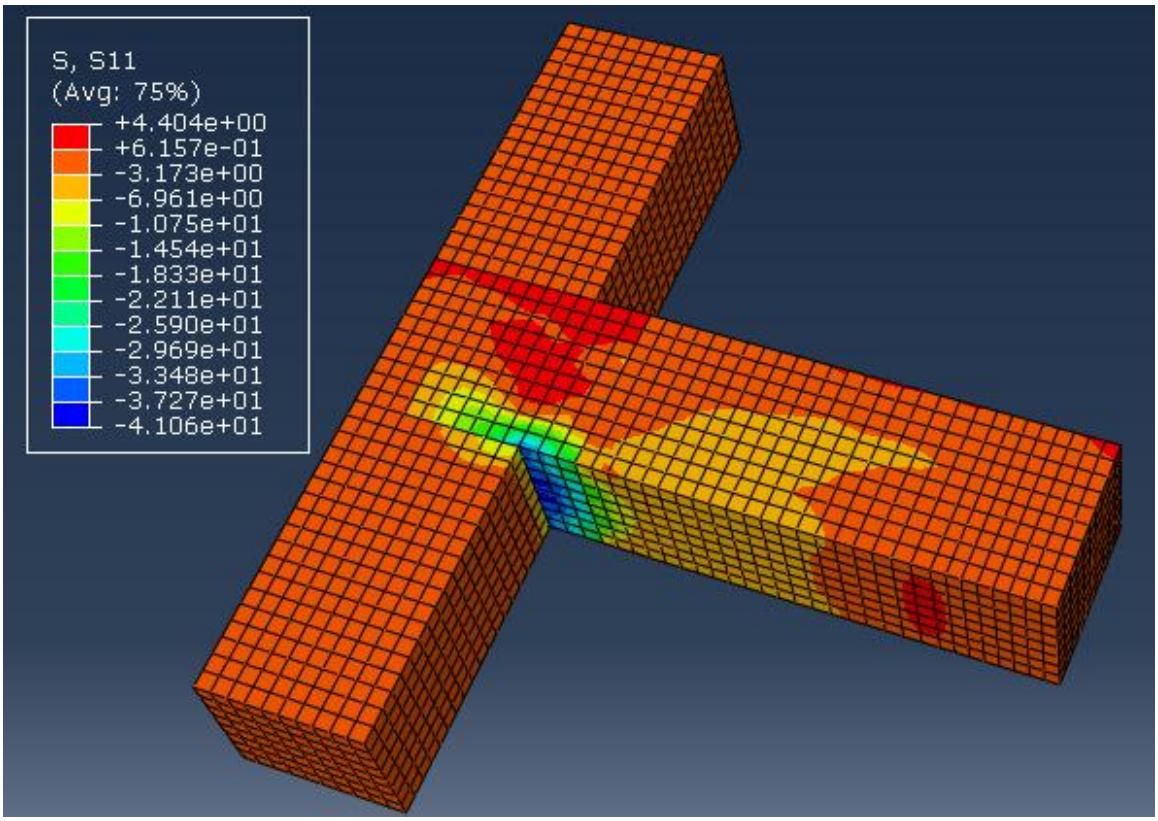

Figure 7-29: Stress S11 in concrete at yielding load (Δ = 14 mm) for SFRC-BCJ-18MM

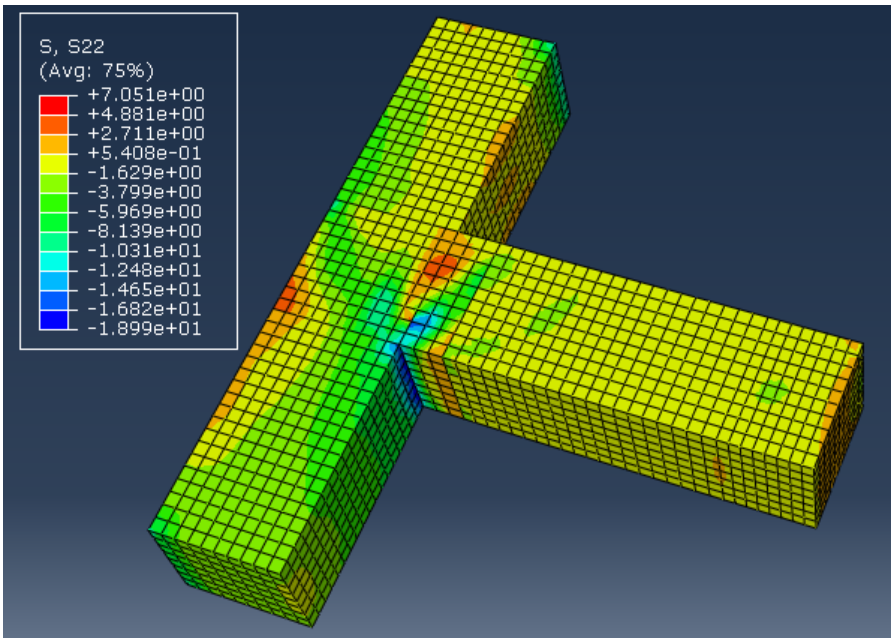

Figure 7-30: Stress S22 in concrete at yielding load (Δ = 14 mm) for SFRC-BCJ-18MM

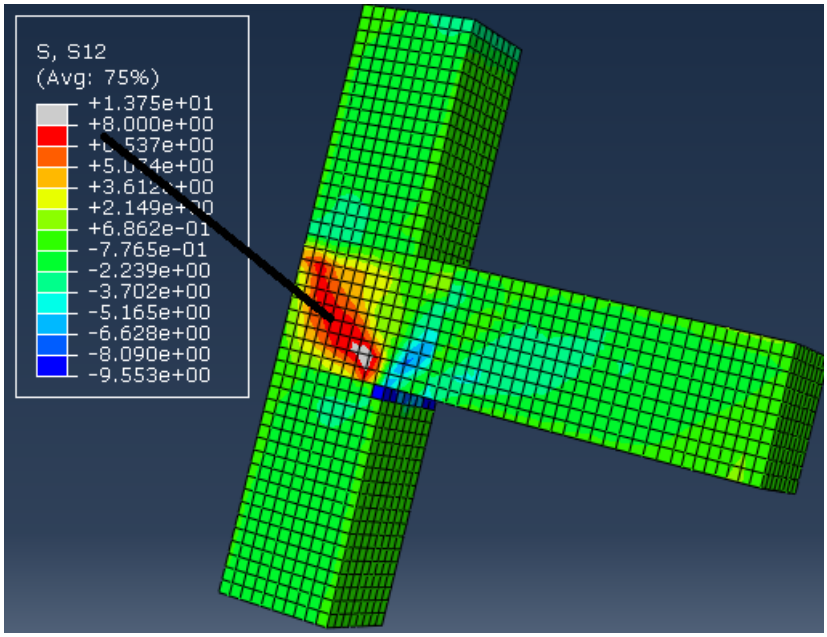

Figure 7-31: Stress S12 in concrete at yielding load (Δ = 14 mm) for SFRC-BCJ-18MM

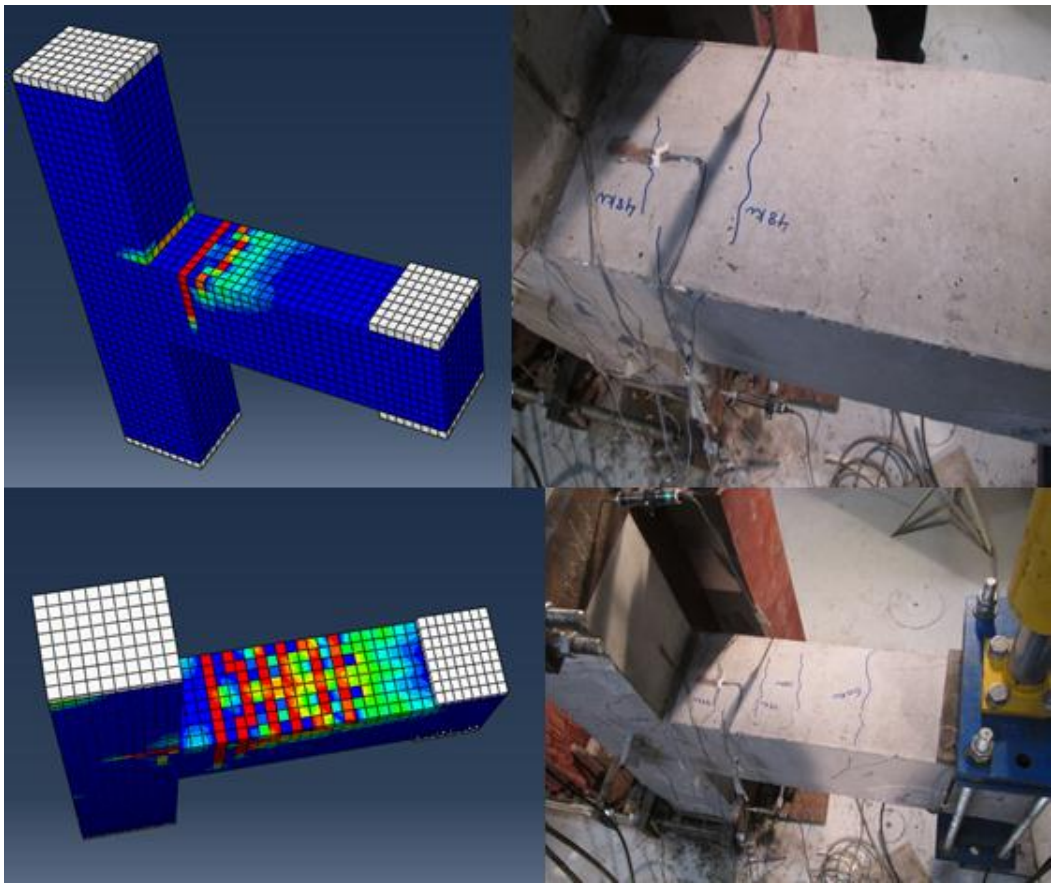

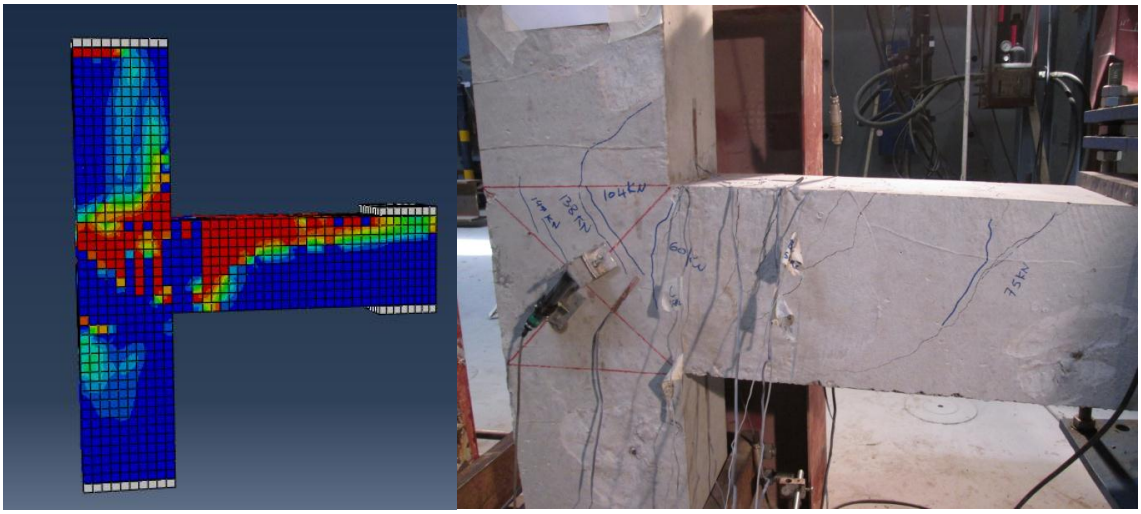

Figure 7-32: Damage propagation and crack pattern SFRC-BCJ-18MM

7.4.6 Numerical Simulation of SFRC-BCJ-S-18MM

The load deflection response for SFRC-BCJ-S-18MM is shown in Figure 7-33. The numerical result is closely matching with the experimental result. The steel stress at the yielding load is shown in Figure 7-34. The concrete stresses S11, S22 and S12 is shown in Figure 7-29 to 7-31 and the cracks pattern in the specimen was correlated with the specimen damage (Figure 7-32).

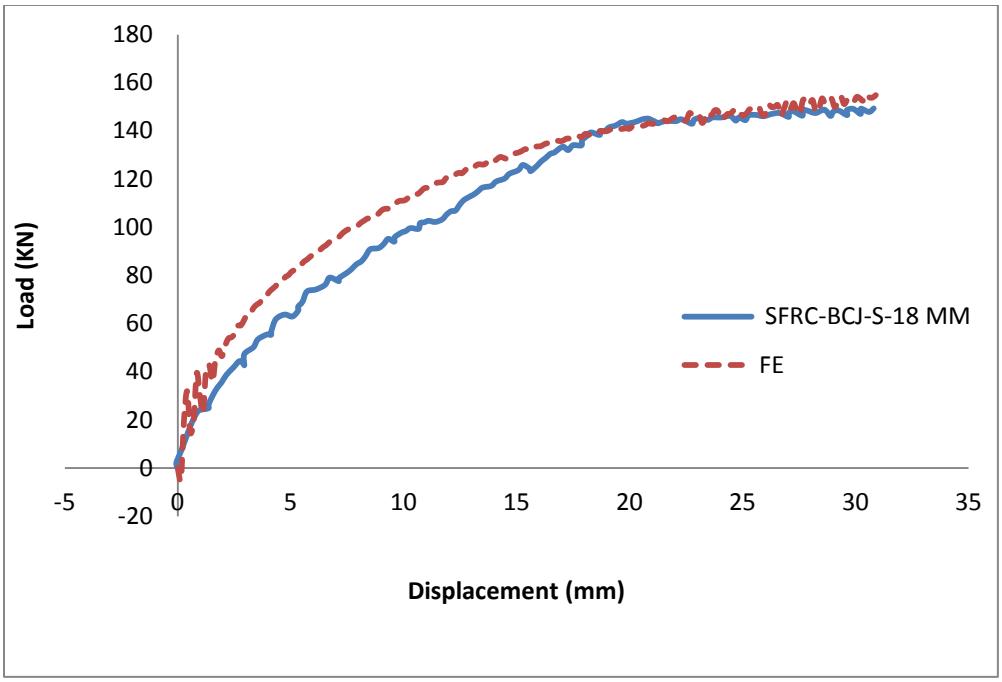

Figure 7-33: Load displacement response for SFRC-BCJ-S-18MM

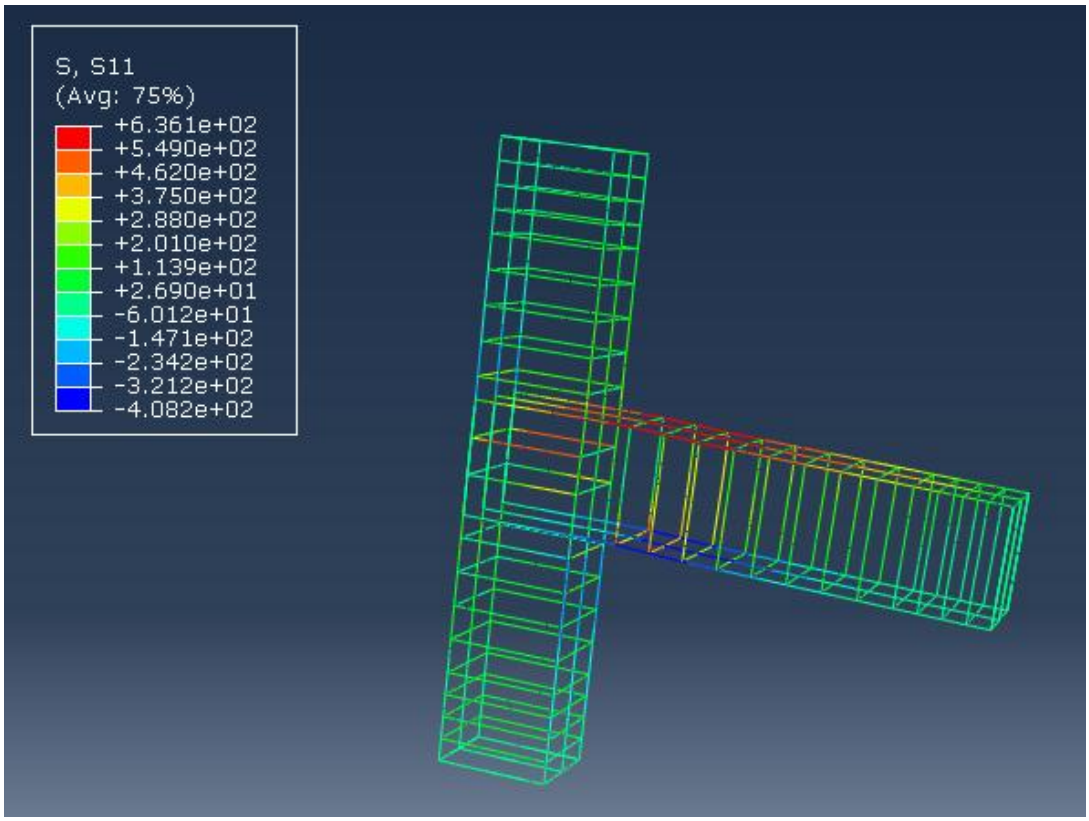

Figure 7-34: Steel stress at ultimate load for SFRC-BCJ-S-18MM

7.4.7 Numerical Simulation of UHPC-BCJ-18MM

The load deflection response for UHPC-BCJ-18MM is shown in Figure 7-35. The numerical result is closely matching with the experimental result. The steel stress at the ultimate load is shown in Figure 7-36. The concrete stresses S11, S22 and S12 is shown in Figure 7-37 to 7-39 and the cracks pattern in the specimen was correlated with the specimen damage (Figure 7-32).

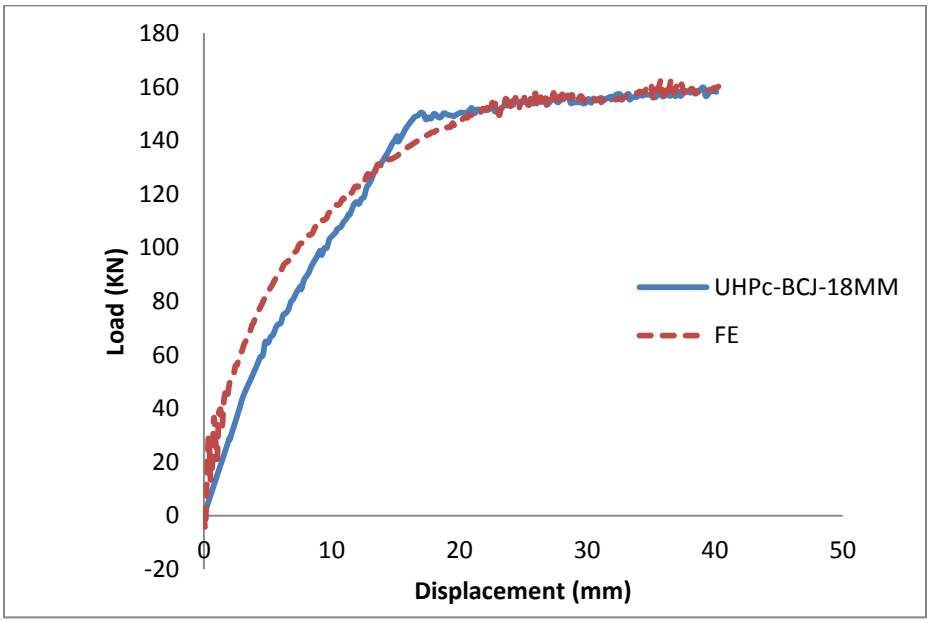

Figure 7-35: Load displacement response for UHPC-BCJ-18MM

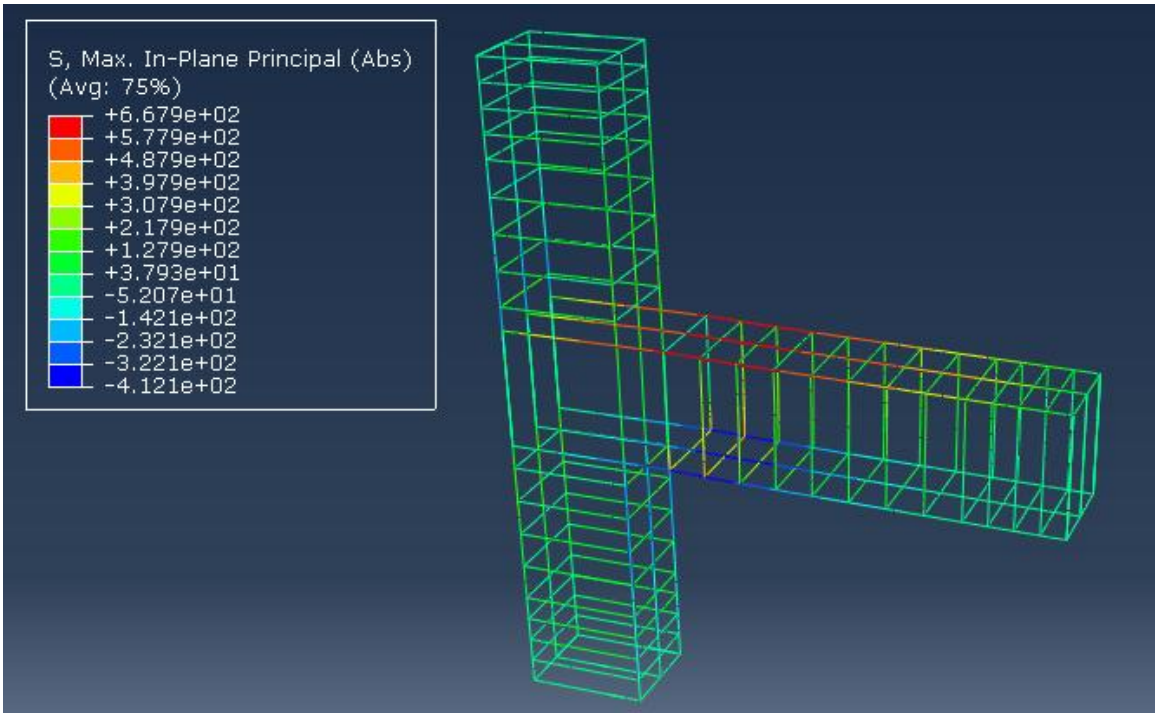

Figure 7-36: Steel stress at ultimate load for SFRC-BCJ-18MM

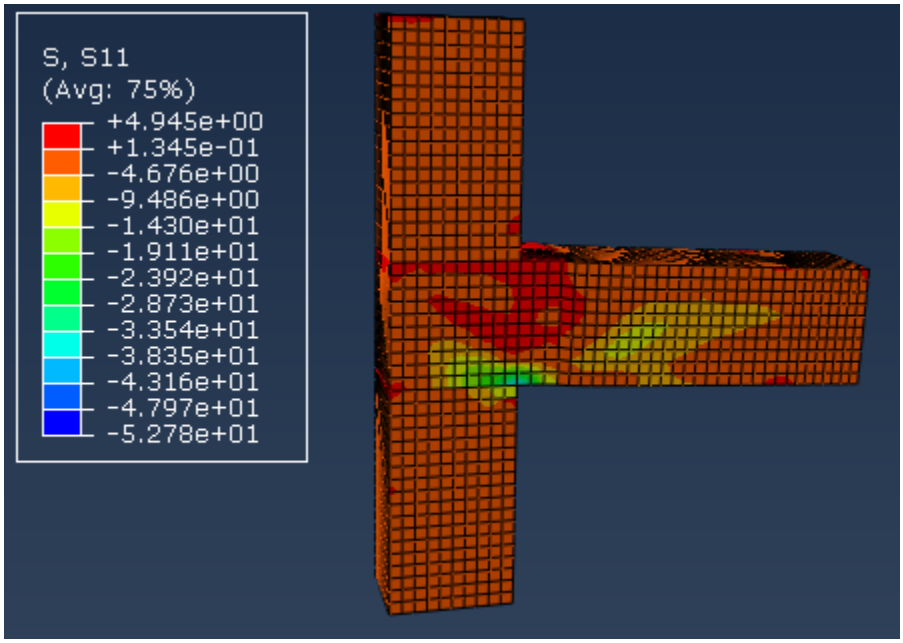

Figure 7-37: Stress S11 in concrete at yielding load (Δ = 15 mm) for UHPC-BCJ-18MM

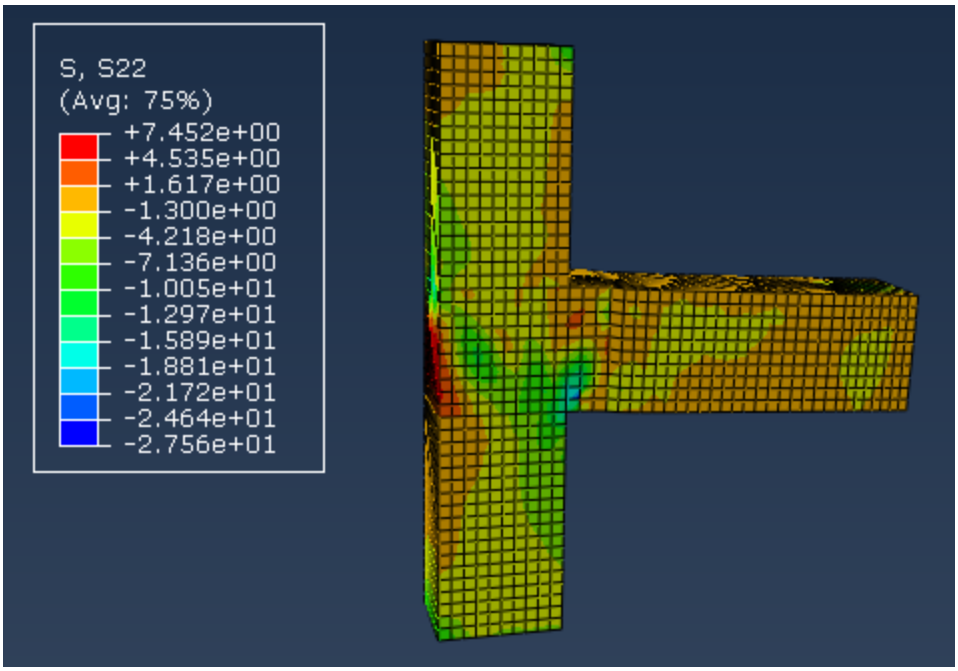

Figure 7-38: Stress S22 in concrete at yielding load (Δ = 15 mm) for UHPC-BCJ-18MM

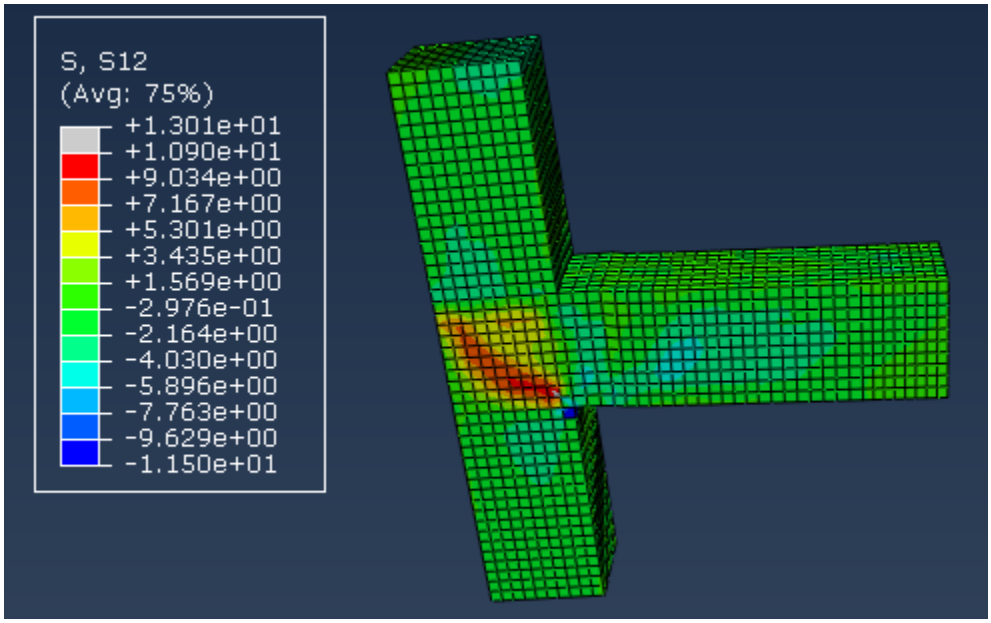

Figure 7-39: Stress S12 in concrete at yielding load (Δ = 15 mm) for UHPC-BCJ-18MM

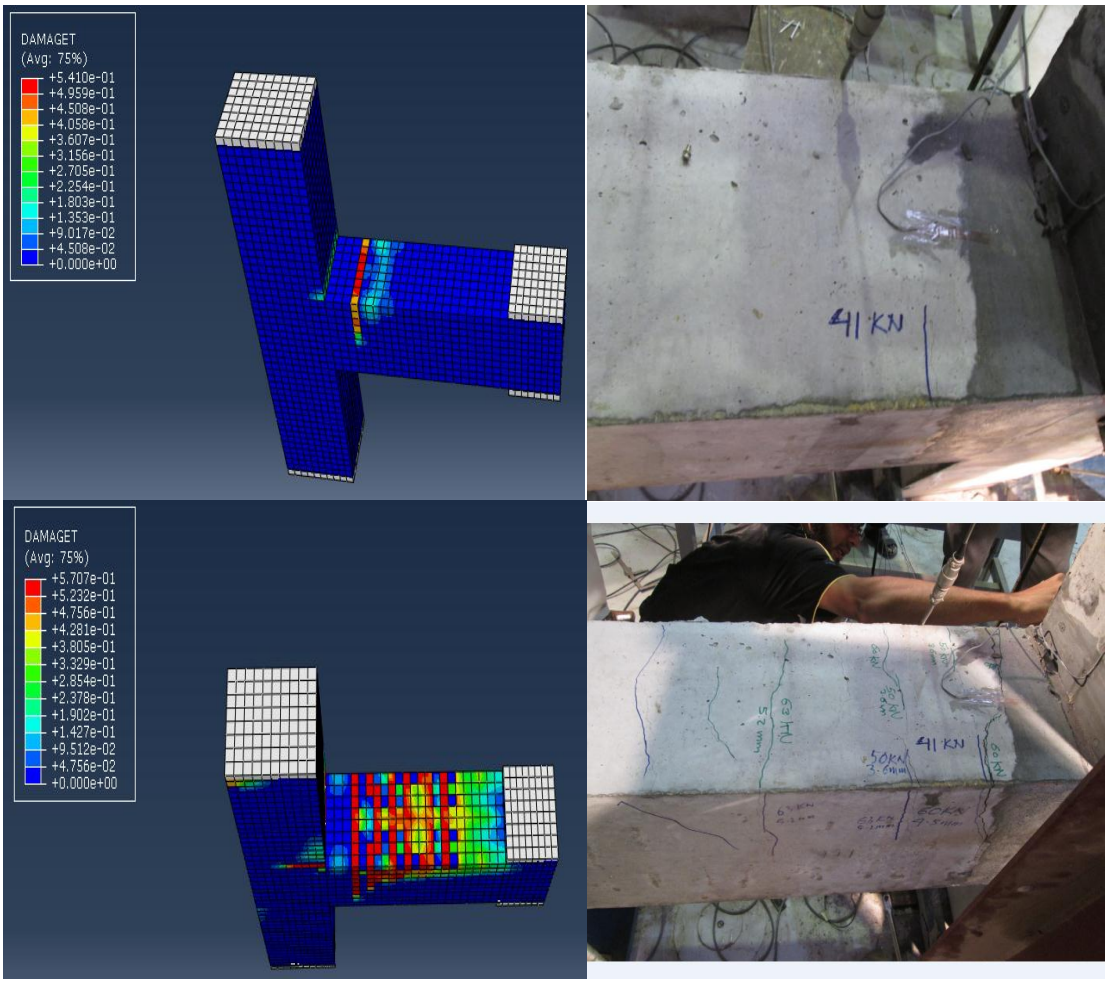

Figure 7-40: Damage propagation and crack pattern UHPC-BCJ-18MM

CHAPTER 8

CONCLUSIONS AND RECOMMENDATION

8.1 Conclusions

In this research, the behavior of BCJ was studied numerically and experimentally. A new type of strengthening of RCBCJ was used. Two types of high strength concrete with different reinforcement detailing were used in this study. As a result of strengthening, the mode of failure was changed from shear failure in the intersection area of the joint to preferred flexural failure in the beam.

From this study the following conclusion are derived:

- Steel fibre played a significant role in enhancing the tensile strength of the concrete and hence the shear capacity of the strengthened joints. However, use of steel fibre reduces significantly the workability of the concrete.
- The first diagonal cracks in the joint intersection area did not represent the failure of the joint. The ultimate load was higher than the first cracking load, showing that the joint has a shear strength that exceeds the first cracking strength, similar to the shear strength for deep and short beams.
- The high strength concrete whether it is SFC or UHPC changed the mode of failure from weak column / strong beam to strong column / weak beam, which is the preferred failure mode.

- Due to the low percentage of beam steel reinforcement in NC-BCJ-12MM control specimen, the mode of failure was flexural beam failure with some damage in the joint intersection region. While in the NC-BCJ-18MM the specimen failed due to the joint shear damage which confirmed by the fact that the flexural strength of the beam was computed as 137 KN which is greater than the ultimate load.

- The stirrups in NC-BCJ-S-18MM specimen played a role in improving the shear carrying capacity and the hysteresis behavior of the joint. The load carrying capacity was improved by 23 %.
- Since the failure in the SFRC-BCJ specimens was flexure dominated failure, the effect of stirrups in the joint could not be observed.
- The SFC concrete in the joint region of SFRC-BCJ-18MM specimen played a significant role in changing the failure in the joint from joint shear failure to preferred beam flexural failure. Due to the high flexural capacity of the beam several fine cracks were appeared in the joint region. After the strengthening, the load carrying capacity was enhanced by 60.49%.

- The high percentage of steel fibre in the UHPC caused the shear and the tensile strength of the concrete to increase significantly. This resulted in only one fine crack in the joint intersection region of UHPC-BCJ-18MM. The failure in the specimen was converted from the joint shear failure to the preferred flexural failure.
- The presence of steel fibre in the SFC caused the shear and the tensile strength of the concrete to increase significantly. This resulted in several fine cracks in the

joint intersection region of SFRC-BCJ-18MM. The failure in the specimen was converted from the joint shear failure to the preferred flexural failure.

- For the strengthened specimens which failed due to flexure, the installed strain gauges on the reinforcement showed that the strain exceeded the yield strain of the reinforcement.
- Regarding the cyclic test, the stiffness and the capacity of the specimens were improved after strengthening.
- The numerical results with damage plasticity model were noted to yield reasonably accurate results of BCJ specimens.
- The concrete damage plasticity model predicted the flexural failure mode as well as the softening failure mode.
- For NC-BCJ-18MM specimens the damage started in the top of the beam, then the damage appeared in the joint intersection region at load of 60KN which confirmed with the experimental result.
- For the specimens which were strengthened with SFC, the damage started in the beam then at load of 107 KN the damage started in the intersection area. While no damage occurred in the intersection region of BCJ specimens which were strengthened with UHPC.
- Regarding NC-BCJ-12MM specimen, the damage started in the beam, then at load of 53 KN the damage started in the joint. After strengthening the BCJ-12MM specimens with SFC, no damage occurred in the intersection area.

8.2 Recommendations for Future Work

- This research was performed on exterior beam column joint specimens, other studies can be conducted on other types of joints.
- In this study steel fibre concrete and ultra-high performance concrete were used in strengthening the BCJ specimens, other types of concrete with different percentages of steel fibre can be used.
- In the coastal areas, Non-metallic fibre can be used in enhancing the concrete tensile strength. Using non-metallic fibre will forbid the corrosion to take place.
- Other types of high strength concrete with less tensile strength can change the mode of failure from flexural failure to joint shear failure. In this case the experimental joint shear capacity will be known.
- Regarding the stirrups in the joint intersection region, other specimens designed for joint shear failure can be studied to investigate the effect of the stirrups on the shear capacity of the high strength concrete joint.
- The possibility of precast SFRC and UHPC joints with dowel bars for use in precast construction should be perused in order to enhance the integrity of precast construction in seismic joints.

References

1. Hakeem, I.Y.A., *Characterization of an ultra-high performance concrete*, King Fahd University of Petroleum & Minerals (Saudi Arabia),MSc Thesis, 2011.

2. Song, P. and S. Hwang, *Mechanical properties of high-strength steel fiber-reinforced concrete.* Construction and Building Materials, 2004. **18**(9): p. 669-673.

3. Shende, A., A. Pande, and M.G. Pathan, *Experimental Study on Steel Fiber Reinforced Concrete for M-40 Grade.* International Refereed Journal of Engineering and Science, 2012. **1**(1): p. 043-048.

4. Gao, J., W. Sun, and K. Morino, *Mechanical properties of steel fiber-reinforced, high-strength, lightweight concrete.* Cement and Concrete Composites, 1997. **19**(4): p. 307-313.

5. Barros, J.A., Santos, S., and Lourento, L., *Flexural behaviour of steel fibre reinforced self-compacting concrete laminar structures.* 2008.

6. Prem, P.R., B. Bharatkumar, and N.R. Iyer. *Mechanical properties of ultra high performance concrete*. in *Proceedings of World Academy of Science, Engineering and Technology*. 2012. World Academy of Science, Engineering and Technology.

7. El-Dieb, A.S., *Mechanical, durability and microstructural characteristics of ultra-high-strength self-compacting concrete incorporating steel fibers.* Materials & Design, 2009. **30**(10): p. 4286-4292.

8. Park, S.H., Kim, D.J., Ryu, G.S., and Koh, K.T., *Tensile behavior of ultra high performance hybrid fiber reinforced concrete.* Cement and Concrete Composites, 2012. **34**(2): p. 172-184.

9. Ramli, M. and E. Dawood, *High-strength flowable mortar reinforced by steel fiber*. Slovak Journal of Civil Engineering, 2011. **19**(3): p. 10-16.

10. Mazloom, M., A. Ramezanianpour, and J. Brooks, *Effect of silica fume on mechanical properties of high-strength concrete.* Cement and Concrete Composites, 2004. **26**(4): p. 347-357.

11. Yew, M., et al., *Strength properties of hybrid nylon-steel and polypropylene-steel fibre-reinforced high strength concrete at low volume fraction.* Int J Phys Sci, 2011. **6**(33): p. 7584-8.

12. Sivakumar, A. and M. Santhanam, *Mechanical properties of high strength concrete reinforced with metallic and non-metallic fibres.* Cement and Concrete Composites, 2007. **29**(8): p. 603-608.

13. Selina, R.G., C. Geethanjali, and P. Jaison Varghese, *Influence of Hybrid Fiber on Reinforced Concrete*, International Journal of Advanced Structures and Geotechnical Engineering, 2014, ISSN 2319-5347, Vol. 03, No. 01.

14. Hsie, M., C. Tu, and P. Song, *Mechanical properties of polypropylene hybrid fiber-reinforced concrete.* Materials Science and Engineering: A, 2008. **494**(1): p. 153-157.

15. Singh, S., A. Singh, and V. Bajaj, *Strength and Flexural Toughness of Concrete Reinforced with Steel-Polypropylene Hybrid Fibres.* Asian Journal of Civil Engineering, 2010. **11**(4): p. 495-507.

16. Nili, M. and V. Afroughsabet, *The effects of silica fume and polypropylene fibers on the impact resistance and mechanical properties of concrete.* Construction and Building Materials, 2010. **24**(6): p. 927-933.

17. Ahmed, D., *Retrofitting of exterior beam-column joints using CFRP*..King Fahd University of Petroleum &Minerals (Saudi Arabia),MSc Thesis, 2012.

18. Braga, F., R. Gigliotti, and M. Laterza, *R/C Existing Structures with Smooth Reinforcing Bars: Experimental Behaviour of Beam-Column Joints Subject to Cyclic Lateral Loads.* Open Construction & Building Technology Journal, 2009. **3**.

19. Pampanin, S., G.M. Calvi, and M. Moratti, *Seismic behavior of RC beam-column joints designed for gravity only.* 2002.

20. *Abdulsamee. H,Modelling ofCyclic Behavior of Retrofitted Beam Column Joint*. King Fahd University of Petroleum & Minerals (Saudi Arabia),PhD Thesis, 2014.

21. Pantelides, C., C. Clyde, and L. Reaveley. *Rehabilitation of R/C building joints with FRP composites*. in 12th World Conference on Earthquake Engineering, Auckland, New Zealand. 2000.

22. Gencoglu, M. and B. Mobasher. *The strengthening of the deficient RC exterior beam-column joints using CFRP for seismic excitation*. in Proceedings of the 3 rd international conference on structural engineering, mechanics and computation. 2007.

23. Sasmal, S., Ramanjaneyulu, Kl., Novak, B., Srinivas, V., and Kumar, K., *Seismic retrofitting of nonductile beam-column sub-assemblage using FRP wrapping and*

steel plate jacketing. Construction and Building Materials, 2011. **25**(1): p. 175-182.

24. Alsayed, S.H., Almusallam, T.H., and Siddiqui, N.A., *Seismic response of FRP-upgraded exterior RC beam-column joints.* Journal of Composites for Construction, 2010. **14**(2): p. 195-208.

25. Karayannis, C.G., C.E. Chalioris, and G.M. Sirkelis, *Local retrofit of exterior RC beam–column joints using thin RC jackets—An experimental study.* Earthquake Engineering & Structural Dynamics, 2008. **37**(5): p. 727-746.

26. M Oinam, R., *Experimental Study on Beam-Column Joint with Fibres under Cyclic Loading.* IOSR Journal of Engineering, 2013. **3**: p. 13-23.

27. Perumal, P. and B. Thanukumari, *Behaviour of M60 Concrete Using Fibre Cocktail in Exterior Beam-Column Joint Under Reversed Cyclic Loading.* Asian Journal Of Civil Engineering (Building And Housing), 2011. **12**(2): P. 255-265.

28. Sarsam, K. and Z.M.K. Al-Azzawi, *Shear Capacity of High-Strength Fiber Reinforced Concrete Beam-Column Joints.*

29. Ganesan, N., P. Indira, and R. Abraham, *Steel fibre reinforced high performance concrete beam-column joints subjected to cyclic loading.* ISET J. Earthq. Technol, 2007. **44**(3-4): p. 445-456.

30. Wang, Y.-C. and M.-G. Lee, *Ultra-high strength steel fiber reinforced concrete for strengthening of rc frames.* Journal of Marine Science and Technology, 2007. **15**(3): p. 210-218.

31. Gencoglu, M. and I. Eren, *An experimental study on the effect of steel fiber reinforced concrete on the behavior of the exterior beam-column joints subjected to reversal cyclic loading.* Turkish Journal of Engineering and Environmental Sciences, 2002. **26**(6): p. 493-502.

32. Röhm, C., Novak, B., Sasmal, S., Karusala, R., and Srinivas., *Behaviour of fibre reinforced beam-column sub-assemblages under reversed cyclic loading.* Construction and Building Materials, 2012. **36**: p. 319-329.

33. Keerthana, J.D. and C.S. Reddy, *Experimental Investigation on Hybrid Steel Fiber Reinforced Concrete Beam–Column Joints Under Cyclic Loading.* 2014.

34. Ha.G. and Shin.J,*Evaluation of Seismic Performance of High Strength Reinforced Concrete Exterior Beam-Column Joints Using High Ductile Fibre-Reinforced Mortar.* Journal of the Korea Concrete Institute, 2013. **25**(4): p. 419-428.

35. Ilki, A., I. Bedirhanoglu, and N. Kumbasar, *Behavior of FRP-retrofitted joints built with plain bars and low-strength concrete.* Journal of Composites for Construction, 2010. **15**(3): p. 312-326.

36. Mostofinejad, D. and S. Talaeitaba, *Finite element modeling of RC connections strengthened with FRP laminates.* Iranian Journal of Science and Technology, Transaction B, Engineering, 2006. **30**(B1): p. 21-30.

37. Ravi, S.R. and G.P. Arulraj, *Finite Element Modeling on behavior of Reinforced Concrete Beam-Column Joints Retrofitted with Carbon Fiber Reinforced Polymer Sheets.* International Journal of Civil & Structural Engineering, 2010. **1**(3): p. 576-582.

38. Sagbas, G., F. Vecchio, and C. Christopoulos, *Computational modeling of the seismic performance of beam-column subassemblies.* Journal of Earthquake Engineering, 2011. **15**(4): p. 640-663.

39. Mitra, N. *Continuum model for RC interior beam-column connection regions*. in *14º Conferência Mundial em Engenharia Sísmica. Beijing, China*. 2008.

40. Kaya, M. and A.S. Arslan, *Analytical modeling of post-tensioned precast beam-to-column connections.* Materials & Design, 2009. **30**(9): p. 3802-3811.

41. Jiuru, T., Chaobin. H., Kaijian. Y,. and Yongcheng. Y,. *Seismic behavior and shear strength of framed joint using steel-fiber reinforced concrete.* Journal of Structural Engineering, 1992. **118**(2): p. 341-358.

42 Tsonos, A.G., Tegos, I.A. and Penelis, G.G.. "*Seismic Resistance of Type 2 Exterior Beam-Column Joints Reinforced with Inclined Bars*", ACI Structural Journal, Vol. 89, No. 1, 2011. pp. 3–12.

43 Park, P. (1997). "A Static Force-based Procedure for the Seismic Assessment of Existing Reinforced ConcreteMoment Resisting Frames." Bulletin of the New Zealand National Society for Earthquake Engineering,1997. 30(3), 213-226.

Vitae

Name	:Anas Mohammad Alkhatib
Nationality	: Palestinian
Date of Birth	:10/20/1987
Email	: anasalkhatib98@gmail.com
Address	: West Bank, Palestine.
Academic Background	: B.Sc. Degree from the Civil Engineering Department, College of Engineering, An-Najah National University"- Nablus, Palestine, August 2009.
	M.Sc. degree in Civil Engineering from the Civil Engineering Department, College of Engineering, King Fahd University of Petroleum and Minerals, Dhahran, Saudi Arabia, May 2015.